APPLICATION OF CHROMIUM DOPED TITANIUM DIOXIDE IN SOLAR-TO-CHEMICAL ENERGY CONVERSION

A THESIS BY
KAZI AKIKUR RAHMAN

THESIS SUBMITTED IN FULFILMENT OF THE REQUIREMENTS FOR THE DEGREE OF
DOCTOR OF PHILOSOPHY (PhD)

SOLAR ENERGY TECHNOLOGIES GROUP
SCHOOL OF COMPUTING, ENGINEERING, AND MATHEMATICS
WESTERN SYDNEY UNIVERSITY, AUSTRALIA
MAY 2018

Statement of Authentication

The work presented in this thesis is, to the best of my knowledge and belief, original except as acknowledged in the text. I do solemnly and sincerely declare that I am the sole author /writer of this work and have not submitted this material, either in full or in part, for a degree at this or any other institution.

…  …..

Kazi Akikur Rahman

Acknowledgment

In the name of God, The Beneficent, The Merciful, I would like to express my utmost gratitude and thanks to the almighty for the help and guidance that he has given me through all these periods of time. I would like to express my gratitude and profound respect to my supervisors Professor Janusz Nowotny and Associate Professor Tadeusz Bak for their enthusiastic support, encouragement and continuous exploration throughout my study period. I would also like to acknowledge my external co-supervisor Professor Mihail Ionescu and Dr. Armand Atanacio for giving me the privilege to use the facilities in ANSTO under their close supervision.

Special thanks are due to Professor Bill Price, Chair of the Solar Energy Technologies Advisory Board. His extensive advices on the research strategy are sincerely appreciated.

I remember the esteem, affection, and inspiration of my parents, brothers, sister and my wife to complete this journey successfully. Their love, motivation, and support always inspire me at every stage of my life. Moreover, I am thankful to my colleagues, Md. Abdul Alim and Md. Elias Mollah from Solar Energy Technologies Lab, to support me directly or indirectly throughout the journey.

I would like to acknowledge the financial support by Western Sydney University, WSU to carry out this research. I gratefully acknowledge the privileges and opportunities offered by the university. I also express my gratitude to the staffs of WSU to help me in different aspect during this time of the study.

I would like to acknowledge the support that I have received from MedipaQ Pty Ltd. This support is sincerely appreciated.

Table of Content

List of Figures

List of Tables

Notation

Symbol	Unit	Term
A	-	Proportionality constant
AES	-	Auger Electron Spectroscopy
AN	-	Anode
BE	eV	Binding energy
CAT	-	Cathode
C_o	mol/L	Initial concentration of methylene blue
CRO	-	Conversion rate optimizer
C_t	mol/L	Concentration of methylene blue at time t
D	m^2/s	Diffusion coefficient
DFT	-	Density function theory
e	C	Elementary charge
E_A	eV	Acceptor energy level
EC	$\Omega^{-1}m^{-1}$	Electrical conductivity
E_{CB}	eV	Energy level of conduction band
E_D	eV	Donor energy level
E_F	eV	Fermi level
EF	-	Enrichment factor
E_g	eV	Bandgap
EPR	-	Electron Paramagnetic Resonance
E_{VB}	eV	Energy level of valence band
f(R)	-	Kubelka-Munk function
h	-	Hour
hv	eV	Photon energy
I	-	Intensity
k	-	Wavevector
K	-	Equilibrium constant
KE	eV	Kinetic energy
KPP	-	Key performance-related property
LDSS	-	Low-dimensional surface structure
MB	-	Methylene blue
min	-	Minute
n	-	Concentration of electrons

NSF	-	Nano size film
NP	-	Nanoparticle
NT	-	Nanotube
p	-	Concentration of electron-holes
PC	-	Polycrystalline
PIXE	-	Proton-induced X-ray emission
$p(O_2)$	Pa	Oxygen activity
ppb	-	Parts per billion
R	-	Reflectance
R	-	Gas constant
r	nm	Radius
s^*	cm^{-1}	Scattering coefficient
SC	-	Single crystal
SEM	-	Scanning electron microscopy
SIMS	-	Secondary ion mass spectrometry
T	K	Absolute temperature
TF	-	Thin film
t	S	Time
UV-vis-NIR	-	Ultraviolet–visible and near-infrared
XPS	-	X-ray photoelectron spectroscopy
α	cm^{-1}	Optical absorption coefficient
σ	$\Omega^{-1}m^{-1}$	Electrical conductivity
λ	nm	Wavelength
Φ	eV	Work function
ϕ_s	eV	Spectrometer work function
μ_n	$m^2V^{-1}s^{-1}$	Mobility of electron-holes

Postulation of the Thesis

Solar energy conversion is a complex process. It has been commonly assumed that the solar energy conversion by oxide semiconductors, such as TiO_2-based solid solutions, is determined by chemical composition, structure and electronic structure, mainly the bandgap.

The present PhD thesis postulates that the performance of oxide semiconductors, including TiO_2-based semiconductors, in solar-to-chemical energy conversion is determined by point defects and a range of defect-related properties that have a competitive effect on the conversion process. The present PhD research project aims at verification of this hypothesis by investigating the effect of defect disorder and a range of defect-related properties of Cr-doped TiO_2 (rutile) on the light-induced partial water oxidation.

The present thesis shows that while the bandgap has an effect on solar energy conversion, the performance of TiO_2-based systems is determined by alternative defect-related properties rather than the bandgap. The established effects and relationships in the present project pave the way for a new type of materials engineering - defect engineering - in the development of a new generation of solar energy conversion systems with enhanced performance.

Abstract

The present PhD research project reports the results of comprehensive studies on defect chemistry and defect-related properties, such as electronic structure, on the light-induced partial water oxidation for Cr-doped TiO_2. The rationale for selecting TiO_2 as the object of these studies was the prominent report of Fujishima and Honda [1] showing, for the first time, that TiO_2 may be applied for water oxidation using sunlight as the only driving force of the process. The rationale for selecting chromium as the main extrinsic lattice element was the reported effect of chromium on bandgap reduction of TiO_2 leading to enhanced absorption of sunlight [2].

Postulate

The thesis postulates that the photocatalytic performance of semiconducting materials based on nonstoichiometric compounds, such as TiO_2-based solid solutions, is determined by point defects. Therefore, the performance of the studied solid solutions in solar energy conversion may be considered in terms of defect-related properties.

Aim

The present research project aimed at verification of the postulate of the thesis. The ultimate aim was to understand the effect of chromium on defect disorder of TiO_2 and its defect-related properties, such as photocatalytic properties. The research involved the determination of the effect of processing conditions of Cr-doped TiO_2 on chromium segregation and the related concentration gradients of defects within the surface layer that is active photo-catalytically. The strategic aim of the research is to develop a new technology of the conversion of solar energy into chemical energy. Such technology may lead to the reduction of the costs of water processing and elimination of the use for this purpose of the electrical energy produced from fossil fuels. Ultimately, the technology could reduce global warming and climate change.

Outline and Approach

The thesis commences with a brief statement about the imperative to address the key community needs to reduce climate change that can be achieved through the

development of new energy generation technologies that are based on renewable energy, such as solar energy [3] (***chapter 1)***.

C***hapter 2*** provides a definition of basic terms used in the topical areas, including defect chemistry and the related electronic structure of TiO_2 and its solid solutions, photocatalytic partial oxidation of water, photoelectrochemical coupling and the phenomenon of segregation. This chapter also provides the relationships between the basic defect-related properties.

C***hapter 3*** provides an overview of the literature reports on the effect of chromium on the electronic structure of TiO_2 [4]. The overview shows that (i) chromium results in a reduction of the bandgap from ~3 eV for pure TiO_2 to ~2 eV for Cr-doped TiO_2 and (ii) the mechanisms of chromium incorporation into the surface layer and the bulk phase of TiO_2 are different. It has been documented that the related experimental data exhibits a substantial scatter. This section also reports the experimental procedures on processing the specimens of Cr-doped TiO_2 with reproducible properties, the chemical analysis using the proton-induced X-ray emission (PIXE) as well as the use of reflectance spectroscopy for the determination of the electronic structure.

C***hapter 4*** considers the effect of chromium segregation on surface vs. bulk composition of Cr-doped TiO_2 [5]. This chapter involves an overview of the literature reports on segregation in oxide materials in general and Cr-doped TiO_2 in particular. The chapter also considers the effect of annealing of Cr-doped TiO_2 in the gas phase of controlled oxygen activity on surface segregation of chromium and the use of secondary ion mass spectrometry (SIMS) for the determination of the segregation-induced surface enrichment.

The subsequent chapter (***chapter 5***) reports the effect of chromium concentration and oxygen activity on photocatalytic properties of both pure and Cr-doped TiO_2 as well as the effect of electrochemical coupling of pure and Cr-doped TiO_2 on photocatalytic performance. The first section involves the literature reports on the effect of chromium on photocatalytic properties of TiO_2 [6]. It is shown that the related data exhibit a substantial scatter. This section considers the experimental procedure on the determination of the rate constant of partial water oxidation that is based on the decomposition of methylene blue (MB) used for testing the photocatalytic properties. This chapter determined the effect of

chromium concentration of the photocatalytic activity for the specimens annealed in reducing and oxidizing conditions. The results were used in the derivation of a theoretical model that is reflective the reactivity of Cr-doped TiO_2 with water and oxygen at anodic and cathodic sites, respectively. This chapter also reports the results on the effect of oxygen activity on the photocatalytic performance of pure and Cr-doped TiO_2 involving 0.04 at% Cr [7]. It is shown that the performance assumes minimum around n-p transition point where the charge transport assumes minimum value. Chapter 5 also considers the effect of electrochemical coupling formed of TiO_2 of different Fermi level, including pure TiO_2 and Cr-doped TiO_2, on the reactivity of anodic and cathodic sites [8].

Chapter 6 provides a brief summary on the effect of the key performance-related properties (KPPs) on the photocatalytic performance of Cr-doped TiO_2, including the bandgap, the concentration of anodic surface sites (titanium vacancies), Fermi level and charge transport. It has been concluded that the results obtained in the thesis pave the way in the development of new type of engineering, defect engineering, which can be applied in the processing of energy materials based on nonstoichiometric compounds.

Summary and Outcomes

The present PhD research project determined the effect of chromium on a range of properties of Cr-doped TiO_2, including electronic structure, segregation-induced surface vs. bulk composition, defect disorder and the light-induced photocatalytic activity in water oxidation. The specific project outcomes include:

1. Determination of the effect of chromium on the bandgap of TiO_2 and the mid-gap energy levels. It is shown that:
   1.1. Chromium incorporation into the TiO_2 lattice results in reduction of the bandgap from 3 eV for pure TiO_2 to 1.4 eV for Cr-doped TiO_2 (1.365 at% Cr).
   1.2. The effect of chromium on bandgap reduction is profoundly influenced by the applied surface processing procedure, such as polishing and subsequent annealing.
2. Determination of chromium segregation in Cr-doped TiO_2. It is shown that:
   2.1. Imposition of high oxygen activity during annealing results in strong chromium segregation.

2.2. The effect of oxygen activity on segregation is markedly larger for single crystals than for polycrystalline specimens.

2.3. Annealing the single crystal of Cr-doped TiO_2 in strongly reducing conditions results in depletion of the surface layer in chromium.

2.4. Annealing of Cr-doped TiO_2 in the gas phase of controlled oxygen activity results in a change of the valence of segregated chromium species. Annealing of Cr-doped TiO_2 in reducing conditions leads to the formation of predominantly tri-valent chromium species. The increase of oxygen activity results in gradual transition from tri-valent species to the mixture of both tri- and hexavalent species of comparable content.

3. Determination of photocatalytic activity tested by oxidation of MB.

3.1. The incorporation of chromium up to 0.04 at% results in an increase of photocatalytic activity of Cr-doped TiO_2 annealed in oxidizing conditions. The effect is considered in terms of chromium incorporation mechanism leading to the formation of anodic surface sites (titanium vacancies).

3.2. The incorporation of chromium above 0.04 at% in oxidizing conditions results in reduced photocatalytic activity, which is considered in terms of the associations of titanium vacancies leading to their weaker activity as acceptors of electrons.

3.3. Annealing of Cr-doped TiO_2 in strongly reducing conditions results in a decrease of photocatalytic activity in the entire range of compositions. This effect is considered in terms of the substitutional mechanism of chromium incorporation leading to the formation of oxygen vacancies that are required for charge compensation.

3.4. The established effect of oxygen activity on photocatalytic activity for pure and Cr-doped TiO_2 indicates that the performance assumes minimum at the n-p transition point that corresponds to minimum of charge transport (see section 2.1.3). This effect indicates that charge transfer related to water oxidation is blocked when the concentration of electronic charge carriers is below a critical level.

3.5. The data of the photocatalytic activity of the electrochemical couples indicate that coupling of TiO_2 specimens of different Fermi level results in either deteriorative

or enhanced performance. The result is determined by the KPPs of coupled structures.

4. This project has derived a theoretical model representing the effect of both intrinsic and extrinsic defects (chromium) on the reactivity mechanism between the surface of Cr-doped TiO_2 and water. The model is based on the following assumptions:
   4.1. The oxidation of water molecules takes place mainly at titanium vacancies acting as the most active anodic sites. The oxidation leads to the formation of hydroxyl radicals and protons. These radicals are the most active species leading to oxidation of organic species in water, such as microbial species or MB. The ultimate effect of the anodic reaction is the transfer of electrons from the adsorbed molecule to the surface of TiO_2.
   4.2. Charge neutrality requires that oxygen dissolved in water is reduced to superoxide species. The active surface cathodic sites for the reduction reaction are the chromium ions located in interstitial sites and the associated tri-valent titanium ions. The superoxide species are involved in subsequent reactions leading to the formation of hydrogen peroxide. The latter also leads to oxidation of organic species in water.
   4.3. The data obtained in this project indicate that chromium exhibits a dual effect on photocatalytic activity of TiO_2. The most spectacular effect is that the incorporation of chromium results in a substantial increase of photocatalytic activity up to 0.04 at% Cr. This effect is surprising since chromium at this concentration level leads to an insignificant change of the bandgap. Therefore, these results can be considered as the strong experimental evidence indicating that bandgap reduction is not the critical KPP. Instead, the KPP that has a critical impact on performance of Cr-doped TiO_2 is the concentration of acceptor-type defects, titanium vacancies. This conclusion is of strategical importance in selection of appropriate research strategy in processing high-performance oxide semiconductors in general and TiO_2-based systems in particular.

Key Findings

1. This project determined the effect of chromium on the bandgap of TiO_2 as well as the mid-gap levels of both the predominant intrinsic defects and chromium. The related

data, which have been determined in well-defined experimental conditions, can be considered as materials-related data that are well reproducible in the specific experimental conditions. The innovative aspects of the research consist of:

1.1. The effect of chemical composition on properties of oxide semiconductors must include lattice oxygen activity and the related defect disorder.

1.2. The effect of chemical composition on the catalytic and photocatalytic activity must be considered in terms of surface vs. bulk properties.

2. The project determined the effect of oxygen activity on:

2.1. The segregation-induced surface layer in chromium for Cr-doped TiO_2 involving 0.04 - 1.365 at% Cr.

2.2. The valence of segregated chromium species within the surface layer.

These data can be considered as materials-related data on the effect of segregation on surface vs. bulk composition of Cr-doped TiO_2.

3. The project determined the effect of oxygen activity in the TiO_2 lattice on defect disorder and the related photocatalytic activity in the oxidation of MB for:

3.1. Pure TiO_2

3.2. Cr-doped TiO_2 (0.04 – 1.365 at% Cr)

These data can be considered as materials-related data with respect to the applied testing organic compound (MB).

4. The project derived a preliminary theoretical model that explains the light-induced reactivity of Cr-doped TiO_2 with water and the related charge transfer.

5. The project established a substantial effect of surface processing, such as polishing, on the band gap.

Refereed Papers Reported by the PhD Candidate during 2015-18

The research activity of the PhD candidate resulted in publication of nine refereed papers published during 2015-18 [3-12]. The 1st pages of these papers are included in the Appendix.

References

[1] Fujishima, A. and K. Honda, *Electrochemical Photolysis of Water at a Semiconductor Electrode.* Nature, 1972. **238**(5358): p. 37-38.

[2] Wilke, K. and H. Breuer, *The influence of transition metal doping on the physical and photocatalytic properties of titania.* Journal of Photochemistry and Photobiology A: Chemistry, 1999. **121**(1): p. 49-53.

[3] Black, D., et al., *Environmentally Clean Energy*, in *Reference Module in Earth Systems and Environmental Sciences*. 2018, Elsevier.

[4] Rahman, K.A., et al., *Toward sustainable energy: photocatalysis of Cr-doped TiO_2: 1. electronic structure.* Ionics, 2018. **24**(2): p. 309-325.

[5] Rahman, K.A., et al., *Towards sustainable energy: photocatalysis of Cr-doped TiO_2. 5. Effect of segregation on surface versus bulk composition.* Ionics, 2018. **24**(4): p. 1211-1219.

[6] Rahman, K.A., et al., *Toward sustainable energy: photocatalysis of Cr-doped TiO_2: 2. effect of defect disorder.* Ionics, 2018. **24**(2): p. 327-341.

[7] Rahman, K.A., et al., *Towards sustainable energy. Photocatalysis of Cr-doped TiO_2: 3. Effect of oxygen activity.* Ionics, 2018. **24**(3): p. 861-872.

[8] Rahman, K.A., et al., *Towards sustainable energy. Photocatalysis of Cr-doped TiO_2: 4. Electrochemical coupling.* Ionics, 2018. **24**(3): p. 873-881.

[9] Nowotny, J., et al., *Effect of Oxygen Activity on the n–p Transition for Pure and Cr-Doped TiO_2.* The Journal of Physical Chemistry C, 2016. **120**(6): p. 3221-3228.

[10] Nowotny, J., et al., *Towards global sustainability: Education on environmentally clean energy technologies.* Renewable and Sustainable Energy Reviews, 2018. **81**(Part 2): p. 2541-2551.

[11] Atanacio, A.J., et al., *Defect Engineering of Photosensitive Oxide Materials. Example of TiO_2 Solid Solutions.* Materials for Sustainable Energy, 2018. **72**.

[12] Bak, T., et al., *Evidence of Low-Dimensional Surface Structures for Oxide Materials. Impact on Energy Conversion.* ACS Applied Energy Materials, 2018.

Chapter 1
Introduction

1.1 Demand for Environmentally Clean Energy Is Rising

The development of the economy requires energy that currently is predominantly produced by using fossil fuels. This, consequently, results in the emission of greenhouse gases and climate changes, which have damaging impact on the environment. Therefore, there is an increasingly urgent need to replace the fossil fuels with environmentally clean renewable energy sources.

In response, the UN established the 10-year research initiative, Future Earth, which aims to develop knowledge to respond and reduce the risk of global environmental changes and support transformations towards global sustainability. The essential part of this initiative is the development of new renewable energy technologies. The present PhD project aims to address the need to develop a new generation of solar materials to inform the development of new technology in solar-to-chemical energy conversion. The novel approach of harvesting sunlight is expected to have an application in water purification using sunlight as the only driving force of water treatment. This, consequently, paves the way in addressing the increasingly urgent need to provide clean drinking water to billions who are still deprived of this basic human right. Alternatively, the material can be used in hydrogen fuel generation from water which is environmentally friendly fuel.

1.2 Access to Clean Drinking Water

The world population is expected to grow by three billion in the next 50 to 75 years. More people mean more demand for safe drinking water. At present, approximately 800 million people globally have limited access to safe drinking water (**Figure 1.1)** [1].

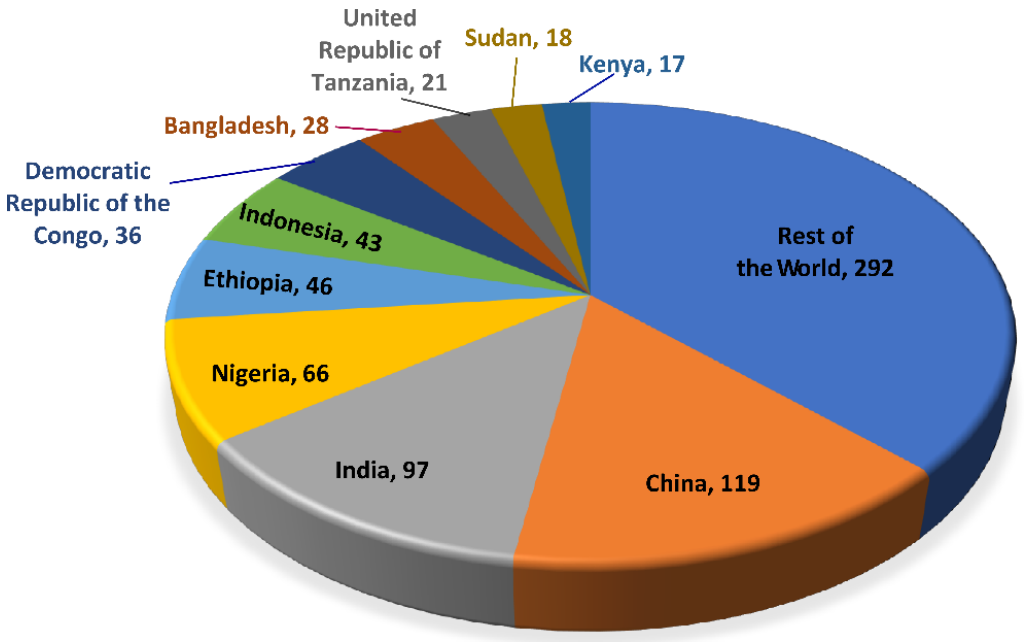

Figure 1.1. *The Earth population (in million - by location) that suffers a lack of access to clean drinking water [1]*

There are many conventional water treatment techniques that are available. These, however, need energy that is expensive. Therefore, intensive research aims at the development of alternative technologies, which are inexpensive and preferably based on the use of renewable energy. The technology of water purification using sunlight, which allows the removal of contaminants from water, such as bacterial species and alternative organic toxic compounds, has huge potential in meeting this need as:

i. The technology based on sunlight is essentially free of charge.
ii. The technology requires low maintenance.
iii. The solar materials are oxide semiconductors, such as TiO_2, that are inexpensive.
iv. The technology is simple and suitable for developing countries.

The following section considers the reasons for selecting TiO_2 as the basic compound for the formations of solid solutions used as a standard system for considering the effect of defect disorder on photocatalytic performance.

1.3 Rationale for Selecting of Titanium Dioxide

The pioneering experiment by Fujishima and Honda [2] attested that TiO_2 may be used for water oxidation using sunlight as the only driving force of the process. Since then, intensive research has aimed at modifying TiO_2 properties in order to increase the solar-to-chemical energy conversion. The most commonly applied procedures are based on the incorporation of a range of ions into the TiO_2 lattice, leading to the formation of donors and acceptors. The main advantage of TiO_2 for water oxidation is that this oxide material is highly resistant to corrosion and photo-corrosion when immersed in water.

The aim of this research is to increase understandings of the effect of point defects in the photocatalytic performance of TiO_2. The ultimate aim is to develop defect engineering to process high-performance photocatalysts based on oxide semiconductors, such as TiO_2.

The present project, which is part of a PhD research program, is based on Cr-doped TiO_2 as a photocatalyst for water purification. The following sections consider the rationale for selecting chromium as the key lattice components and the applied research strategy to address the scientific and applied problems.

The strong photo-reactivity of TiO_2 makes it a promising material for solar-to-chemical energy conversion in the application of water oxidation, including partial oxidation, that aims at the oxidation of organic compounds in water and total oxidation leading to water splitting [3-11]. The first process can yield reactive agents like hydroxyl radicals (OH^*), which are the most reactive species for the sanitization of water from a large variety of organics, viruses, bacteria, fungi, algae as well as cancer cells. The process of full water oxidation results is a promising approach in the production of solar hydrogen fuel. Some other advantages of TiO_2 are its high chemical stability, non-toxicity and low cost [12].

The main disadvantage of TiO_2 is the large bandgap (3 eV for rutile and 3.2 eV for anatase) leading to low quantum yield. The large bandgap value allows only the use of

UV radiation which is 3-5% of solar energy while visible light holds 45% [12]. Therefore, mainstream research on TiO_2 for solar energy conversion applications aims at lowering the bandgap [13-20]. Another approach consists in forming heterogeneous systems involving TiO_2 and small bandgap semiconductors, such as CdS and WO_3 [21-30].

1.4 Rationale for Selecting Chromium as the Dopant of TiO_2

There are several reasons why chromium is an interesting dopant of TiO_2:

i) According to many reports, chromium results in a substantial reduction of the bandgap of TiO_2 [31-44]. The bandgap of pure TiO_2 is approximately 3 eV. On the other hand, the optical bandgap that allows for maximal solar energy conversion is in the range 1.5 – 2 eV [37]. Therefore, chromium is the ion that allows for processing TiO_2 with optimal light absorption.

ii) Chromium is known to have a tendency to be incorporated into the titanium site of TiO_2 [45, 46]. When trivalent chromium ions are incorporated into four-valent titanium ions, the formed defected site assumes a negative charged compared to the lattice and is singly ionized. Therefore, tri-valent chromium incorporated into the titanium site results in the formation of anodic sites, which are required for water oxidation.

iii) Chromium concentration at the surface of Cr-doped TiO_2 may be tailored by segregation. It has been shown that chromium surface segregation in Cr-doped TiO_2 depends on the annealing conditions, including the temperature, the annealing time and the oxygen activity of the surrounding gas phase [47].

1.5 Research Strategy

The objective of the present research project, which is focused on TiO_2-based semiconductors as a photocatalyst for solar energy conversion, is to understand the photocatalytic performance of Cr-doped TiO_2 and the associated semiconducting properties. It is important to note that addressing this objective requires the recognition of the significance of point defects in explaining both photocatalytic and semiconducting properties of TiO_2. The rationale of this approach is the highly defective structure of TiO_2, which is a nonstoichiometric compound. Therefore, its properties are determined by the

related defect disorder. The defect disorder has an impact on electronic structure and the related ability of the TiO_2-based semiconductors on light absorption and the light-induced reactivity.

It is important to realize that the effect of chromium on properties of TiO_2, including photocatalytic properties, should be considered in terms of the mechanism of chromium incorporation into the host lattice and the related defect disorder, as well as the associated semiconducting properties. Besides chromium, which is the key external dopant, the thesis involves two innovative approaches:

i) *The effect of oxygen activity*. It is shown that oxygen activity is the key parameter in considering defect disorder and the defect-related properties, such as electronic structure and reactivity.

ii) *The effect of segregation*. It is shown that the phenomenon of segregation may be used as the technology in surface processing aims at imposition-controlled surface vs. bulk composition.

The thesis concludes with the theoretical model that explains the light-induced reactivity of Cr-doped TiO_2 with water and the related charge transfer.

1.6 Questions of the Research

The objectives of the presented work can be considered in terms of several questions addressing certain scientific problems. Consequently, the following questions can be formulated:

i) What is the effect of chromium on defect disorder of TiO_2? (Discussed in section 2.1.2)

ii) What is the effect of oxygen activity on defect disorder of Cr-doped TiO_2? (Discussed in section 2.1.3)

iii) What is the effect of chromium on the electronic structure of Cr-doped TiO_2 including band gap and mid-band energy levels? (Discussed in section 3.4.1)

iv) What is the effect of oxygen activity on the electronic structure of Cr-doped TiO_2? (Discussed in section 3.4.2)

v) What is the effect of segregation on the surface composition of Cr-doped TiO_2? (Discussed in section 4.3.1)

vi) What is the effect of oxygen activity on surface segregation of chromium for Cr-doped TiO_2? (Discussed in section 4.3.2)

vii) What is the effect of segregation on interactions between defects within the surface layer? (Discussed in section 4.3.3)

viii) What is the difference in surface segregation of chromium between single crystal and polycrystalline specimens of Cr-doped TiO_2? (Discussed in section 4.3.4)

ix) What is the driving force of chromium segregation in Cr-doped TiO_2? (Discussed in section 4.3.3)

x) What is the effect of segregation-induced enrichment of the surface layer on the formation of low-dimensional surface structures? (Discussed in section 4.3.5)

xi) What is the effect of chromium on photocatalytic activity of TiO_2? (Discussed in section 5.3.3)

xii) What is the effect of oxygen activity on photocatalytic properties of Cr-doped TiO_2? (Discussed in section 5.3.3)

1.7 References

[1] *Safe Drinking Water is Essential*. Available from: https://www.koshland-science-museum.org/water/html/en/Treatment/index.html.

[2] Fujishima, A. and K. Honda, *Electrochemical Photolysis of Water at a Semiconductor Electrode.* Nature, 1972. **238**(5358): p. 37-38.

[3] Fujishima, A., K. Hashimoto, and T. Watanabe, *TiO_2 photocatalysis: fundamentals and applications*. 1999: BKC Incorporated.

[4] Hoffmann, M.R., et al., *Environmental applications of semiconductor photocatalysis.* Chemical Reviews, 1995. **95**(1): p. 69-96.

[5] Linsebigler, A.L., G. Lu, and J.T. Yates Jr, *Photocatalysis on TiO_2 surfaces: principles, mechanisms, and selected results.* Chemical Reviews, 1995. **95**(3): p. 735-758.

[6] Fujishima, A., T.N. Rao, and D.A. Tryk, *Titanium dioxide photocatalysis.* Journal of Photochemistry and Photobiology C: Photochemistry Reviews, 2000. **1**(1): p. 1-21.

[7] Nowotny, J. and T. Bak. *TiO_2-based photosensitive oxide semiconductors for solar hydrogen*. in *SPIE Solar Energy+ Technology*. 2009. International Society for Optics and Photonics.

[8] Antonucci, V., E. Passalacqua, and N. Giordano, *TiO_2-based photoelectrodes in photoelectrochemical cells: Performance and mechanism of O_2 evolution.* International Journal of Hydrogen Energy, 1987. **12**(5): p. 305-313.

[9] Nozik, A.J. and R. Memming, *Physical chemistry of semiconductor-liquid interfaces.* The Journal of Physical Chemistry, 1996. **100**(31): p. 13061-13078.

[10] Heller, A., *Conversion of sunlight into electrical power and photoassisted electrolysis of water in photoelectrochemical cells.* Accounts of Chemical Research, 1981. **14**(5): p. 154-162.

[11] Carp, O., C.L. Huisman, and A. Reller, *Photoinduced reactivity of titanium dioxide.* Progress in Solid State Chemistry, 2004. **32**(1–2): p. 33-177.

[12] Zainullina, V., V. Zhukov, and M. Korotin, *Influence of oxygen nonstoichiometry and doping with 2p-, 3p-, 6p- and 3d-elements on electronic structure, optical properties and photocatalytic activity of rutile and anatase: Ab initio approaches.* Journal of Photochemistry and Photobiology C: Photochemistry Reviews, 2015. **22**: p. 58-83.

[13] Lee, J.S., K.H. You, and C.B. Park, *Highly Photoactive, Low Bandgap TiO_2 Nanoparticles Wrapped by Graphene.* Advanced Materials, 2012. **24**(8): p. 1084-1088.

[14] Asahi, R., et al., *Visible-light photocatalysis in nitrogen-doped titanium oxides.* Science, 2001. **293**(5528): p. 269-271.

[15] Chen, D., et al., *Carbon and Nitrogen Co-doped TiO_2 with Enhanced Visible-Light Photocatalytic Activity.* Industrial & Engineering Chemistry Research, 2007. **46**(9): p. 2741-2746.

[16] Hao, W. and P.L. James, *Effects of dopant states on photoactivity in carbon-doped TiO_2.* Journal of Physics: Condensed Matter, 2005. **17**(21): p. L209.

[17] Nagaveni, K., et al., *Synthesis and structure of nanocrystalline TiO_2 with lower band gap showing high photocatalytic activity.* Langmuir, 2004. **20**(7): p. 2900-2907.

[18] Zhu, W., et al., *Band gap narrowing of titanium oxide semiconductors by noncompensated anion-cation codoping for enhanced visible-light photoactivity.* Physical Review Letters, 2009. **103**(22): p. 226401.

[19] Waterhouse, G.I.N., et al., *Hydrogen production by Tuning the Photonic Band Gap with the Electronic Band Gap of TiO_2.* Scientific Reports, 2013. **3**: p. 2849.

[20] Cong, Y., et al., *Preparation, Photocatalytic Activity, and Mechanism of Nano-TiO_2 Co-Doped with Nitrogen and Iron (III).* The Journal of Physical Chemistry C, 2007. **111**(28): p. 10618-10623.

[21] Bessekhouad, Y., et al., *UV–vis versus visible degradation of Acid Orange II in a coupled CdS/TiO_2 semiconductors suspension.* Journal of Photochemistry and Photobiology A: Chemistry, 2006. **183**(1): p. 218-224.

[22] Zhang, Y.J., et al., *Synthesis of TiO_2 nanotubes coupled with CdS nanoparticles and production of hydrogen by photocatalytic water decomposition.* Materials Letters, 2008. **62**(23): p. 3846-3848.

[23] DohĿeviĿ-MitroviĿ, Z., et al., *WO_3/TiO_2 composite coatings: Structural, optical and photocatalytic properties.* Materials Research Bulletin, 2016. **83**: p. 217-224.

[24] Kim, H.-M., D. Kim, and B. Kim, *Photoinduced hydrophilicity of TiO_2/WO_3 double layer films.* Surface and Coatings Technology, 2015. **271**: p. 18-21.

[25] Miyauchi, M., et al., *A highly hydrophilic thin film under 1 $\mu W/cm^2$ UV illumination.* Advanced Materials, 2000. **12**(24): p. 1923-1927.

[26] Momeni, M.M. and Y. Ghayeb, *Visible light-driven photoelectrochemical water splitting on ZnO–TiO_2 heterogeneous nanotube photoanodes.* Journal of Applied Electrochemistry, 2015. **45**(6): p. 557-566.

[27] Siripala, W., et al., *A Cu_2O/TiO_2 heterojunction thin film cathode for photoelectrocatalysis.* Solar Energy Materials and Solar Cells, 2003. **77**(3): p. 229-237.

[28] Tristão, J.C., et al., *Electronic characterization and photocatalytic properties of CdS/TiO_2 semiconductor composite.* Journal of Photochemistry and Photobiology A: Chemistry, 2006. **181**(2): p. 152-157.

[29] Wu, L., C.Y. Jimmy, and X. Fu, *Characterization and photocatalytic mechanism of nanosized CdS coupled TiO_2 nanocrystals under visible light irradiation.* Journal of Molecular Catalysis A: Chemical, 2006. **244**(1): p. 25-32.

[30] Bessekhouad, Y., D. Robert, and J.V. Weber, *Photocatalytic activity of Cu_2O/TiO_2, Bi_2O_3/TiO_2 and $ZnMn_2O_4/TiO_2$ heterojunctions.* Catalysis Today, 2005. **101**(3–4): p. 315-321.

[31] Kim, R., et al., *Charge and magnetic states of rutile TiO_2 doped with Cr ions.* Journal of Physics: Condensed Matter, 2014. **26**(14): p. 146003.

[32] Hajjaji, A., et al., *Cr-Doped TiO_2 Thin Films Prepared by Means of a Magnetron Co-Sputtering Process: Photocatalytic Application.* American Journal of Analytical Chemistry, 2014. **2014**.

[33] Radecka, M., et al., *Study of the TiO_2–Cr_2O_3 system for photoelectrolytic decomposition of water.* Solid State Ionics, 2003. **157**(1): p. 379-386.

[34] Dholam, R., et al., *Efficient indium tin oxide/Cr-doped-TiO_2 multilayer thin films for H_2 production by photocatalytic water-splitting.* International Journal of Hydrogen Energy, 2010. **35**(18): p. 9581-9590.

[35] Diaz-Uribe, C., W. Vallejo, and W. Ramos, *Methylene blue photocatalytic mineralization under visible irradiation on TiO_2 thin films doped with chromium.* Applied Surface Science, 2014. **319**: p. 121-127.

[36] Mardare, D., et al., *Chromium-doped titanium oxide thin films.* Materials Science and Engineering: B, 2005. **118**(1): p. 187-191.

[37] Wilke, K. and H. Breuer, *The influence of transition metal doping on the physical and photocatalytic properties of titania.* Journal of Photochemistry and Photobiology A: Chemistry, 1999. **121**(1): p. 49-53.

[38] López, R., R. Gómez, and S. Oros-Ruiz, *Photophysical and photocatalytic properties of TiO_2-Cr sol–gel prepared semiconductors.* Catalysis Today, 2011. **166**(1): p. 159-165.

[39] Jaimy, K.B., et al., *An aqueous sol–gel synthesis of chromium (III) doped mesoporous titanium dioxide for visible light photocatalysis.* Materials Research Bulletin, 2011. **46**(6): p. 914-921.

[40] Choudhury, B. and A. Choudhury, *Dopant induced changes in structural and optical properties of Cr^{3+} doped TiO_2 nanoparticles.* Materials Chemistry and Physics, 2012. **132**(2): p. 1112-1118.

[41] Michalow, K.A., et al., *Flame-made visible light active TiO_2:Cr photocatalysts: Correlation between structural, optical and photocatalytic properties.* Catalysis Today, 2013. **209**: p. 47-53.

[42] Zhang, S., et al., *Synthesis, characterization of Cr-doped TiO_2 nanotubes with high photocatalytic activity.* Journal of Nanoparticle Research, 2008. **10**(5): p. 871-875.

[43] Gong, J., et al., *A simple electrochemical oxidation method to prepare highly ordered Cr-doped titania nanotube arrays with promoted photoelectrochemical property.* Electrochimica Acta, 2012. **68**: p. 178-183.

[44] Momeni, M.M. and Y. Ghayeb, *Photoelectrochemical water splitting on chromium-doped titanium dioxide nanotube photoanodes prepared by single-step anodizing.* Journal of Alloys and Compounds, 2015. **637**: p. 393-400.

[45] Bechstein, R., et al., *Evidence for vacancy creation by chromium doping of rutile titanium dioxide (110).* The Journal of Physical Chemistry C, 2009. **113**(8): p. 3277-3280.

[46] Sasaki, J., N. Peterson, and K. Hoshino, *Tracer impurity diffusion in single-crystal rutile (TiO_{2-x}).* Journal of Physics and Chemistry of Solids, 1985. **46**(11): p. 1267-1283.

[47] Jayamaha, U., et al., *Effect of oxygen activity on chromium segregation in Cr-doped TiO_2 single crystal.* Ionics, 2015. **21**(3): p. 785-790.

Chapter 2
Basic Terms, Relationships, and Concepts

This chapter first defines the basic terms and relationships on defect chemistry and the electronic structure of TiO_2 and its solid solutions. The chapter then considers the basic concepts on the photocatalysis of TiO_2-based semiconductors and segregation in oxide materials, including TiO_2-based solid solutions, as well as the formation and photo-catalytically active electrochemical couples. This chapter also summarizes the processing of the studied specimens.

2.1 Defect Chemistry

The structure of crystals is not perfect as crystalline solids involve a range of structural imperfections (defects). The most common structural defects include point defects, linear defects and planar defects [1]. The present thesis focuses on the point defects, which are thermodynamically reversible. This section considers the basic relationships of defect chemistry in application to TiO_2 and Cr-doped TiO_2.

2.1.1 Pure TiO_2

The properties of nonstoichiometric oxides, such as TiO_2, are closely related to semiconducting properties and the associated defect disorder. The defect disorder of TiO_2 involves a variety of ionic point defects, such as:

- Oxygen vacancies
- Titanium interstitials
- Titanium vacancies

Moreover, TiO_2 involves both types of electronic defects: electrons and electron holes, which are formed by the ionization of ionic defects.

The ionic defects exhibit different degrees of ionization. The defect disorder of TiO_2 including fully ionized defects, as well as electronic defects located on the lattice sites, is represented schematically in **Figure 2.1**:

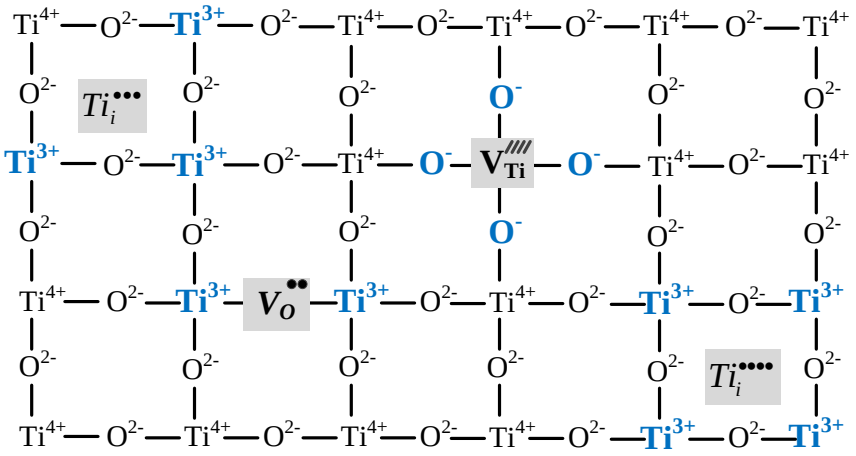

Figure 2.1. *Schematic representation of intrinsic defects in the TiO_2 lattice [2]. The defects are represented according to the Kröger-Vink notation [3].*

In **Figure 2.1** the electrons are located on the titanium lattice sites, leading to the formation of trivalent ions, Ti^{3+}. On the other hand, electron holes are located on oxygen lattice sites leading to the formation of single ionized oxygen ions, O^-. The defect reactions leading to the formation/removal of defects are shown in **Table 2.1** [2].

Table 2.1. *Basic defect equilibria for pure TiO_2 and the notation of defects.*

Intrinsic Defect Equilibria		Kröger-Vink notation	Description
$O_O^x \leftrightarrow V_O^{\bullet\bullet} + 2e' + \frac{1}{2}O_2$	(2.1)	O_O^x	O^{2-} ion in the oxygen lattice site
		$V_O^{\bullet\bullet}$	Fully ionized oxygen vacancy
$2O_O^x + Ti_{Ti}^x \leftrightarrow Ti_i^{\bullet\bullet\bullet} + 3e' + O_2$	(2.2)	Ti_{Ti}^x	Ti^{4+} ion in titanium lattice site
		$Ti_i^{\bullet\bullet\bullet}$	Ti^{3+} ion in the interstitial site
$2O_O^x + Ti_{Ti}^x \leftrightarrow Ti_i^{\bullet\bullet\bullet\bullet} + 4e' + O_2$	(2.3)	$Ti_i^{\bullet\bullet\bullet\bullet}$	Ti^{4+} ion in the interstitial site
$O_2 \leftrightarrow 2O_O^x + V_{Ti}^{\prime\prime\prime\prime} + 4h^{\bullet}$	(2.4)	$V_{Ti}^{\prime\prime\prime\prime}$	Fully ionized titanium vacancy
$nil \leftrightarrow e' + h^{\bullet}$	(2.5)	e'	Quasi-free electron located on the Ti^{3+} ion in the titanium lattice site
		$h^{\bullet}$	Quasi-free electron-hole located on the O^- ion in the oxygen lattice site

As seen, the equilibria (**2.1**) - (**2.4**) in **Table 2.1** involve oxygen as a product or reactant species. Therefore, oxygen activity is involved in the related equilibrium constants, which are outlined in **Table 2.2**, along with the associated charge neutrality conditions [2, 4].

Table 2.2. *Equilibrium constants, charge neutrality conditions and the associated enthalpy and entropy terms related to Equilibria (2.1.) – (2.5) in* ***Table 2.1 (****n and p denote the concentration of electrons and electron holes, respectively, ΔH° and ΔS° denote the enthalpy and entropy terms, respectively, T is absolute temperature, R is gas constant).*

	Equilibrium constant	Charge neutrality	ΔH° [kJ/mol]	ΔS° [J/(mol.K)]
1	$K_1 = [V_O^{\bullet\bullet}]n^2p(O_2)^{1/2}$	$n = 2[V_O^{\bullet\bullet}]$	493.1	106.5
2	$K_2 = [Ti_i^{\bullet\bullet\bullet}]n^3p(O_2)$	$n = 3[T_i^{\bullet\bullet\bullet}]$	879.2	190.8
3	$K_3 = [Ti_i^{\bullet\bullet\bullet\bullet}]n^4p(O_2)$	$n = 4[T_i^{\bullet\bullet\bullet\bullet}]$	1025.8	238.3
4	$K_4 = [V_{Ti}^{\prime\prime\prime\prime}]p^4p(O_2)^{-1}$	$p = 4[V_{Ti}^{\prime\prime\prime\prime}]$	354.5	-202.1
5	$K_i = np$	$n = p$	222.1	44.6
	$\ln K = [(\Delta S^o)/R] - [(\Delta H^o)/RT]$			

2.1.2 Chromium-doped TiO_2

Chromium may be incorporated into the TiO_2 lattice by several mechanisms entering different lattice sites (titanium sites and interstitial sites). Chromium in the TiO_2

lattice exhibits different degree of ionization. The mechanism depends on a range of factors, such as:

(i) Concentration of chromium

(ii) Temperature

(iii) Oxygen activity in the surrounding gas phase

(iv) Distance from the surface

The most commonly considered mechanism consists in the incorporation of trivalent chromium ions into titanium sites of TiO_2 leading to the formation of oxygen vacancies [5]:

$$Cr_2O_3 \leftrightarrow 2Cr'_{Ti} + V_O^{\bullet\bullet} + 3O_O^x \tag{2.6}$$

This reaction results in a defect disorder that is governed by the ionic charge compensation:

$$[Cr'_{Ti}] = 2[V_O^{\bullet\bullet}] \tag{2.7}$$

where the square brackets denote the concentration of species inside the brackets.

The incorporation of trivalent chromium in strongly oxidizing conditions may be represented by the following mechanism:

$$Cr_2O_3 + \frac{1}{2}O_2 \leftrightarrow 2Cr'_{Ti} + 2h^{\bullet} + 4O_O^x \tag{2.8}$$

In this case, the defect disorder is governed by electronic charge neutrality:

$$p = [Cr'_{Ti}] \tag{2.9}$$

where p is the concentration of electron holes. Alternative mechanisms of tri-valent chromium incorporation may be represented by the following respective reactions:

$$\frac{1}{2}O_2 + Cr_2O_3 \leftrightarrow 2Cr_i^{\bullet\bullet\bullet} + 2V''''_{Ti} + 2h^{\bullet} + 4O_O^x \tag{2.10}$$

$$2Cr_2O_3 \leftrightarrow 4Cr_i^{\bullet\bullet\bullet} + 3V''''_{Ti} + 6O_O^x \tag{2.11}$$

$$Cr_2O_3 \leftrightarrow 2Cr_i^{\bullet\bullet\bullet} + 6e' + \frac{3}{2}O_2 \tag{2.12}$$

These reactions are governed by the following charge compensations, respectively:

$$p + 3[Cr_i^{\bullet\bullet\bullet}] = 4[V''''_{Ti}] \tag{2.13}$$

$$3[Cr_i^{\bullet\bullet\bullet}] = 4[V_{Ti}^{''''}] \tag{2.14}$$

$$n = 3[Cr_i^{\bullet\bullet\bullet}] \tag{2.15}$$

The incorporation of divalent chromium into TiO_2 may be considered in terms of the following mechanisms:

$$\frac{1}{2}O_2 + CrO \leftrightarrow Cr_{Ti}'' + 2h^{\bullet} + 2O_O^x \tag{2.16}$$

$$CrO + \frac{1}{2}O_2 \leftrightarrow Cr_i^{\bullet\bullet} + V_{Ti}^{''''} + 2h^{\bullet} + 2O_O^x \tag{2.17}$$

These equilibria are governed by the respective charge neutrality conditions:

$$p = 2[Cr_{Ti}''] \tag{2.18}$$

$$p + 2[Cr_i^{\bullet\bullet}] = 4[V_{Ti}^{''''}] \tag{2.19}$$

The incorporation of hexavalent chromium ions may be represented by the following respective reactions:

$$2CrO_3 \leftrightarrow 2Cr_{Ti}^{\bullet\bullet} + V_{Ti}^{''''} + 6O_O^x \tag{2.20}$$

$$\frac{1}{2}O_2 + CrO_3 \leftrightarrow Cr_i^{\bullet\bullet\bullet\bullet\bullet\bullet} + 2V_{Ti}^{''''} + 2h^{\bullet} + 4O_o^x \tag{2.21}$$

$$CrO_3 \leftrightarrow Cr_i^{\bullet\bullet\bullet\bullet\bullet\bullet} + 6e' + \frac{3}{2}O_2 \tag{2.22}$$

These are governed by the following respective charge neutralities:

$$[Cr_{Ti}^{\bullet\bullet}] = 2[V_{Ti}^{''''}] \tag{2.23}$$

$$p + 6[Cr_i^{\bullet\bullet\bullet\bullet\bullet\bullet}] = 4[V_{Ti}^{''''}] \tag{2.24}$$

$$n = 6[Cr_i^{\bullet\bullet\bullet\bullet\bullet\bullet}] \tag{2.25}$$

Carpentier et al. [6] claim that chromium is incorporated into TiO_2 according to the mechanism leading to the formation of tetra-valent interstitial titanium ions:

$$2Cr_2O_3 + 2O_o^x + Ti_{Ti}^x \leftrightarrow 4Cr_{Ti}' + Ti_i^{\bullet\bullet\bullet\bullet} + 8O_o^x \tag{2.26}$$

The common approach in assessing the effect of doping on defect disorder is based on the experimental determination of the effect of oxygen activity on the concentration of electronic defects and the subsequent verification of the obtained data against the theoretical models. For example, doping of TiO_2 with chromium, according to the reaction

expressed by **equation (2.6)** and the charge neutrality condition **(2.7)**, results in the following relation between the concentration of electrons and oxygen activity:

$$n = \left(\frac{2K_1}{[Cr_{Ti}^{'}]} \right)^{1/2} p(O_2)^{-1/4} \tag{2.27}$$

where K_1 is the equilibrium constant of the formation of oxygen vacancies. The concentration of electrons may be determined using the measurements of the electrical conductivity:

$$\sigma = e\mu_n n \tag{2.28}$$

where e is elementary charge and μ_n is the mobility of electron holes. Assuming that the mobility term is independent of oxygen activity, the electrical conductivity measurements may be used for the verification of the model expressed by **equation (2.27)**.

It is important to note at this stage that the surface mechanism of chromium incorporation may differ entirely from that of the bulk phase because of the excess of surface energy [7, 8].

In considering the different mechanism of chromium incorporation, leading to either oxygen vacancies or titanium vacancies, their concentrations must always satisfy the Schottky-type defect disorder:

$$K_S = [V_{Ti}^{''''}][V_O^{\bullet\bullet}] \tag{2.29}$$

Where K_S is the equilibrium constant of the Schottky-type defect disorder [9]:

$$nil \leftrightarrow V_{Ti}^{''''} + 2V_O^{\bullet\bullet} \tag{2.30}$$

2.1.3 Effect of Oxygen Activity on Defect Disorder of TiO_2 vs. Cr-doped TiO_2

The effect of oxygen activity on the defect disorder of pure and Cr-doped TiO_2 is shown in the upper part of **Figure 2.2 (a** and **b)**. **Figure 2.2b** is derived assuming that chromium in the titanium site is a singly ionized acceptor, $Cr_{Ti}^{'}$.

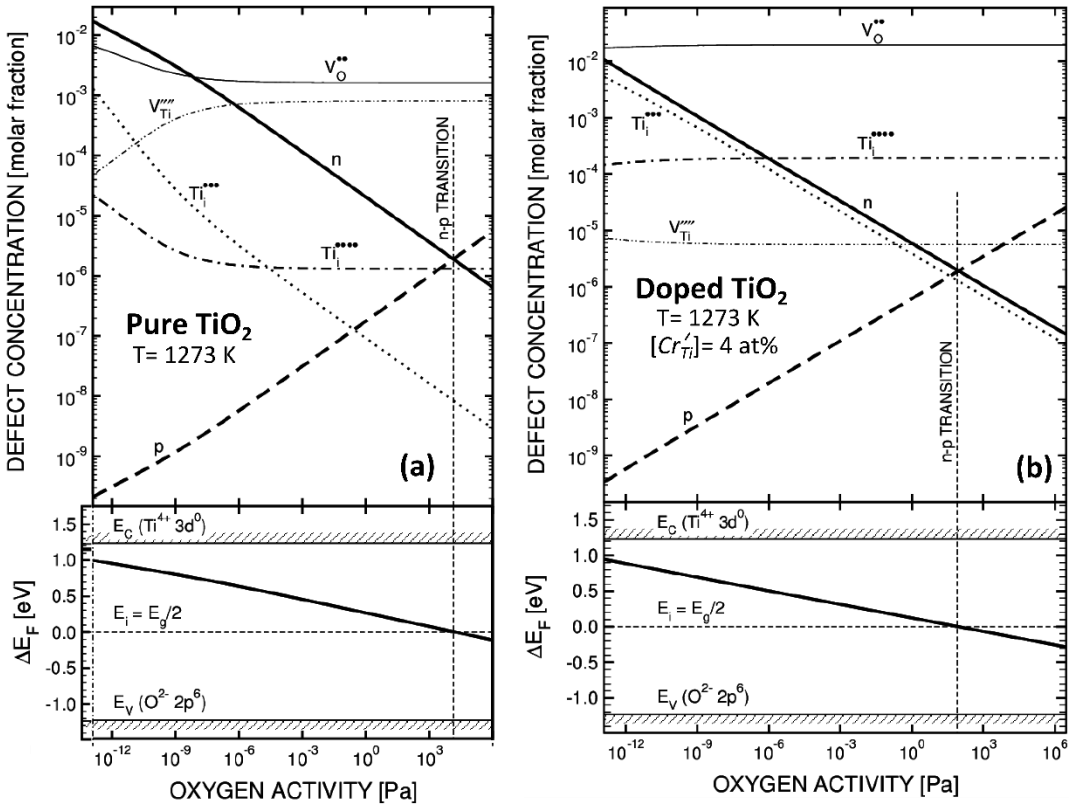

Figure 2.2. *Isothermal plots of the effect of oxygen activity on the concentration of intrinsic defects for pure TiO_2 at 1273 K (a, upper part) as well as acceptor doped TiO_2 (b, upper part) and the relative changes of the Fermi level (a & b, lower part). The symbols n and p denote the concentration of electrons and electron holes, respectively (the remaining symbols are according to the Kröger-Vink notation represented in* ***Table 2.1*** *[3]). The effect of chromium on properties of TiO_2 is reported in ref [10-12], respectively.*

As seen, the incorporation of chromium results in a shift of the n-p transition point towards the lower $p(O_2)$, as well as a change in the $p(O_2)$ dependence of the concentration of all intrinsic defects compared to pure TiO_2. The n-p transition point, marked by the intersection of the n- and p-lines, is around $p(O_2) = 10^4$ Pa for pure TiO_2 while it moves to $p(O_2) = 80$ Pa for Cr-doped TiO_2. The increase of $p(O_2)$ above this value leads to the formation of p-type properties. The observed n-p transition point is associated with a minimum of charge transport. Therefore, the n-p transition point can be modified by imposition of controlled concentration of both the extrinsic defects, such as chromium and the intrinsic defects by a change in oxygen activity, $p(O_2)$.

2.2 Electronic Structure

The effect of light on properties of semiconductors depends mainly on its bandgap, which is the difference of energy between the top of the valence band and the bottom of the conduction band. The valence band of TiO_2 is formed by filled 2p orbitals of two-valent oxygen ions and the conduction band is formed by empty 3d states of four-valent Ti ions [2, 13]. The bandgap of TiO_2 is 3.2 eV for anatase and 3 eV for rutile [13].

The intrinsic electronic transitions between the valence band (VB) and the conduction band (CB), induced by light or temperature, can be considered in terms of either direct or indirect transition, as represented schematically in **Figure 2.3**.

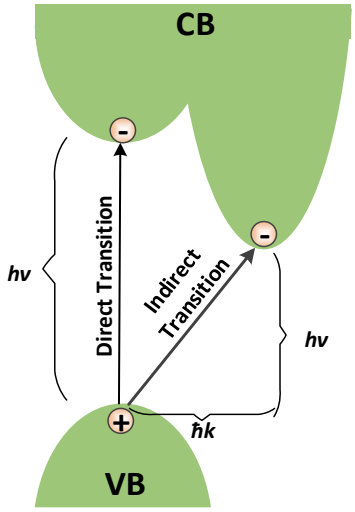

Figure 2.3. *Schematic representation of the optical transitions in TiO_2.*

As seen, during the direct transition the energy of the electron is changed only by the value of photon energy, *hv*. During the indirect transition, the electron's momentum is changed as well, by the value of *ħk*, where *k* is the wave vector of emitted/absorbed phonon and $\hbar = h/2\pi$.

One of the important parameters in electronic structure is Fermi level, which is the parameter is the Fermi-Dirac function *F(E)* that is given as:

$$F(E) = \frac{1}{1 + \exp(\frac{E - E_F}{kT})} \tag{2.31}$$

The position of the Fermi in semiconductors like TiO_2 depends on the concentration of donor and acceptor levels and their ionization degree.

2.3 Photocatalysis

This section considers the basic concepts of photocatalysis on the light-induced partial oxidation of water. It is shown the TiO_2, which exhibits a strong chemical stability in water, reacts with both light and water.

This research project is focused on photocatalytic partial water oxidation using Cr-doped TiO_2 as well as the electrochemical couples formed of TiO_2 of different Fermi levels. The photocatalytic performance is determined by the light-induced reactivity of the semiconducting photocatalyst. The primary reaction is the light-induced ionization over the bandgap, which can be represented by:

$$TiO_2 + hv\ (photon\ energy) \leftrightarrow h^{\bullet} + e' \tag{2.32}$$

The light-induced electronic charge carriers, which are formed at the depth of the light penetration distance beneath the surface, are subsequently transported to the surface leading to the formation of both anodic and cathodic reaction sites. The primary reaction of water oxidation is the anodic reaction between water molecules and electron-hole leading to the formation of hydroxyl radicals and protons:

$$H_2O + h^{\bullet} \leftrightarrow HO^{*} + H^{+} \tag{2.33}$$

The charge neutrality, which requires that the excess of electrons in the semiconductor and the driving force of the cathodic reaction between the electrons and oxygen dissolved in water. The reaction, leading to the formation of superoxide species, can be represented by the following equilibrium:

$$O_2 + e' \leftrightarrow O_2^{*-} \tag{2.34}$$

The photocatalytic effect on semiconductors is commonly considered by a schematic representation of the light-induced ionization over the bandgap leading to the formation of anodic and cathodic sites, as represented schematically in **Figure 2.4**.

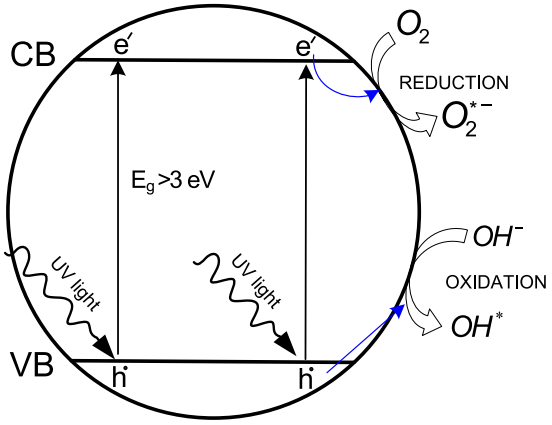

Figure 2.4. *Schematic representation of the light-induced reaction mechanism for Cr-doped TiO_2 photocatalyst.*

As seen, the schematic drawing represents the light-induced bandgap ionization, leading to the formation of electrons and electron holes, which are involved in the reactions (2.33) and (2.34), respectively. In addition to these two primary reactions, there are several subsequent reactions, which lead to the formation of alternative species:

$$O_2^{*-} + 2H^+ + e' \leftrightarrow H_2O_2 \quad (2.35)$$

$$H_2O + 2H^+ \leftrightarrow H_2O_2 \quad (2.36)$$

$$H_2O_2 + e' \leftrightarrow OH^* + OH^- \quad (2.37)$$

$$H_2O_2 + H^+ + e' \leftrightarrow OH^* + H_2O \quad (2.38)$$

2.3.1 Anticipated Effect of Chromium on Photocatalytic Properties of TiO_2

The effect of chromium on the photocatalytic properties of TiO_2 has been mainly considered in terms of the beneficial effect of chromium on bandgap reduction and the resulting increase of light absorption. Therefore, the primary effect of chromium on the properties of TiO_2 is the bandgap, however, its effect on photocatalytic performance is not obvious for the following reasons:

1) The bandgap is one of several performance-related properties which should be taken into account, such as, (i) the concentration of surface active sites, (ii) Fermi level and (iii) charge transport, in addition to (iv) the bandgap. So far, little is known about the effect of (i) - (iii) on performance.

2) The effect of chromium depends on the mechanism of incorporation into the surface layer, which is entirely different than that in the bulk phase. This effect, which impacts the oxidation state of chromium, is unknown.
3) The effect of chromium is profoundly influenced by the resulting changes of the Fermi level at the outermost surface layer. This effect is unknown as well.
4) The effect of chromium on reactivity depends on surface chromium concentration that is determined by segregation. So far, little is known in this matter.

This thesis aims to address the effects related to (1) – (4).

2.3.2 Formation and Performance of Electrochemical Coupled TiO_2

The formation of heterogeneous systems aims to i) imposition of the properties that are not available for isolated system components and ii) understand the impact of coupling on the performance. The strategy for this approach consists in deposing small islets of alternative phases on the surface of the basic photocatalyst, such as TiO_2, that act as functional co-catalysts. The alternative phases involve either small particles of noble metals or compounds, such as Au [14], Pt [15], WO_3 [16], CdS [17], which are deposited on the surface of TiO_2. The rationale behind the deposition of such phases is that their Fermi level is different from that of the basic TiO_2. As a consequence, the deposited islets result in a charge transfer leading to the formation of either anodic or cathodic sites. The main innovative aspect of this approach is the formation of the electrochemical couples formed of TiO_2 of different Fermi levels. The advantage of this approach is that the Fermi levels of TiO_2-based components may be imposed in a controlled manner using the procedure discussed in **chapter 5**.

The performance concept of electrochemical couples forming heterogeneous photocatalytic systems for light-induced water oxidation is represented in **Figure 2.5**.

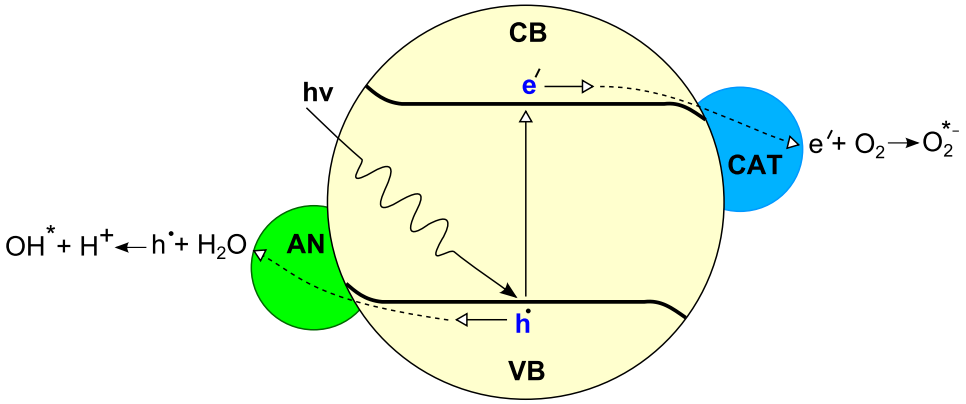

Figure 2.5. *Schematic representation of the charge transfer within a photocatalytic system involving both anodic- and cathodic-type co-catalysts, denoted by AN and CAT, respectively, and the related reactions.*

As seen, the chain involves the basic semiconducting catalysts, such as TiO_2, and the co-catalysts, termed as *AN* and *CAT*, acting as anodic and cathodic sites respectively. The related reactions for partial water oxidation are represented by equations (**2.33**) and (**2.34**) respectively. The functional aim of co-catalysts AN and CAT is to enhance the supply of the electronic charge carriers required for the reactions (**2.33**) and (**2.34**) respectively.

The formation of the electrochemical couple consisting of TiO_2-based semiconductors of different Fermi level is represented in **Figure 2.6**. Both n-type TiO_2 and p-type TiO_2 are shown in **Figure 2.6**, including (a) the component in isolation, and (b) the components involved in galvanic contact, where Φ_1 and Φ_2 are reflective of work functions of the couple components and E_F is the Fermi level.

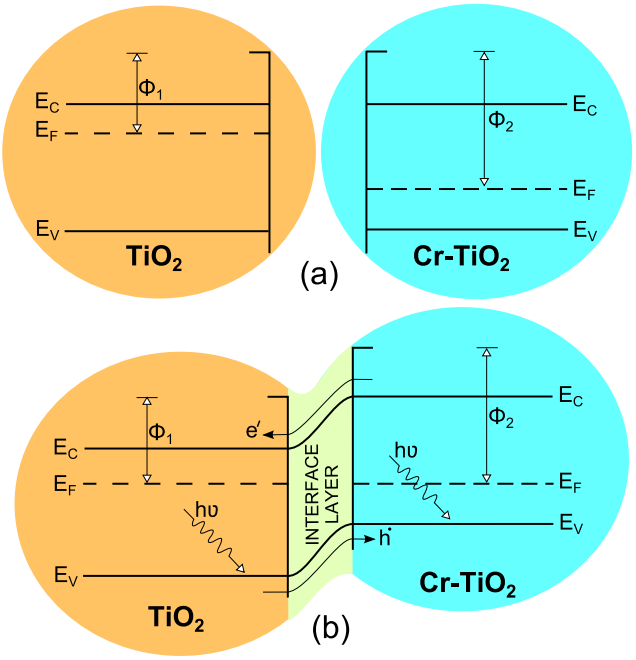

Figure 2.6. *Schematic representation of n-type pure TiO_2 and p-type Cr-doped TiO_2 (a) before galvanic contact and (b) after the interface layer is formed.*

The charge transfer takes place when the couple components enter into galvanic contact. This leads to the diffusion of electrons from p-type to n-type component and the diffusion of electron holes in the opposite directions. The diffusion results in the formation of an electrical potential barrier that is determined by the difference of the Fermi levels. The resulting electric field is reflective of band bending within the depletion zone. Ultimately there is no net charge transfer across the interphase if the system is in thermal equilibrium. The related electric field is the driving force of charge separation when the system is exposed to light, leading to bandgap ionization. Therefore, the barrier formed across the junction may be considered as an electrochemical pump for the transfer of the light-induced electronic charge carriers in the desired direction.

The deposition of small islets of noble metals, such as gold, platinum, palladium, silver, ruthenium, and iridium, results in a strong enhancement of photocatalytic performance [14, 15, 18-27]. The band model representing the effect of light on the charge transfer across the chain involving the couple formed of metallic islets deposited on the surface of TiO_2, as well as the oxygen species adsorbed on the islet forming a cathodic site, is represented in **Figure 2.7**.

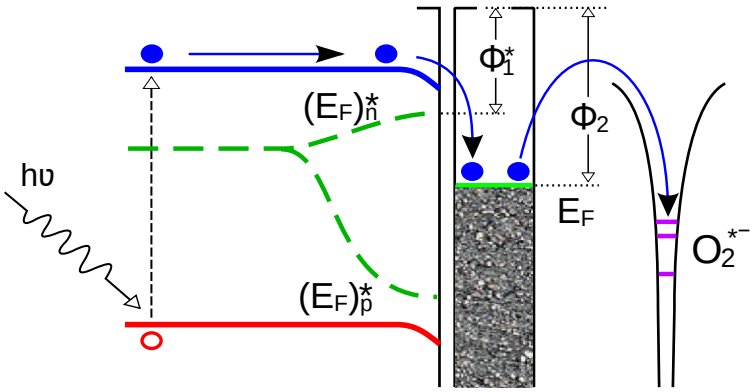

Figure 2.7. *Band model representation of the light-induced charge transfer within the electrochemical system formed of n-type semiconductor and a metallic islet acting as a reduction site (where* Φ_1^* *and* Φ_2 *denote the work function of the semiconductor under light and the metal islet, respectively).*

The driving force for the charge transfer within the system in **Figure 2.7** is the light-induced ionization over the bandgap leading to a split of the Fermi level into the quasi-Fermi level components related to electrons and electron holes [$(E_F)_n^*$ and $(E_F)_n^*$ respectively].

2.3.3 Key Performance-related Properties

It has been shown that the photocatalytic performance of TiO_2-based semiconductors should be considered in terms of a range of defect-related properties, including the bandgap, concentration of surface active sites, Fermi level and charge transport [28].

2.3.3.1 Bandgap (KPP-1)

The key elements of the electronic structure, which influence light absorption, are the bandgap and the energy levels within the bandgap. These may be modified by the imposition of variable oxygen activity and the incorporation of aliovalent ions. The bandgap is the property of semiconductors, which is critical for light absorption. If the bandgap is the critical KPP, one should expect that decreasing the bandgap value results in enhanced photocatalytic performance within the entire range.

2.3.3.2 Concentration of Surface Active Sites (KPP-2)

It has been shown that the reactivity of TiO_2 with water depends on the local property of the reaction site that remains in contact with the adsorbed water molecule. Not all sites are equal. Since water oxidation requires the removal of electrons from water molecules, the most effective surface local active sites for the related charge transfer are the lattice species that tend to accept electrons. If this KPP is the critical property, the effect of chromium on photocatalytic performance should be observed only in the case of the incorporation mechanisms leading to the formation of titanium vacancies.

2.3.3.3 Fermi Level (KPP-3)

The Fermi level is the collective property related to the chemical potential of electrons, which is reflective of the ability of a semiconductor either to accept or donate electrons. The Fermi level of nonstoichiometric compounds is a complex function of the defect disorder and the ionization degree of all defects involved. The reactivity of semiconductors is influenced by the Fermi level, which is the collective factor, and the local factor that depends on the nature and the concentration of surface active sites.

2.3.3.4 Charge Transport (KPP-4)

Photocatalytic performance requires that the light-induced electronic charge carriers are transported from the site(s) of their generation within the light penetration distance beneath the surface, to the surface reaction sites. Therefore, the charge transport has an essential effect on performance. The effect of chromium on charge transport depends on the associated concentration of electronic charge carriers and their mobility.

2.4 Segregation

Surface composition of solids differs from that of the bulk phase as a result of the phenomenon of segregation [29]. So far, little is known about the segregation of metal oxides.

Segregation is a mass transport phenomenon of intrinsic defects from their lattice position to the interfaces under the driving force of free energy minimization (lattice and interfacial) [30]. It has been shown that the dopant in TiO_2 in the bulk phase segregates to

the surface [29, 31]. Consequently, the intendant dopant concentration in the bulk and at the surface changes after the specimen processing, depending on the processing temperature, time and surrounding gas phase. Since the photocatalytic reaction relates to the surface properties, knowledge on the dopant concentration gradient from the surface to the bulk is important [29, 31].

The theory of interfacial segregation first derived for metals and alloys [32]. Awareness is growing that the effect of segregation is essential to correctly understand the catalytic and photocatalytic properties taking place on the surface in ionic solids of nonstoichiometric compounds. The complication in the latter case results in the characterization of surface properties. Certain progress in this area has been achieved by determining the segregation-induced surface concentration of solutes in metal oxides, such as MgO [33], Al_2O_3 [34], ZrO_2 [35], NiO [36] and CoO [37]. The effect of segregation on oxide materials may be predicted in terms of theoretical models based on regular solid solutions of oxides with isovalent cations being used to predict surface segregation [38].

The regular solution approximation may be described by the following expression:

$$\frac{x_2^s}{x_1^s} = \frac{x_2^b}{x_1^b} \exp\left(\frac{-\Delta H_{seg}}{kT}\right) \tag{2.39}$$

where subscripts *s* and *b* are related to the surface and the bulk phase, respectively, and ΔH_{seg} is the enthalpy of segregation. The latter term involves the components related to different driving forces of segregation:

$$\Delta H_{seg} = \Delta H_{\gamma} + \Delta H_{w} + \Delta H_{str} + \Delta H_{el} \tag{2.40}$$

where

a. ΔH_{γ} - the surface energy contribution tends to increase the surface mole fraction of the component of lower surface energy;
b. ΔH_{w} - the binary solution interaction contribution depends on crystallographic orientation;
c. ΔH_{str} is the elastic solute strain energy contribution that is related to the mismatch between the species of solute and solvent;
d. ΔH_{el} is the electrostatic interactions contribution. It has been shown that the component ΔH_{el} has a substantial impact on nonstoichiometric compounds [11, 29].

The certain complication in considering segregation in polycrystalline solids is related to linear defects that are formed by intersections of grain boundaries with the external surface. In this work, it will be shown (in **Chapter 4**) that the effect of grain boundaries on surface segregation of polycrystalline materials is substantial and must be taken into account in considering the segregation-induced surface composition.

2.5 Specimens

2.5.1 Processing

The studied specimens involved pure TiO_2 as well as Cr-doped TiO_2, and included both single crystals and polycrystalline specimens, with controlled oxygen activity in the oxide lattice. The single crystal of Cr-doped TiO_2 was purchased from SurfaceNet, Germany, and annealed in the gas phase of controlled oxygen activity. The polycrystalline specimens of Cr-doped TiO_2 were processed using the sol-gel technique and subsequently also annealed in the gas phase of controlled oxygen activity in order to impose the desired oxygen activity in the oxide lattice. The summary of the applied processing conditions and the characterization techniques of the studied specimens are represented in **Figure 2.8**.

The processing details are reported in the following chapters.

2.5.2 Protocol Representing Processing Procedure Step-by-step

The details of the processing procedure and the capacity of the specific facilities for the characterization of surface properties are represented in **Figures 2.8** and **2.9**. The specimens were characterized by different techniques, such as the surface properties were determined by x-ray photoelectron spectroscopy (XPS) and secondary ion mass spectrometry (SIMS), whereas the bulk compositions were examined by proton induced x-ray emission spectroscopy (PIXE). Moreover, the information related to the surface grain size of the specimen was examined by scanning electron microscope (SEM). Later, the optical and photocatalytic properties were determined using UV-vis-NIR spectrophotometer.

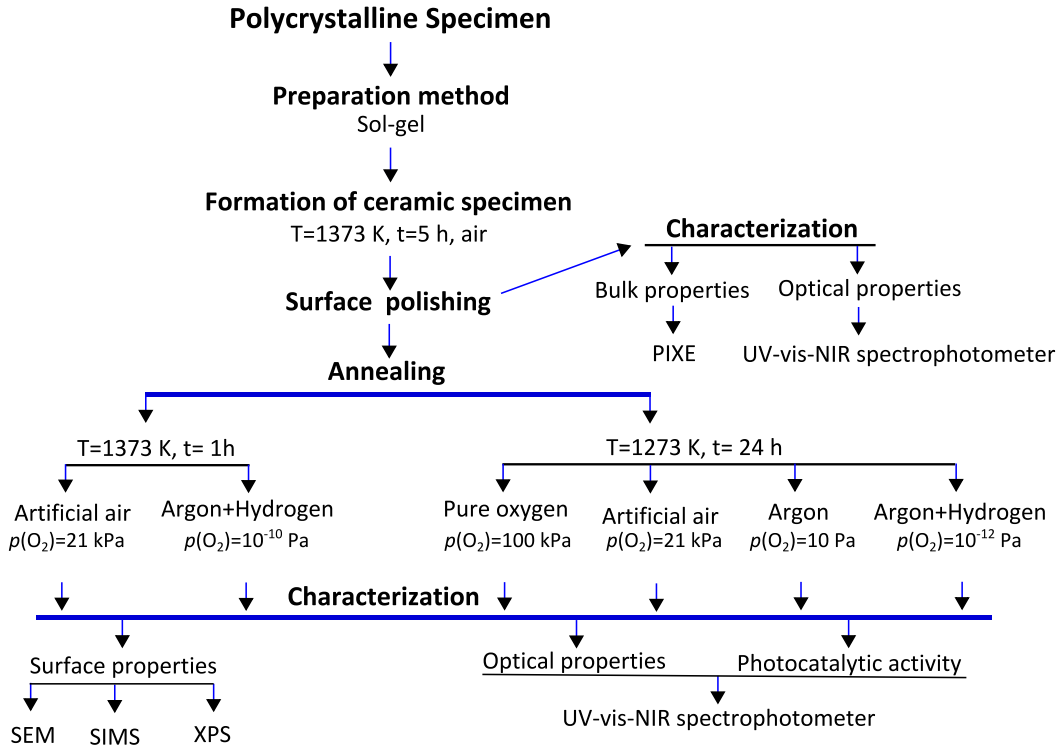

Figure 2.8. *Flowchart representing the summary of the studied specimen's preparation method, processing conditions, and characterization techniques. The notation PIXE, SEM, SIMS, and XPS corresponds to Proton Induced X-ray Emission spectroscopy, scanning electron microscope, Secondary Ion Mass Spectrometry, and X-ray Photoelectron Spectroscopy respectively.*

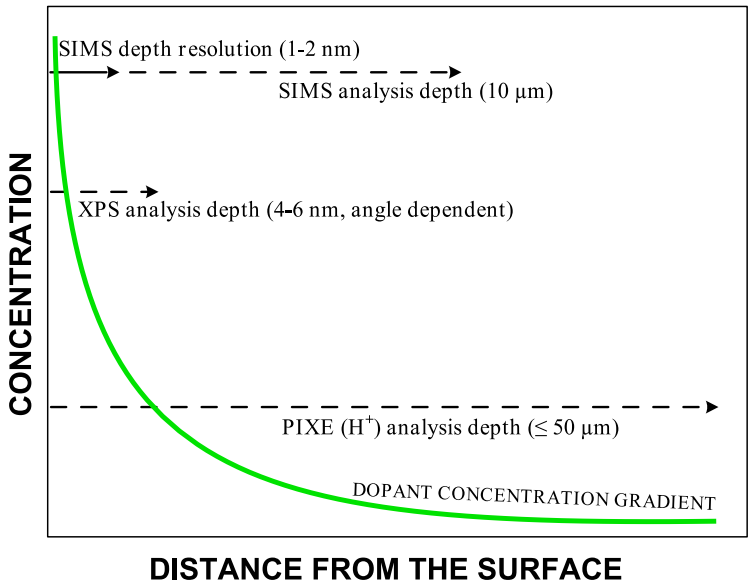

Figure 2.9. *Schematic representation comparing the approximate penetration depth of SIMS, XPS, and PIXE analysis techniques.*

2.6 References

[1] Kofstad, P., *Nonstoichiometry, diffusion, and electrical conductivity in binary metal oxides*. 1972: Wiley-Interscience New York.

[2] Nowotny, J., *Oxide Semiconductors for Solar Energy Conversion: Titanium Dioxide*. 2011: CRC Press.

[3] Kröger, F. and H. Vink, *Relations between the concentrations of imperfections in crystalline solids.* Solid State Physics, 1956. **3**: p. 307-435.

[4] Bak, T., et al., *Defect chemistry and semiconducting properties of titanium dioxide: I. Intrinsic electronic equilibrium ☆.* Journal of Physics and Chemistry of Solids, 2003. **64**(7): p. 1043-1056.

[5] Bechstein, R., et al., *Evidence for vacancy creation by chromium doping of rutile titanium dioxide (110).* The Journal of Physical Chemistry C, 2009. **113**(8): p. 3277-3280.

[6] Carpentier, J.-L., A. Lebrun, and F. Perdu, *Point defects and charge transport in pure and chromium-doped rutile at 1273 K.* Journal of Physics and Chemistry of Solids, 1989. **50**(2): p. 145-151.

[7] Ghosh, A.K., F. Wakim, and R. Addiss Jr, *Photoelectronic processes in rutile.* Physical Review, 1969. **184**(3): p. 979.

[8] Xu, M., et al., *Photocatalytic Activity of Bulk TiO_2 Anatase and Rutile Single Crystals Using Infrared Absorption Spectroscopy.* Physical Review Letters, 2011. **106**(13): p. 138302.

[9] He, J., et al., *Prediction of high-temperature point defect formation in TiO_2 from combined ab initio and thermodynamic calculations.* Acta Materialia, 2007. **55**(13): p. 4325-4337.

[10] Bak, T., et al., *Charge transport in Cr-doped titanium dioxide.* The Journal of Physical Chemistry C, 2008. **112**(18): p. 7255-7262.

[11] Jayamaha, U., et al., *Effect of oxygen activity on chromium segregation in Cr-doped TiO_2 single crystal.* Ionics, 2015. **21**(3): p. 785-790.

[12] Nowotny, J., et al., *Effect of Oxygen Activity on the n–p Transition for Pure and Cr-Doped TiO_2.* The Journal of Physical Chemistry C, 2016. **120**(6): p. 3221-3228.

[13] Zainullina, V., V. Zhukov, and M. Korotin, *Influence of oxygen nonstoichiometry and doping with 2p-, 3p-, 6p- and 3d-elements on electronic structure, optical properties and photocatalytic activity of rutile and anatase: Ab initio approaches.* Journal of Photochemistry and Photobiology C: Photochemistry Reviews, 2015. **22**: p. 58-83.

[14] Li, H., et al., *Mesoporous Au/TiO_2 nanocomposites with enhanced photocatalytic activity.* Journal of the American Chemical Society, 2007. **129**(15): p. 4538-4539.

[15] Wang, X., et al., *A mesoporous Pt/TiO_2 nanoarchitecture with catalytic and photocatalytic functions.* Chemistry-A European Journal, 2005. **11**(10): p. 2997-3004.

[16] Kim, H.-M., D. Kim, and B. Kim, *Photoinduced hydrophilicity of TiO_2/WO_3 double layer films.* Surface and Coatings Technology, 2015. **271**: p. 18-21.

[17] Zhang, Y.J., et al., *Synthesis of TiO_2 nanotubes coupled with CdS nanoparticles and production of hydrogen by photocatalytic water decomposition.* Materials Letters, 2008. **62**(23): p. 3846-3848.

[18] Chandrasekharan, N. and P.V. Kamat, *Improving the photoelectrochemical performance of nanostructured TiO_2 films by adsorption of gold nanoparticles.* The Journal of Physical Chemistry B, 2000. **104**(46): p. 10851-10857.

[19] Subramanian, V., E.E. Wolf, and P.V. Kamat, *Catalysis with TiO_2/gold nanocomposites. Effect of metal particle size on the Fermi level equilibration.* Journal of the American Chemical Society, 2004. **126**(15): p. 4943-4950.

[20] Chen, T., et al., *Mechanistic studies of photocatalytic reaction of methanol for hydrogen production on Pt/TiO_2 by in situ Fourier transform IR and time-resolved IR spectroscopy.* The Journal of Physical Chemistry C, 2007. **111**(22): p. 8005-8014.

[21] Zou, J.-J., et al., *Highly efficient Pt/TiO_2 photocatalyst for hydrogen generation prepared by a cold plasma method.* International Journal of Hydrogen Energy, 2007. **32**(12): p. 1762-1770.

[22] Ranjit, K., T.K. Varadarajan, and B. Viswanathan, *Photocatalytic reduction of nitrite and nitrate ions to ammonia on Ru/TiO_2 catalysts.* Journal of Photochemistry and Photobiology A: Chemistry, 1995. **89**(1): p. 67-68.

[23] Zhang, H. and G. Chen, *Potent antibacterial activities of Ag/TiO_2 nanocomposite powders synthesized by a one-pot sol-gel method.* Environmental Science & Technology, 2009. **43**(8): p. 2905-2910.

[24] Zhong, J.B., et al., *Characterization and photocatalytic property of Pd/TiO_2 with the oxidation of gaseous benzene.* Journal of Hazardous Materials, 2009. **168**(2): p. 1632-1635.

[25] Chen, P., et al., *Characterizations of Ir/TiO_2 catalysts with different Ir contents for selective hydrogenation of crotonaldehyde.* Reaction Kinetics, Mechanisms and Catalysis, 2012. **106**(2): p. 419-434.

[26] Pan, X. and Y.-J. Xu, *Defect-mediated growth of noble-metal (Ag, Pt, and Pd) nanoparticles on TiO_2 with oxygen vacancies for photocatalytic redox reactions under visible light.* The Journal of Physical Chemistry C, 2013. **117**(35): p. 17996-18005.

[27] Wu, G., et al., *H_2 production with low CO selectivity from photocatalytic reforming of glucose on metal/TiO_2 catalysts.* Science in China Series B: Chemistry, 2008. **51**(2): p. 97-100.

[28] Bak, T., et al., *Photocatalytic Properties of TiO_2: Evidence of the Key Role of Surface Active Sites in Water Oxidation.* The Journal of Physical Chemistry A, 2015. **119**(36): p. 9465-9473.

[29] Atanacio, A.J., T. Bak, and J. Nowotny, *Effect of Indium Segregation on the Surface versus Bulk Chemistry for Indium-Doped TiO_2.* ACS Applied Materials & Interfaces, 2012. **4**(12): p. 6626-6634.

[30] Sheppard, L., et al. *Effect of niobium segregation on surface properties of titanium dioxide*. in *SPIE Optics+ Photonics*. 2006. International Society for Optics and Photonics.

[31] Atanacio, A.J., J. Nowotny, and K.E. Prince, *Effect of Oxygen Activity on Surface Composition of In-Doped TiO_2 at Elevated Temperatures.* The Journal of Physical Chemistry C, 2012. **116**(36): p. 19246-19251.

[32] McLean, D. and A. Maradudin, *Grain boundaries in metals*. 1958, AIP.

[33] Cotter, M., et al., *Surface segregation of Ba in MgO.* Surface Science, 1989. **208**(3): p. 267-284.

[34] Marcus, H. and M. Fine, *Grain-Boundary Segregation in MgO-Doped Al_2O_3.* Journal of the American Ceramic Society, 1972. **55**(11): p. 568-570.

[35] Aoki, M., et al., *Solute Segregation and Grain-Boundary Impedance in High-Purity Stabilized Zirconia.* Journal of the American Ceramic Society, 1996. **79**(5): p. 1169-1180.

[36] Adamczyk, Z. and J. Nowotny, *Effect of segregation on near-surface and bulk transport phenomena in ionic crystals.* Journal of Physics and Chemistry of Solids, 1986. **47**(1): p. 11-27.

[37] Haber, J., et al., *Electron spectroscopy in studies of surface segregation of Cr in Cr-doped CoO.* Applications of Surface Science, 1984. **17**(3): p. 324-330.

[38] Wynblatt P, M.R.C., *Surface Segregation in Metal Oxides*, in *Surface and Near-Surface Chemistry of Oxide Materials*, J.N.a.L. Dufour, Editor. 1988, Elsevier: Amsterdam. p. 247-279.

Chapter 3
Electronic Structure

This chapter considers the effect of chromium on the electronic structure of TiO_2-based semiconductors, including the bandgap and mid-gap energy levels. The substantial scatter of the bandgap reported in the literature is considered in terms of the effects related to processing conditions, such as the oxygen activity of the gas phase during annealing and annealing temperature. The experimental part considers the processing conditions of polycrystalline specimens of Cr-doped TiO_2 and its basic characterizations, including bulk composition and the related electronic structure.

3.1 Literature Overview

3.1.1 Effect of Chromium on Electronic Structure

3.1.1.1 Band Model

The semiconducting properties of TiO_2 are profoundly influenced by electronic charge carriers that are formed by ionization of ionic point defects, including intrinsic defects for pure TiO_2 and both intrinsic and extrinsic defects for its solid solutions [1]. The bandgap and the energy levels within the bandgap are the key quantities affecting the semiconducting properties. This section considers the effect of chromium and oxygen activity of the oxide lattice on the electronic structure of TiO_2.

The reported data on the energy levels of the intrinsic ionic defects, as well as chromium incorporated into the titanium site, forming donors and acceptors, are represented in **Figure 3.1** [2].

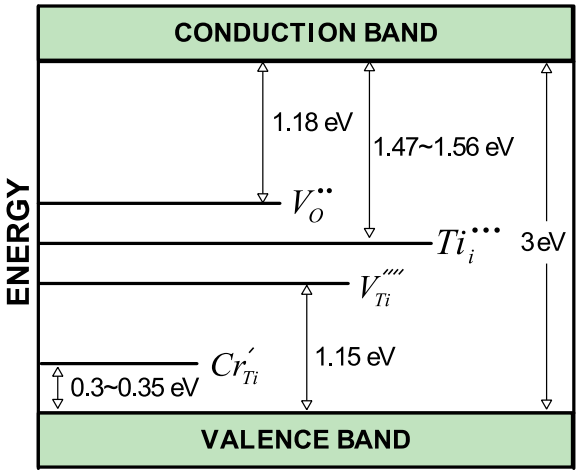

Figure 3.1. *Band model for TiO_2 (rutile) including the energy levels of different intrinsic defects as well as trivalent chromium ions in titanium sites [2-6].*

The lattice of pure TiO_2 involves positively charged intrinsic ionic defects, including oxygen vacancies (the predominant defects), titanium interstitials (the minority defects), as well as negatively charged intrinsic ionic defects, which are titanium vacancies. In addition to the ionic defects, the oxide lattice involves electronic defects, which are formed by light and thermal ionization of both ionic defects and the bandgap.

The effect of light on bandgap ionization depends on the mechanism of the related electronic transitions that may be considered in terms of either direct or indirect transition.

3.1.1.2 Direct vs. Indirect Transitions

The bandgap can be determined from optical spectra using the theoretical models, which are based on either direct or indirect transition. Therefore, the proper determination of the bandgap requires knowledge of the transition mechanism.

The present section considers the optical properties in terms of the reflection spectrum applied in this work. The related Kubelka–Munk function, *f*(R), [7] can be used to convert the reflectance spectrum in light absorption spectrum as follows:

$$f(R) = \frac{(1-R)^2}{2R} = \frac{\alpha}{s^*} \tag{3.1}$$

where R is reflectance, α is absorption coefficient and s^* is the scattering coefficient. The absorption coefficient of an ideal material that exhibits the parabolic dependence of electron energy vs. electron wave vector grows with photon energy, according to the Tauc Equation [8]:

$$\alpha h\nu = A\left(h\nu - E_g\right)^n \tag{3.2}$$

where *A* is a proportionality constant, E_g is the optical bandgap and n =1/2, 3/2, 2, and 3 for the direct allowed, direct forbidden, indirect allowed, and indirect forbidden transitions, respectively. The bandgap could be graphically estimated from the intersection of extrapolated linear part of the plot of $[f(R)h\nu]^2$ vs $h\nu$ for direct and $[f(R)h\nu]^{1/2}$ vs $h\nu$ for indirect transitions.

According to the density functional theory, DFT studies on the electronic structure of TiO_2, the electronic transitions in anatase and rutile take place according to the indirect and direct models, respectively [9-11].

Selected data on the bandgap of pure TiO_2, determined by optical methods is presented in **Table 3.1**.

Table 3.1. *The literature data on the bandgap for pure TiO_2.*

Authors	Transition Model	Phase	Approach	Bandgap [eV]
Persson and da Silva [12]	Direct	Rutile	Optical	3.08
Yang et al. [13]	-	Anatase	Optical	3.30
Marzec et al. [14]	Indirect	Anatase	Optical	3.18
Tang et al. [15]	Indirect	Anatase	Optical	3.20

As seen, the experimentally obtained value of bandgaps for rutile and anatase are approximately 3 eV and 3.2 eV.

3.1.1.3 Effect of Chromium on Bandgap

Extensive studies have reported the effect of chromium on the bandgap of TiO_2 [16-27]. The reported experimental and theoretical results for Cr-doped TiO_2 are depicted in **Figure 3.2**. Since the effect of chromium on the bandgap depends on the morphology of studied specimens, the results are grouped according to the reported morphology, including single crystal (**Figure 3.2a**) [26], thin films (**Figure 3.2b**) [18, 21-23, 27], powder specimens (**Figure 3.2c**) [16, 17, 19, 20, 25] and nanotubes (**Figure 3.2d**) [28-30].

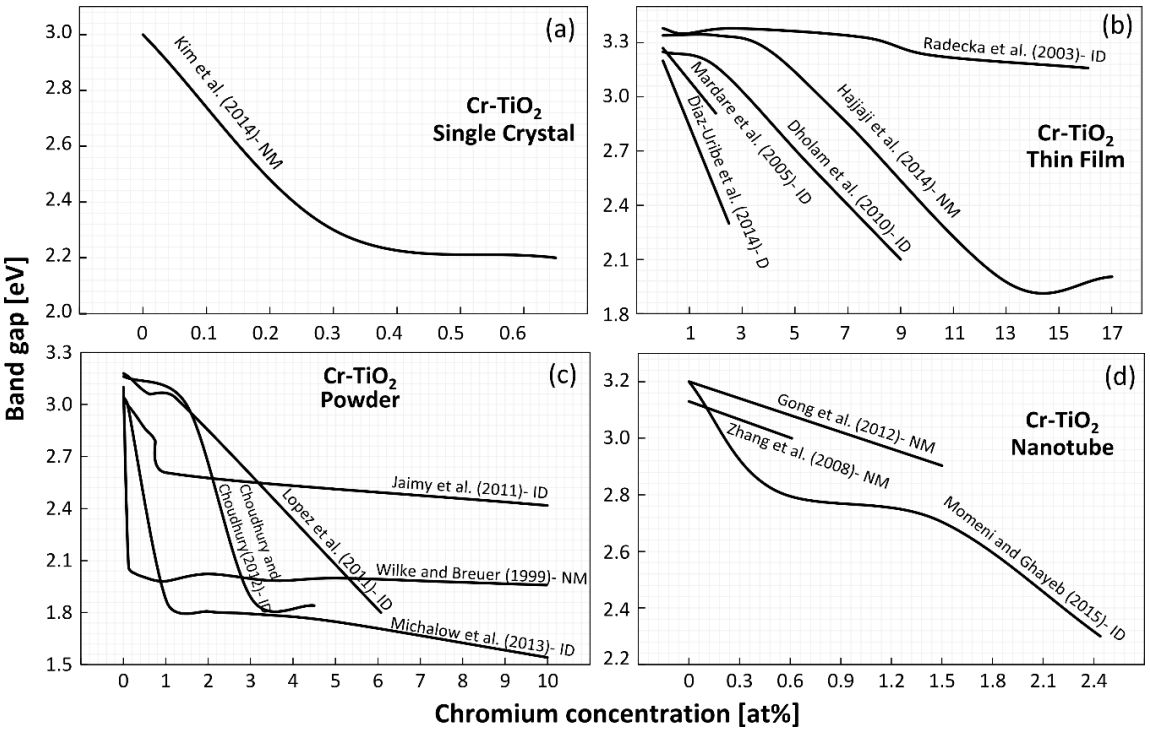

Figure 3.2. *Literature data on the effect of chromium concentration on the bandgap of TiO_2 of different morphology [16-23, 25-30] (the notation D and ID correspond to reported bandgap transitions, including direct and indirect, respectively, and NM denotes not mentioned.*

As seen, the character of the observed effect of chromium on the bandgap depends on the morphology. However, the scatter of data – even within the same morphology category - is substantial.

Single Crystal. As seen in **Figure 3.2a**, chromium incorporation into the TiO_2 lattice results in a decrease of the bandgap from 3 eV for pure TiO_2 to approximately 2.2 eV for Cr-doped TiO_2 containing 0.65 at% Cr. The effect is substantial. The character of the observed dependence indicates that the effect of chromium on the bandgap is limited to the concentration of approximately 0.4 at%. Since this concentration corresponds to the solubility limit, which is in the range of 5-8 at% [31, 32], one may assume that the mechanisms of chromium incorporation below and above that level, in the case of the single crystal, are different. The results for the single crystal are relatively well defined since the specimen is free of grain boundaries, which are expected to have a strong impact on the incorporation mechanism.

Thin Films. The effect of chromium on the bandgap of TiO_2 thin films is shown in **Figure 3.2b.** As seen, the effect is more substantial than that for the single crystal. However, the reported slopes of the bandgap change vs. the concentration of chromium and exhibit a substantial scatter. According to Diaz-Uribe et al. [23], the incorporation of chromium results in a decrease of the bandgap to the level of 2.2 eV at 3 at% Cr, while the same effect of the single crystal is observed at 0.4 at% Cr. The difference between the two effects is a strong indication that the mechanism of chromium incorporation and its effect on properties are different in the bulk phase of the single crystal and grain boundaries of the polycrystalline thin film. The lower slope of the bandgap changes vs. chromium concentration and is a consequence of the minor effect of chromium on the bandgap. As seen, the minimal slope reported by Radecka et al. [21] indicates that their experimental procedure does not lead to chromium being incorporated into the TiO_2 lattice.

Powder. As seen in **Figure 3.2c**, the shape of the reported effects of chromium on the bandgap for powder-type specimens consists of an initial strong decrease and subsequent little change when the chromium content is above a certain critical limit that ranges between 0.12 at% [16] and 3 at% Cr [20]. This behavior indicates that, in analogy to the single crystal (**Figure 3.2a**), the amount of chromium incorporated into TiO_2, and leading to a reduction of the bandgap, is limited and chromium above this limit results in a minimal change of bandgap.

Nanotube. In **Figure 3.2d**, shows chromium incorporation into nanotube-type specimen results in a steady decrease of the bandgap as a function of concentration. This effect suggests that the content of chromium leading to a decrease of bandgap is much lower than that for thin films.

The scatter of data in **Figure 3.2**, which is substantial, may be considered in terms of the following effects:

i) *Kinetic Factor.* The effect is related to the amount of chromium being effectively incorporated into the lattice due to the kinetic reason.

ii) *Composition*. The amount of chromium incorporation differs from that determined by the applied analytical procedure.

iii) Solubility. The properties of solid solutions are well defined only within the solubility limit. The amount of solute, more than the solubility limit results in the formation of heterogeneous precipitates. Their properties are not well-defined.

iv) Structure. The studied specimens frequently involve the mixture of both rutile and anatase phases [25, 33-36]. Since the related properties, such as light-induced transition models, are entirely different, knowledge of phase composition is required.

v) Morphology. The effect of different morphology of the studied specimens on properties can be substantial and is not well-defined.

vi) Oxygen Activity. It has been attested that oxygen activity has a substantial effect on the properties of TiO_2 [37]. Unfortunately, most of the reported data does not further inform or confirm this effect.

3.1.2 Chromium Incorporation Mechanisms

The effect of chromium on surface and bulk properties of TiO_2 has been studied using a range of surface vs. bulk experimental approaches. The most commonly used surface techniques include secondary ion mass spectrometry, SIMS, and X-ray photoelectron spectroscopy, XPS. The alternative properties include the electron paramagnetic resonance, EPR, electrical conductivity, as well as theoretical methods. The reported data and the related conclusions are summarised in **Table 3.2**.

As seen, both SIMS and XPS data indicate that chromium in oxidizing conditions strongly segregates to the surface leading to a substantial enrichment of the surface layer in chromium. The enrichment, consequently, results in the formation of LDSSs [38]. At the same time, it has been shown that 25% - 60% of chromium incorporated leads to the formation of donors. As a result, segregation leads to the formation of concentration gradients of chromium and related potential barriers.

Table 3.2. *The reported studies on surface and bulk properties of Cr-doped TiO_2 (LDSS denotes low-dimensional surface structure).*

Authors	Approach	Outcomes	Conclusions
Jayamaha et al. (2015) [39]	SIMS	• Chromium segregates to Cr-TiO_2 surface in oxidizing condition leading to surface enrichment • Chromium segregation driving force in oxidizing conditions is imposed by a low-dimensional surface structure • Chromium is removed from the Cr-TiO_2 surface in reducing condition leading to surface depletion	The enrichment leads to strong interactions between defect in the surface layer leading to the formation of LDSSs
Colmenares et al. (2013) [40]	XPS	• At low concentration, chromium enters into titanium sites as Cr^{3+} and Cr^{6+} • Chromium segregates to the surface in oxidizing conditions (enrichment 2-7) • The Cr^{6+}/Cr^{3+} ratio at the surface in oxidizing conditions is 2/3	At low concentrations chromium results in formation of both Cr'_{Ti} and $Cr^{\bullet\bullet}_{Ti}$ in the surface layer
Mardare et al. (2010) [41]			
Lopez et al. (2011) [17]			
Zhu et al. (2010) [42]			
Li et al. (2013) [43]			
Yin et al. (2004) [44]			
Kohler et al. (1993) [45]	EPR	• Chromium segregates to the surface in oxidizing conditions • The Cr^{6+}/Cr^{3+} ratio at the surface in oxidizing conditions 1:4	25% - 60% of chromium at the surface results in the formation of donors, such as $Cr^{\bullet\bullet}_{Ti}$
Carpentier et al. (1989)[46]	Electrical conductivity	Introduction of chromium results in a change of electrical conductivity (EC) of TiO_2 (**Figure 3.3**): • In oxidizing conditions, the EC of pure TiO_2 is larger than that of Cr-TiO_2 • In reducing condition, the EC of pure TiO_2 is smaller than that of Cr-TiO_2	In oxidizing conditions chromium in the bulk results in the formation of acceptors, such as Cr'_{Ti} In reducing condition chromium in the bulk leads to donor-type defects, such as $Cr^{\bullet\bullet}_{Ti}$ or $Cr_i^{\bullet\bullet\bullet}$ or $Cr_i^{\bullet\bullet\bullet\bullet\bullet\bullet}$
Radecka and Rekas (1994) [47]			
Tani and Baumard (1980) [48]			
Açıkgöz (2012) [49]	Theoretical method	Tri-valent chromium enters both substitutional and interstitial sites	Chromium in the TiO_2 lattice results in the formation of Cr'_{Ti} and $Cr_i^{\bullet\bullet\bullet}$ ions
Yang et al. (2009) [50]	DFT	In oxidizing conditions both tri- and tetra-valent chromium enters substitutional sites In reducing conditions tri-valent chromium enters interstitial sites	In oxidizing conditions chromium results in the formation of acceptors. In reducing conditions chromium results in formation of donors, such as $Cr_i^{\bullet\bullet\bullet}$
Sasaki et al. (1985) [51]	Diffusion	Chromium is transported in rutile via interstitial sites	The diffusion mechanism is consistent with the formation of donors

Choudhury and Choudhury, 2012 [20]	Raman	Chromium is incorporated according to both substitutional and interstitial mechanism	Chromium results in the formation of both Cr'_{Ti} and $Cr_i^{\bullet\bullet\bullet}$

A very sensitive probe for the determination of the effect of extrinsic ions, such as chromium, on properties of oxide semiconductors, is the measurement of the electrical conductivity. The common approach is based on determining the effect of oxygen activity on the electrical conductivity at elevated temperatures corresponding to gas/solid equilibrium. The reported data on the effect of oxygen activity on the electrical conductivity for pure and Cr-doped TiO_2 are represented in **Figure 3.3** showing the data of Tani and Baumard [48], Carpentier et al. [46] and Radecka and Rekas [47].

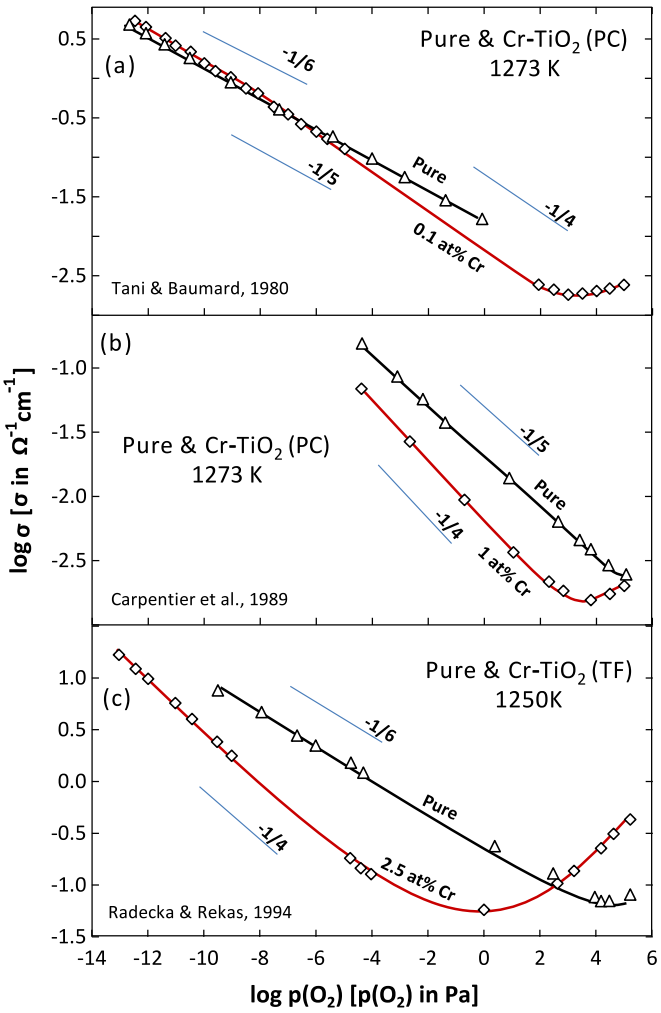

Figure 3.3. *The reported data on the effect of oxygen activity on the electrical conductivity, where σ is the electrical conductivity and p(O_2) is oxygen activity [46-48]. The notation PC and TF represents polycrystalline and thin film, respectively.*

As seen, the plots of chromium on the log $p(O_2)$ vs. log σ indicate the following effects:

i) The slope of the log $p(O_2)$ vs. log σ dependence assumes negative and positive values in the n- and p-type regimes respectively. The slope may be considered in terms of the defect disorder (see Chapter 2).

ii) The minimum of the electrical conductivity corresponds to the n-p transition, if the mobility terms are the same. As seen, the incorporation of chromium results in lowering the $p(O_2)$-related to the n-p transition point.

iii) The incorporation of chromium in the n-type regime results in a decrease of the electrical conductivity. This effect is consistent with the acceptor-type mechanism of chromium incorporation.

3.1.3 Unresolved Problems

While the literature indicates that chromium results in a reduction of the bandgap, the following problems are still unresolved:

i) The scatter of data on the effect of chromium on the bandgap is substantial. Therefore, there is a need to determine the effect that is well defined, reproducible and free of processing conditions and morphology.

ii) Little is known on the effect of oxygen activity on the bandgap. There is a need to investigate this effect in more detail.

iii) The reported data on the energy levels of ionic defects in TiO_2 is based on theoretical calculations. There is a need to verify these data experimentally.

This chapter aims at addressing these unresolved problems.

3.2 Specimen Processing

3.2.1 Processing of Powder Specimens

The specimens of solid solutions of TiO_2 with chromium were prepared using the sol-gel method. The precursors included titanium isopropoxide (TTIP), $Ti[OCH(CH_3)_2]_4$, and chromium-chloride hexahydrate, $CrCl_3.6H_2O$. The required amount of $CrCl_3.6H_2O$ powder was calculated to achieve chromium concentrations of 0.05, 0.08, 0.16, 0.5, and 1.5 at% in the final TiO_2 solid solutions.

The sol-gel technique involves several steps that are related to the formation of the sol of the right composition, its subsequent conversion into gel and calcination. Hydrolysis of titanium alkoxide, TTIP, is commonly performed in the presence of acetic acid acting as a catalyst that allows modification of the rate of the hydrolysis process. Since, the gelation process is profoundly influenced by the content of TTIP, acetic acid, and water, selection of the appropriate ratio of these components allow to achieve the desired reaction rates. The optimum volumes of acetic acid and deionized H_2O can be determined from the ratios of CH_3COOH:Ti and H_2O:Ti that is equal to 1.5:1 and 4:1, respectively. Finally, the formation of a monolithic gel at room temperature requires an optimum amount of ethanol. Hence, the volume of anhydrous ethanol was adjusted to achieve the concentration of 0.8 mol/L of titanium in the final solution [52].

The processing procedure involves the following steps:

Step 1: The mixture of $CrCl_3.6H_2O$ powder and a small amount of ethanol (Beaker-1) was vigorously stirred until the $CrCl_3.6H_2O$ was completely dissolved. Then, in a separate beaker (Beaker-2) the $Ti[OCH(CH_3)_2]_4$ was mixed with the acetic acid by vigorous stirring.

Step 2: The Beaker-1 solution was slowly added to the Beaker-2 solution and stirred for 1 hour.

Step 3: After 1 hour, the mixture of remaining ethanol and deionized water solution was added drop-wise to the Beaker-2 solution and stirred until the viscosity of the formed gel hindered the rotation of the stirring bar.

Step 4: The stirrer was taken out and the beaker was placed on a hot plate at approximately 353 K and left in the fume cabinet to dry for 1 to 2 days. The resulting crystals were then ground into a fine powder using an agate mortar and pestle.

A similar procedure was applied for processing pure TiO_2; however, in this case, Beaker-1 was not involved.

3.2.2 Formation of Ceramic Pellets

The powders of both pure and Cr-doped TiO_2 were prepared following steps 1-4, and then used to form ceramic pellets according to the following procedure:

i) Calcination the powder at 773 K during 5 h in air.

ii) Mixing the powder with the binder (1% of paraffin).

iii) Uniaxial pressing at 50 – 60 MPa into 13 mm discs.

iv) Annealing the pellets at 873 K in air during 10 h (binder removal).

v) Sintering at 1373 K for 5 h in artificial air (the mixture of 79% argon and 21% of oxygen).

The heating and cooling programs involved in steps (i), (iv) and (v) are shown in **Figure 3.4**.

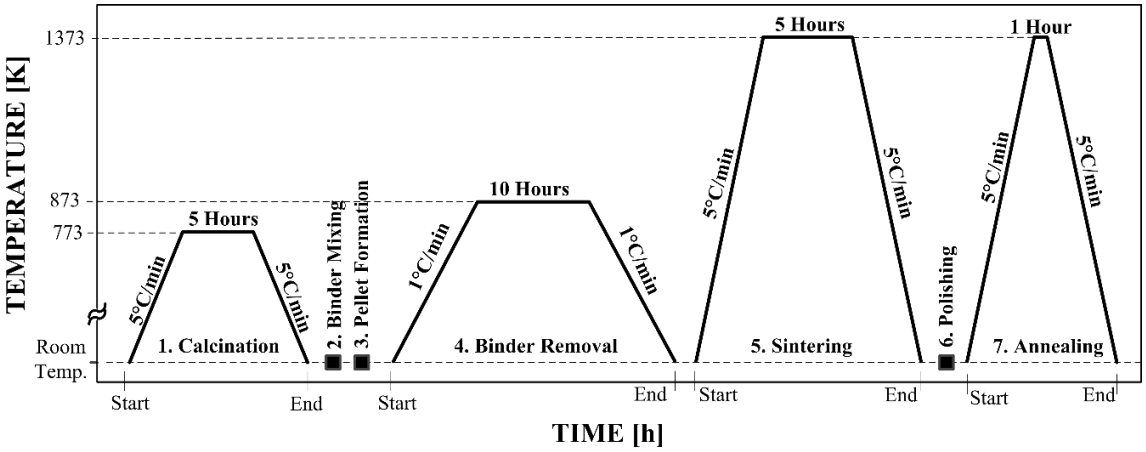

Figure 3.4. *The applied processing procedure in the formation of polycrystalline specimens of both pure and Cr-doped TiO_2 (the numbers correspond to the processing steps described in text).*

Calcination. The pulverized powders of pure or Cr-doped TiO_2 were placed in a platinum lined alumina boat. The calcination, which takes place in a tube furnace in air at 773 K, aims at removing residue water and organic compounds. The powder specimens, before and after the calcination process are shown in **Figure 3.5 a-b**.

Binder Mixing. The paraffin wax (1%) was mixed with calcined powder.

Pellet Formation. The powder was pressed uniaxially into cylindrical pellets using a 13-mm diameter hardened stainless steel die at 50-60 MPa.

Binder Removal. The pellets were again placed in a tube furnace for 10 hours dwelling at 873 K in air for binder removal.

Sintering. The pellets were sintered in artificial air at 1373 K for 5 hours for densification into a polycrystalline solid. The images of the obtained ceramic polycrystalline specimens after sintering are presented in **Figure 3.5 c-h**.

Polishing. The specimens were polished using sandpaper (1200 grit).

Annealing. The specimens were annealed for 1 h at 1373 K in the gas phase of controlled oxygen activity in order to impose the desired oxygen activity in the oxide lattice. The formation of the gas phases of different compositions is discussed below.

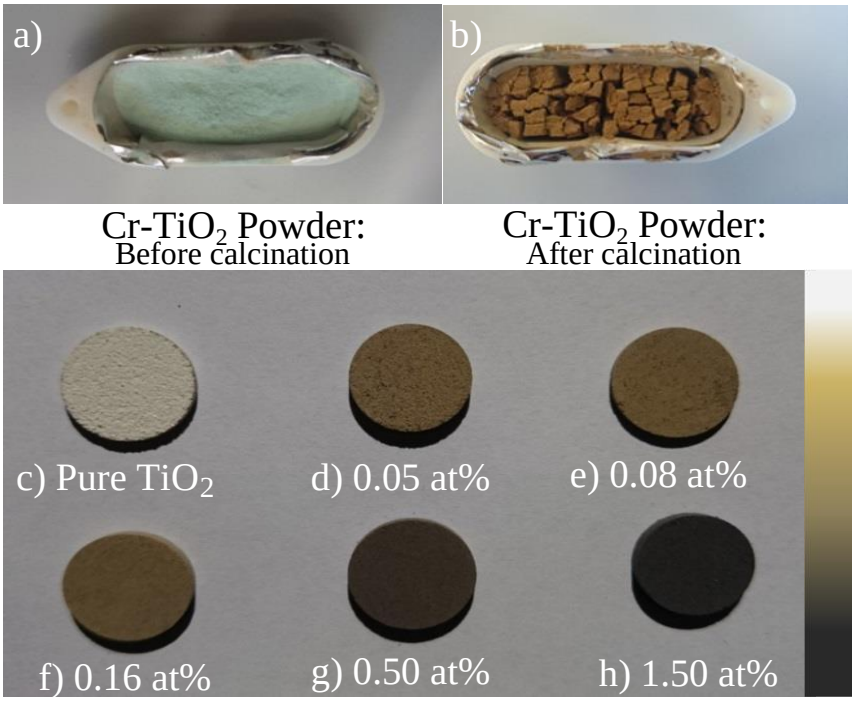

Figure 3.5. *Pictorial representation of Cr-doped TiO_2 powder (a & b) before and after calcination and (c-h) the polycrystalline ceramic samples.*

3.2.3 Gas Phase

The experimental set-up of the gas flow system is represented in **Figure 3.6**. As seen, the system involved the gas flow controllers, the tube furnace and the bubbler to prevent the backflow of air. The specimen was placed in the alumina tube dedicated to the present series of specimens with chromium.

The following gas phase mixtures were used:

i) Pure oxygen, $p(O_2)$ = 100 kPa

ii) Artificial air (79% argon + 21% oxygen)- related oxygen activity), $p(O_2)$ = 21 kPa

iii) Argon (99%) - hydrogen (1%) mixture. The related oxygen activities are

a. At 1373 K: $p(O_2) = 10^{-10}$ Pa

b. At 1273 K: $p(O_2) = 10^{-12}$ Pa

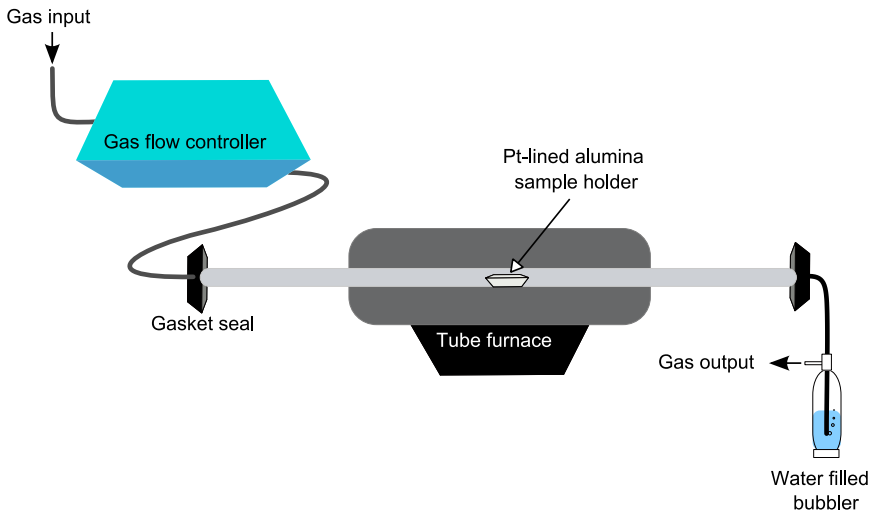

Figure 3.6. *Schematic illustration of the experimental set-up used during high-temperature heat treatment.*

The oxygen activity in the gas phase was monitored throughout the experiment using the zirconia-based electrochemical sensor [53].

3.3 Characterization

According to a range of literature reports the incorporation of chromium into the anatase form of TiO_2 results in the transition of the anatase structure into the rutile structure [25, 33-36]. The transition effect depends on the concentration of chromium. It has also been shown that annealing of the anatase form of TiO_2, including both pure and Cr-doped TiO_2, results in the transition of anatase to the rutile structure [54, 55]. The transition is complete at 1073 K and above (details are discussed in Chapter 5, section 5.1.1.2). Consequently, taking into account the processing procedure described in section 3.2.2, it was assumed the specimen studied in this research project exhibited the rutile structure.

3.3.1 Proton Induced X-ray Emission Spectroscopy

Proton Induced X-ray Emission spectroscopy (PIXE) is an analytical technique for the elemental analysis of solids with high accuracy at the level of parts per billion. Through the application of an ion beam, PIXE measures the radiation emitted by electron state changes and identifies each element based on its unique emissions, records it as a spectral peak. It is one of the most powerful and relatively simple non-destructive analytical techniques. The principle of the PIXE technique is shown in **Figure 3.7.**

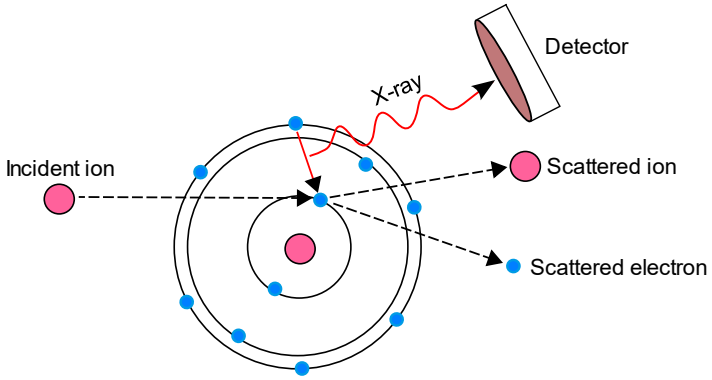

Figure 3.7. *Schematic representation of the basic working principle of photon-induced x-ray emission technique.*

As seen in the schematic diagram, the accelerated ion particle beam ejects an inner-shell electron from the atoms present in the target sample which produces a shell vacancy. When that vacancy is filled by an outer-shell electron, an X-ray of characteristic energy, related to that particular atom is emitted. The intensity of the emitted X-rays is detected as a spectral peak by the energy dispersive detector.

The PIXE analysis was used to perform an elemental bulk phase analysis of the studied specimens. The instrumentation included a 2MV STAR tandem accelerator at the Australian Nuclear Science and Technology Organization (ANSTO). The experimental procedure involved the following steps:

- A 2.6 MeV proton beam of 10-15nA beam current was applied to the sample surface for analysis.
- The X-rays were recorded using a Si(Li) detector fitted with a 25 μm thick Be window at the 45° angle.

- Due to the limited ability of Si(Li) detectors to cope with very high-count rates resulting from solid samples, an additional pin-hole filter (1700 μm thick acrylic) with a 2%-hole area, was used.
- The pin-hole filter was placed over the X-ray detector to minimize pile-up and dead time during sample analysis.
- The pin-hole filter was also fitted with an additional 4 μm thick mylar film to further decrease the intensity of the low energy X-rays excited with high cross-sections.
- The collected charge generated by the ion beam for each sample was 30 μC.
- The acquired X-ray spectra were processed using the GUPIXWIN software package (Version 2.1.4, University of Guelph, Canada) to determine the elemental concentration.

The obtained PIXE spectra for pure and Cr-doped TiO_2 samples are shown in **Figure 3.8** (the inserts show the enlarged chromium-related peak).

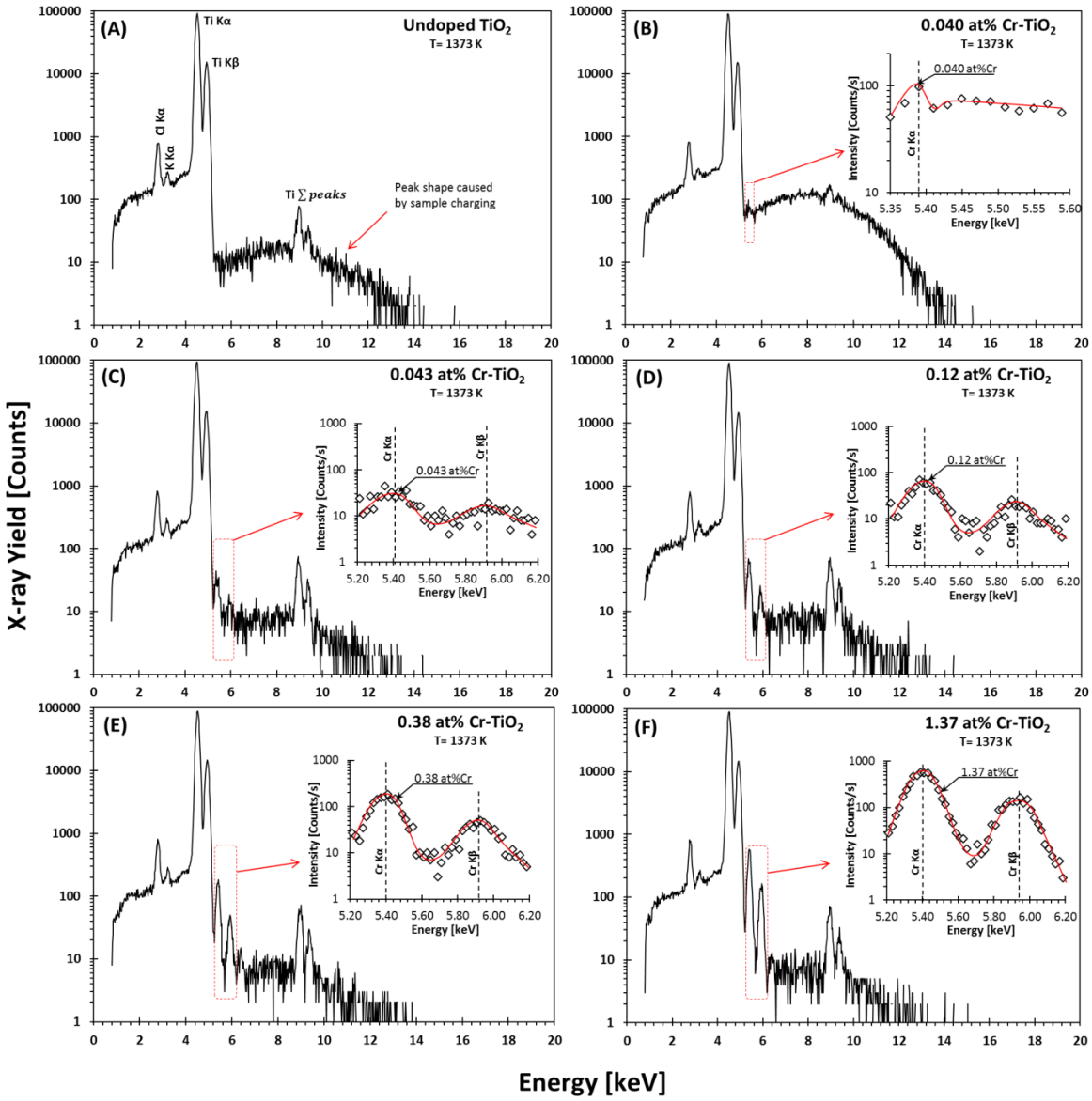

Figure 3.8. *Schematic representation of PIXE analysis data for undoped and Cr-doped TiO_2 specimens after sintering at 1373 K for 5 h (the inserts represent the enlargements of chromium-related peaks). From now, the studied specimens will be addressed according to the value obtained from PIXE analysis.*

The results of the PIXE quantitative analysis are collected in **Table 3.3**.

Table 3.3. *Elemental bulk analysis data for undoped and Cr-doped TiO_2 samples conducted by PIXE technique.*

Projected chromium content [at%]	Experimentally determined chromium concentrations and main impurities [at%]			
	Cr	Ti	K	Cl
1	2	3	4	5
0.00	0.000	99.778	0.010	0.211
0.05	0.040±0.014	99.780	0.013	0.168
0.08	0.043±0.009	99.723	0.017	0.217
0.16	0.116±0.007	99.711	0.006	0.166
0.50	0.376±0.005	99.388	0.017	0.218
1.50	1.365±0.004	98.362	0.015	0.259

As seen, the results of chromium concentrations according to the PIXE analysis performed after sintering (stage 5 of the applied processing shown in Figure 3.4), shown in column 2, are lower from the amount of chromium introduced during processing (column 1). The difference between the two values, which is approximately 20% - 30%, corresponds to the loss of chromium during processing. The increase of chromium content (column 2) is consistent with the decrease of titanium content (column 3). This consistency suggests that the majority of chromium is incorporated into titanium sites. The level of potassium is insignificant. The effect of chlorine on properties of Cr-doped TiO_2 is considered later in this chapter.

3.3.2 Optical Properties

The study of optical properties aims at determining the reflectance spectra that can be used for graphical estimation of the bandgap. The introductory discussion on the bandgap determination from the reflectance spectra is presented before (section 3.1.1.2).

The reflectance spectra were determined using the Agilent Cary 5000 UV−vis−NIR spectrophotometer fitted with a 150 mm diameter integrating sphere (external diffuse reflectance accessory, DRA-2500). The instrument was turned on 30 minutes before the reflectance measurement to warm-up the light sources. The system baseline and 100% R were calibrated with polytetrafluoroethylene (PTFE) standard plate

on the reference port. The reflectance was measured within the wavelength range 200 to 800 nm.

The graphical estimation of bandgap from the intersection of the extrapolated linear part of the plot of $[f(R)hv]^2$ vs hv for direct transitions with the energy axis is shown in **Figure 3.9.**

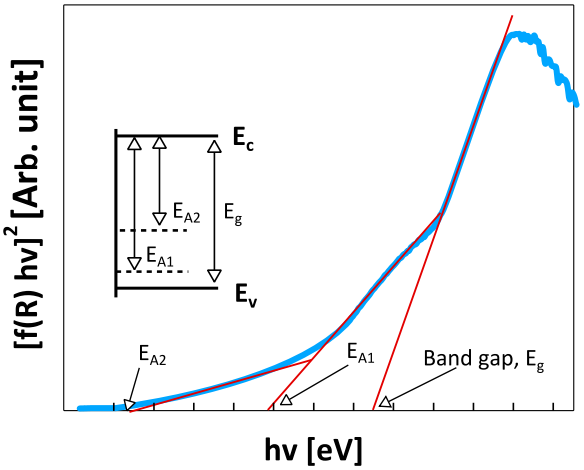

Figure 3.9. *Schematic representation of Tauc plot showing the determination technique of bandgap as well as mid-band energy level within the electronic structure (denoted by E_{A1} and E_{A2}).*

As seen, different mid-band energy levels in the forbidden gap can be determined from the Tauc plot [21].

3.4 Results and Discussion

This section studies the results on optical properties in terms of the effect of chromium on the electronic structure of TiO_2 with controlled oxygen activity. The aim is to determine the effect of processing, such as annealing, in the gas phase of controlled oxygen activity and surface polishing on the band gap and the mid-gap levels.

3.4.1 Effect of Chromium Concentration on Electronic Structure

This section considers the reflectance spectra as a function of photon energy (light wavelength) for Cr-doped TiO_2 involving two kinds of specimens; the 1st corresponding

to the as-polished specimens after stage 6 in **Figure 3.4** and the 2nd specimen after subsequent annealing in air. The related spectra are shown in **Figures 3.10 a and b**.

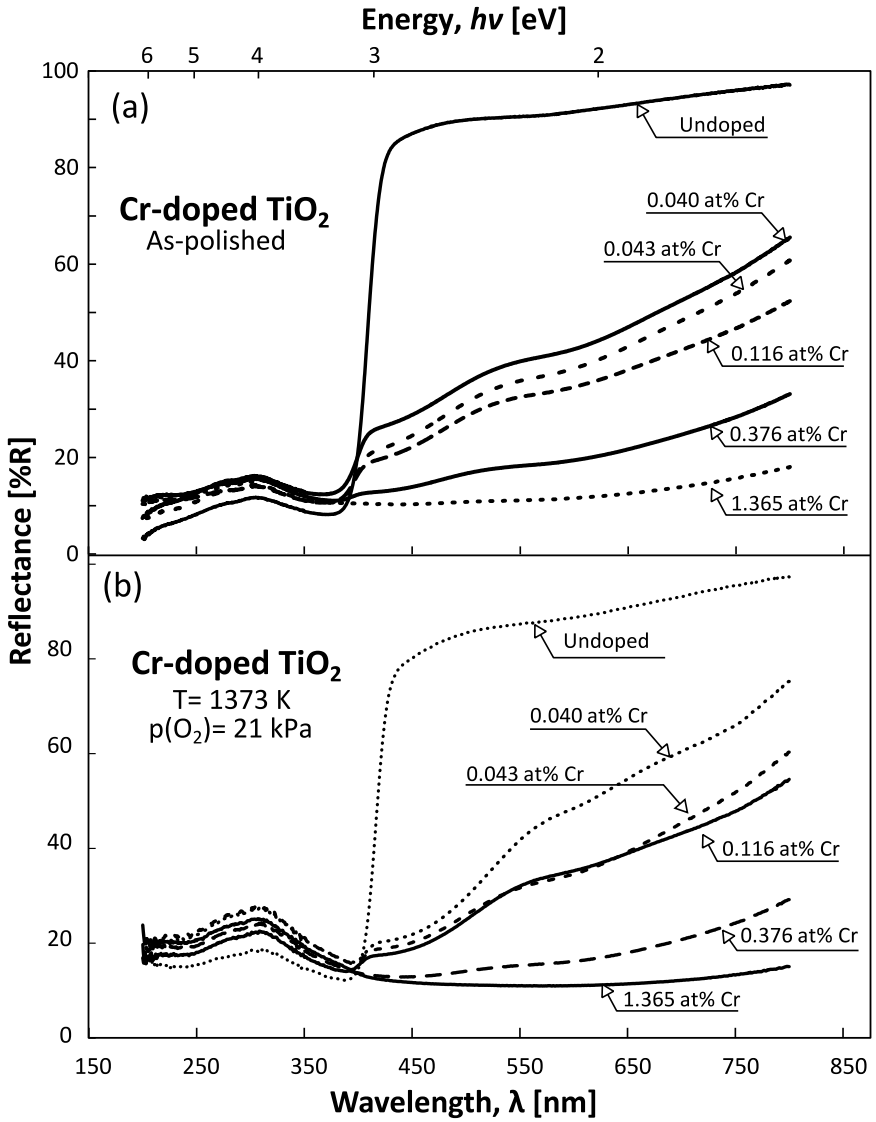

Figure 3.10. *Effect of chromium concentration on the reflectance spectra of TiO_2 for (a) as-polished specimens and (b) the specimens subsequently annealed at 1373 K in artificial air, $p(O_2)$ = 21 kPa.*

The reflectance data in **Figure 3.10** was transformed to the form according to the Kubelka-Munk function, *f(R)*, expressed by equation (3.1). Subsequently, the *f(R)* function was represented in the form of the Tauc plots using equation (3.2), as shown in **Figure 3.11** and **Figure 3.12** for the specimens as-polished (processing stage 6) and subsequently annealed (processing stage 7) respectively.

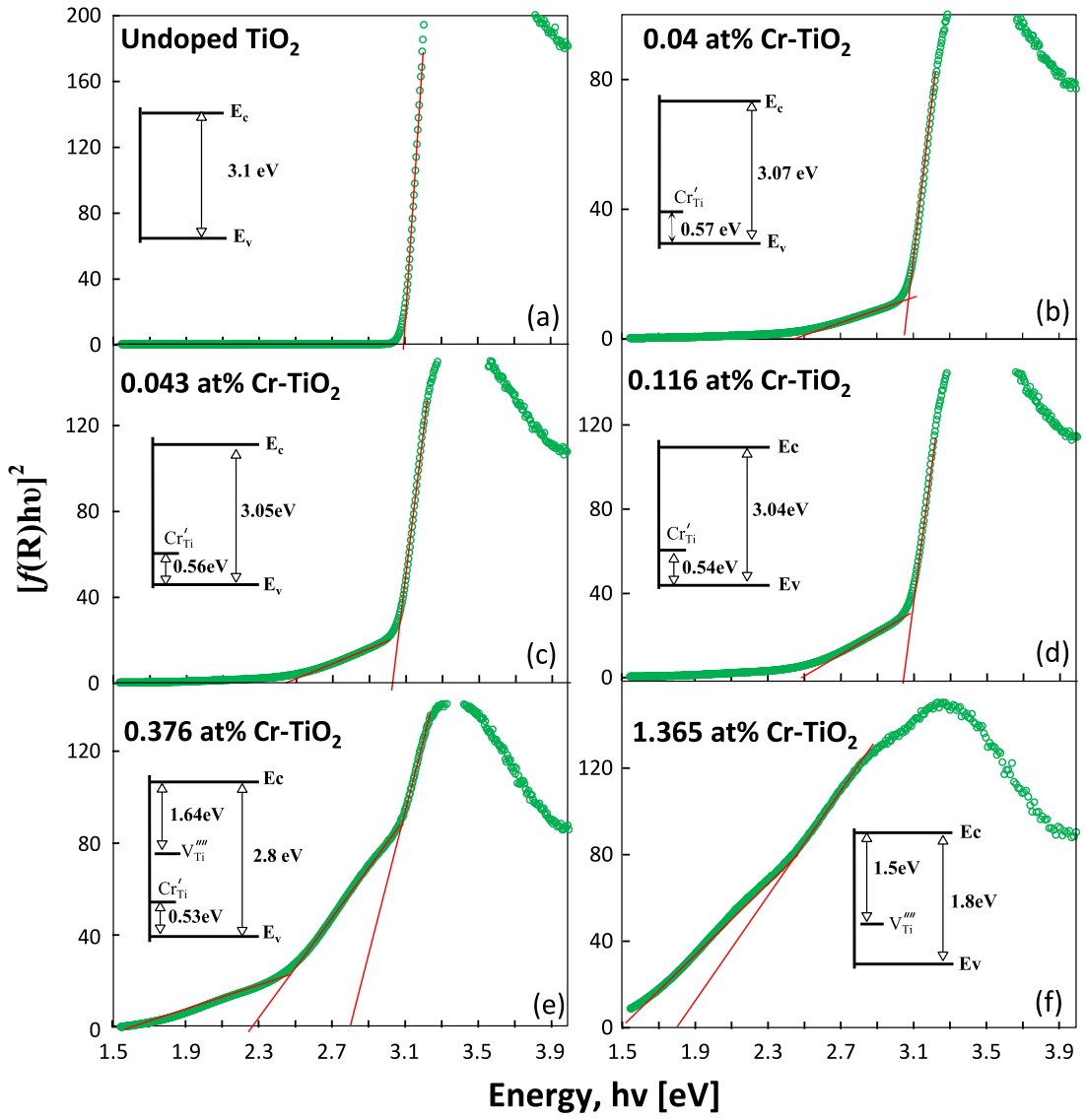

Figure 3.11. *Effect of chromium on the Tauc plots for Cr-doped TiO_2 and the related models of the electronic structure for the as-polished specimen. The mid-band levels are determined following the method described in* ***Figure 3.9.***

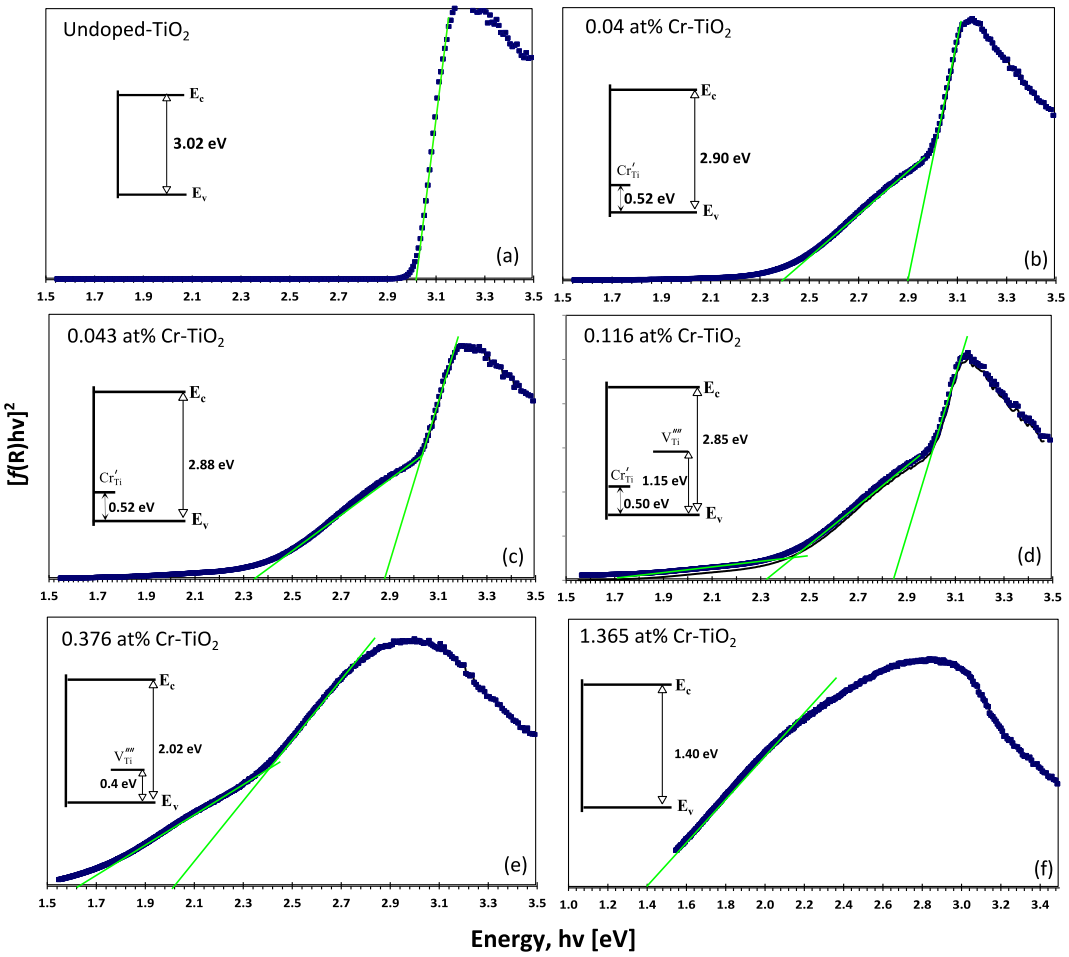

Figure 3.12. *Effect of chromium on the Tauc plots for Cr-doped TiO_2 after polishing and subsequent annealing at 1373 K in $p(O_2)$ = 21 kPa and the related models of the electronic structure. The mid-band levels are determined following the method described in* ***Figure 3.9****.*

The spectra in **Figures 3.11** and **3.12** can be used for the determination of the bandgap (determined assuming direct electronic transitions) as well as the mid-gap energy levels, which are represented by the inserts. The results in **Figures 3.11 and 3.12** allow the following points to be made:

(i) ***Bandgap.*** The incorporation of chromium results in a bandgap reduction, (a) from 3.1 eV for pure TiO_2 to 1.8 eV for Cr-doped TiO_2 involving 1.365 at% Cr for the as-polished specimen, and (b) from 3.02 eV for pure TiO_2 to 1.4 at% Cr for involving 1.365 at% Cr for the specimen polished and subsequently annealed in air. The difference between the two values, which is substantial, is strong

evidence that surface processing, such as polishing, has a substantial effect on the optical properties and the related bandgap. Since the effect of polishing is expected to be sensitive to the applied polishing procedure, the optical properties determined after annealing in the gas phase of controlled oxygen activity can be considered as the specific material property.

(ii) ***Chromium-related Energy Level.*** The new edge corresponding to 0.57 eV above the valence band reflects an acceptor energy level, which is consistent with the chromium ions in the titanium sites, Cr'_{Ti}. These ions are formed according to the mechanisms expressed by equations **(2.6), (2.8)** and **(2.26)**. The mechanism **(2.6)** is preferred because oxygen vacancies are the predominant defects in oxidizing conditions in the applied processing conditions. The energy level related to chromium is approximately 0.57 eV above the band gap at 0.04 at% for the as-polished specimen and its band widens as the chromium content increases. The energy level of chromium at the same bulk content is 0.52 eV for the annealed specimen, however, the widening effect for the chromium-related band is more substantial because of the effect of segregation leading to surface enrichment with chromium (details are in Chapter 4).

(iii) ***Fully Ionized Titanium Vacancies.*** The energy of these defects is around the middle of the band gap for both specimens. The energy level above the valence band corresponding to 1.15 eV is consistent with the reported energy level of titanium vacancies, V''''_{Ti} [56].

(iv) ***Oxygen Vacancy-Related Energy Level.*** The incorporation of chromium leads to an increase in the concentration of donor-type oxygen vacancies, however, their concentration is below the detection limit of the applied procedure.

3.4.2 Effect of Oxygen Activity on Electronic Structure

The former section considered the effect of polishing and subsequent annealing in air on optical properties of Cr-doped TiO_2. It is concluded that annealing in oxygen results in the formation of TiO_2 with reproducible properties that can be considered as materials-related. The aim of the present section is to consider the effect of oxygen activity on the

optical properties and the related bandgap. The related reflection spectra for pure and Cr-doped TiO_2 involving 0.04 at% Cr are shown in **Figure 3.13** (a and b, respectively).

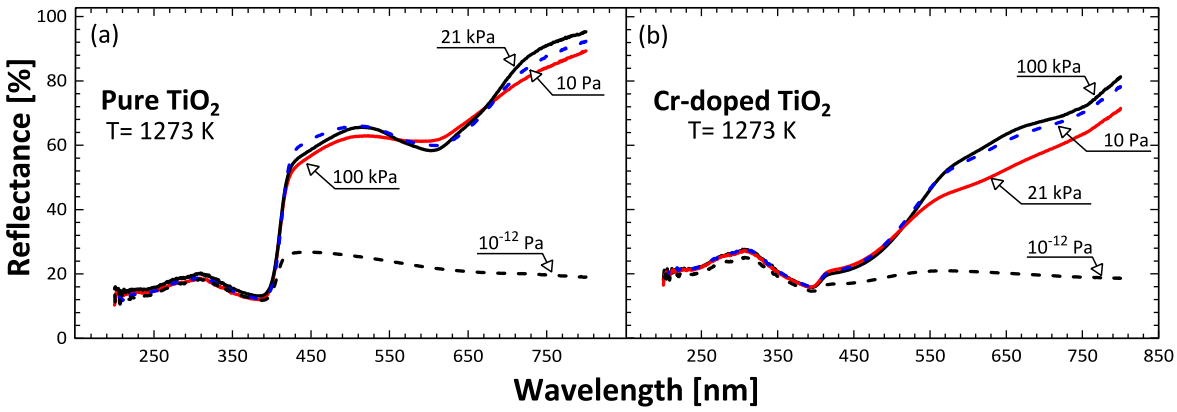

Figure 3.13. *The changes of reflectance spectra of (a) pure and (b) 0.04 at% Cr-doped TiO_2 specimens annealed in different oxygen activity as a function of wavelength.*

Assuming a direct transition model, the bandgap was graphically estimated from the intersection of the extrapolated linear part of the Tauc plot of $[f(R)hv]^2$ vs. hv with the energy axis shown in **Figure 3.14**.

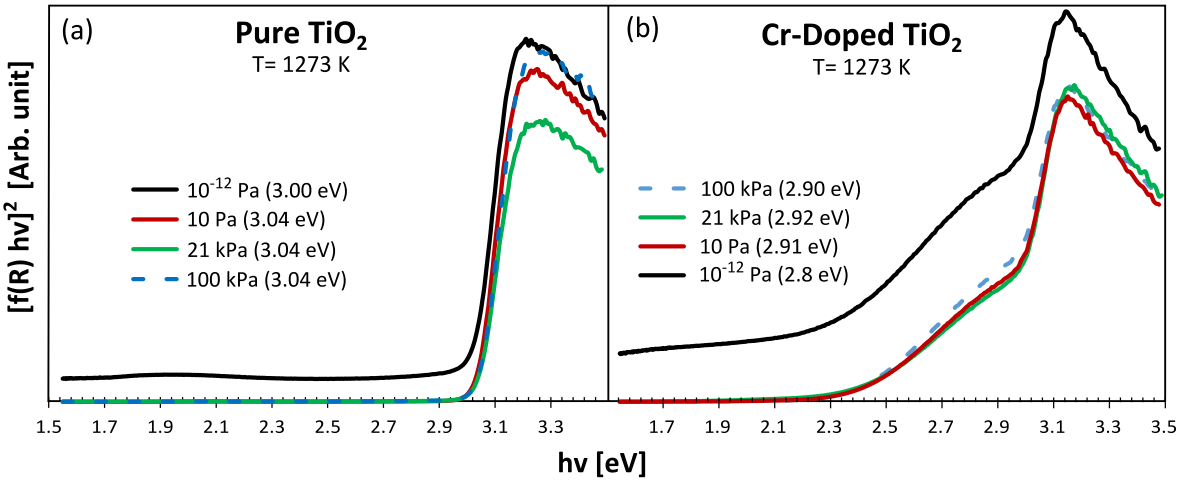

Figure 3.14. *Schematic representation of Tauc plot for direct transition of photo-excited electron for (a) pure and (b) 0.04 at% Cr-doped TiO_2 samples treated at different oxygen activity.*

The effect of chromium concentration on the bandgap for TiO_2 annealed in the gas phase of the controlled oxygen activity, along with the data for the as-polished specimen, is shown in **Figure 3.15**.

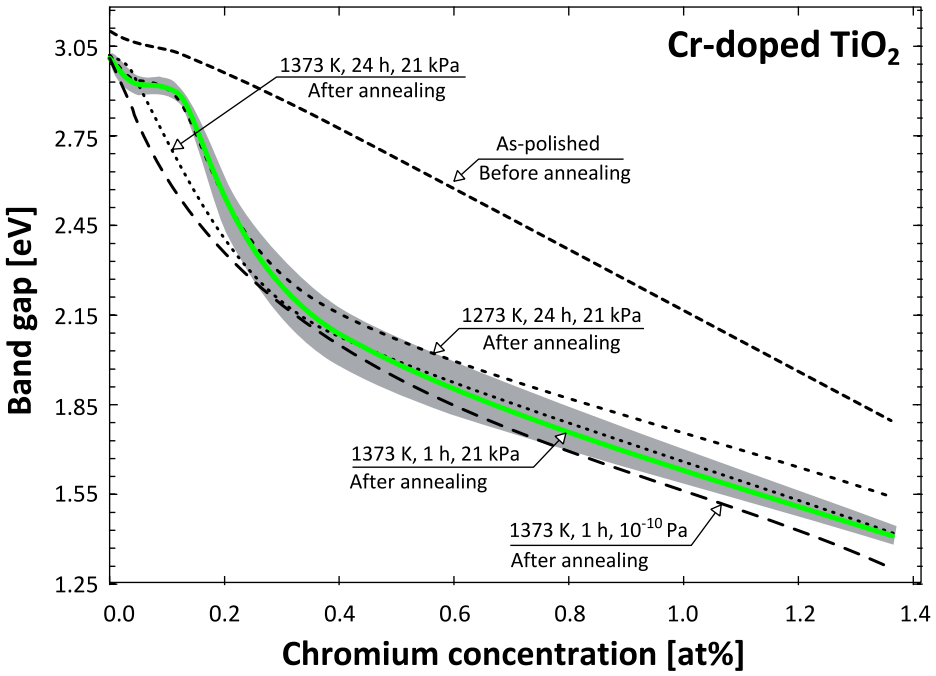

Figure 3.15. *The effect of composition on the bandgap for Cr-doped TiO_2 before annealing (as -polished) as well as after annealing in $p(O_2) = 10^{-10}$ Pa and 21 kPa, respectively. The shaded region shows the variation of the bandgap for three different sets of specimen annealed at 1373 K for 1 hour in controlled oxygen activity related to $p(O_2) = 21$ kPa.*

These data can be summarized as:

i) Chromium results in a strong reduction of the bandgap of TiO_2, however:
   a. The effect of bandgap reduction for the as-polished specimen is lower and depends on the applied processing procedure.
   b. The effect of bandgap reduction for the polished and subsequently annealed specimen at 1273 K and 1373 K is much stronger and the related data, which are well reproducible, may be considered as material-related data.
   c. The effect of oxygen activity in the gas phase during annealing on the bandgap is insignificant, however, annealing at 1373 K results in the removal of a step-like effect observed for dilute solid solution of chromium in TiO_2.

ii) The observed effect of polishing on the bandgap indicates that the determined reflection spectra before polishing are reflective of the bandgap of the surface layer that is removed during polishing. This effect also indicates that the surface layer exhibits the bandgap that is essentially different from that of the bulk phase beneath.

3.4.3 Effect of Chlorine Ions on Electronic Structure

The results from the PIXE chemical analysis (**Table 3.3**) indicate the studied specimens of Cr-doped TiO_2 involve a certain amount of chlorine (0.166 at%-0.259 at%). The contamination present at this level, which for dilute solid solutions is comparable to the content of intentionally introduced dopant, cannot be ignored.

The incorporation of chlorine into the TiO_2 lattice may be represented by the following equilibrium:

$$Cl_2 \leftrightarrow 2Cl_O^{\bullet} + V_{Ti}'''' + 2h^{\bullet} \tag{3.3}$$

As seen, the incorporation of chlorine results in the formation of titanium vacancies and electron holes, however, the effect of both chlorine-related species and titanium vacancies depends on their ionization degrees. According to Long et al. [57], the effect of chlorine on the properties of TiO_2 calcined above 573 K can be ignored.

3.5 Summary and Theoretical Models

The optical properties reported in this chapter determine the electronic structure of both pure and Cr-doped TiO_2. It has been documented that the related data, which are based on the reflection spectra, including the bandgap and mid-gap levels, are very sensitive to the applied processing procedure, especially surface processing, such as polishing. The obtained experimental material may be summarised in terms of the models showing the effect of the composition on the electronic structure for the specimens (a) after polishing and also (b) after subsequent annealing in the gas phase of the controlled composition (**Figure 3.16**).

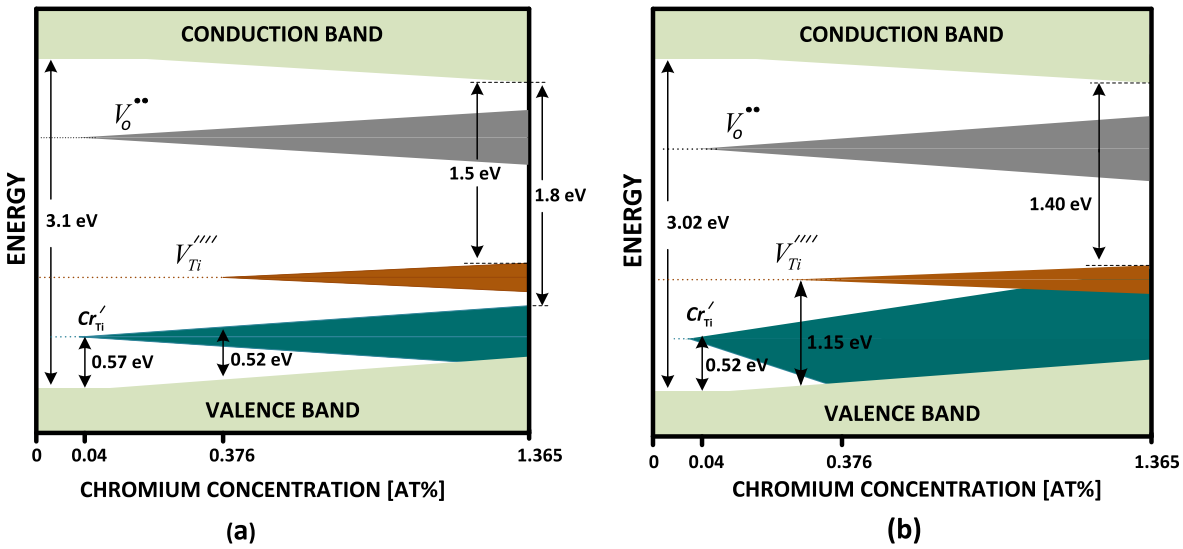

Figure 3.16. *Semi-quantitative representation of the effect of chromium on the electronic structure of TiO_2 for (a) as polished and (b) annealed specimen.*

As seen, these diagrams essentially confirm the theoretical model reported in the literature shown in **Figure 3.1**. However, this work represents a conceptual advance in terms of the effect of processing on the picture of the electronic structure. The data indicate that the interpretation of the optical properties requires recognition that the optical reflection data are sensitive to the applied processing procedure. The present work considers three surface-related effects:

i. *Effect of polishing*. The effect of polishing on the reflection spectra and the related data on electronic structure is substantial and must not be ignored. The effects established in this work indicates that in fact the electronic structure for solids, such as TiO_2 for the bulk phase, is entirely different from that of the surface layer.

ii. *Effect of annealing*. Annealing allows restoration of the surface that is essentially determined by the annealing conditions, such as temperature and oxygen activity, of the gas phase during annealing.

iii. *Effect of oxygen activity*. The effect of oxygen activity on the determined optical properties is insignificant but measurable.

iv. *Effect of segregation*. The phenomenon of segregation has a substantial effect on surface properties, including chemical composition and structure. Therefore, the time and the temperature of annealing should allow the segregation equilibrium to be reached.

The effects of (i) oxygen activity during annealing and (ii) polishing on the bandgap for Cr-doped TiO_2 are summarized in **Figure 3.17**.

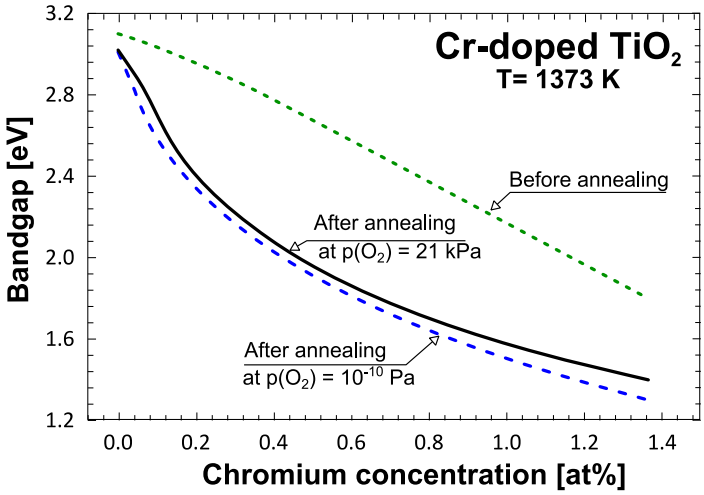

Figure 3.17. *Bandgap vs. chromium concentration showing an insignificant effect of oxygen activity during annealing and a substantial effect of polishing.*

In conclusion, the incorporation of chromium into the TiO_2 lattice results in a decrease of the band gap from 3.1 eV or 3.04 eV for pure TiO_2 to either 1.8 eV or 1.4 eV for Cr-doped TiO_2 involving 1.365 at% Cr before and after the final annealing in oxidizing conditions, respectively. The character of the reflectance spectra reveals that the observed reduction of the band gap is associated with the formation of acceptor-type energy levels, that are related to trivalent chromium ions incorporated into the titanium sub-lattice at [Cr]=0.04 at% Cr (E=0.52-0.57 eV). However, the analysis of the optical absorption spectra indicate that chromium exhibits a dual mechanism, including the acceptor-type as well as donor-type mechanism leading to the formation is hexavalent ions that are compensated by titanium vacancies. The derived defect disorder model is applicable to the ceramic specimens of Cr-doped TiO_2 solid solutions equilibrated in dry air.

3.6 References

[1] Kofstad, P., *Nonstoichiometry, diffusion, and electrical conductivity in binary metal oxides*. 1972: Wiley-Interscience New York.

[2] da Silva, R.C., E. Alves, and M.M. Cruz, *Conductivity behaviour of Cr implanted TiO_2*. Nuclear Instruments and Methods in Physics Research Section B: Beam Interactions with Materials and Atoms, 2002. **191**(1–4): p. 158-162.

[3] Ghosh, A.K., F. Wakim, and R. Addiss Jr, *Photoelectronic processes in rutile.* Physical Review, 1969. **184**(3): p. 979.

[4] Miyagi, T., et al., *Superior Schottky electrode of RuO_2 for deep level transient spectroscopy on anatase TiO_2.* Applied Physics Letters, 2003. **83**(9): p. 1782-1784.

[5] Nowotny, M., et al., *Defect chemistry of titanium dioxide. Application of defect engineering in processing of TiO_2-based photocatalysts.* The Journal of Physical Chemistry C, 2008. **112**(14): p. 5275-5300.

[6] Cronemeyer, D., *Infrared Absorption of Reduced Rutile TiO_2 Single Crystals.* Physical Review, 1959. **113**(5): p. 1222.

[7] Nobbs, J.H., *Kubelka—Munk theory and the prediction of reflectance.* Coloration Technology, 1985. **15**(1): p. 66-75.

[8] Tauc, J., *Optical properties and electronic structure of amorphous Ge and Si.* Materials Research Bulletin, 1968. **3**(1): p. 37-46.

[9] Zhang, J., et al., *New understanding of the difference of photocatalytic activity among anatase, rutile and brookite TiO_2.* Physical Chemistry Chemical Physics, 2014. **16**(38): p. 20382-20386.

[10] Xu, M., et al., *Photocatalytic Activity of Bulk TiO_2 Anatase and Rutile Single Crystals Using Infrared Absorption Spectroscopy.* Physical Review Letters, 2011. **106**(13): p. 138302.

[11] Wang, Y., et al., *First-principles study on transition metal-doped anatase TiO_2.* Nanoscale Research Letters, 2014. **9**(1): p. 46.

[12] Persson, C. and A. Ferreira da Silva, *Strong polaronic effects on rutile TiO_2 electronic band edges.* Applied Physics Letters, 2005. **86**(23): p. 231912-231912.

[13] Yang, T.-S., C.-B. Shiu, and M.-S. Wong, *Structure and hydrophilicity of titanium oxide films prepared by electron beam evaporation.* Surface Science, 2004. **548**(1–3): p. 75-82.

[14] Marzec, A., et al., *Structural, optical and electrical properties of nanocrystalline TiO_2, SnO_2 and their composites obtained by the sol–gel method.* Journal of the European Ceramic Society, 2016. **36**(12): p. 2981-2989.

[15] Tang, H., et al., *Electrical and optical properties of TiO_2 anatase thin films.* Journal of Applied Physics, 1994. **75**(4): p. 2042-2047.

[16] Wilke, K. and H. Breuer, *The influence of transition metal doping on the physical and photocatalytic properties of titania.* Journal of Photochemistry and Photobiology A: Chemistry, 1999. **121**(1): p. 49-53.

[17] López, R., R. Gómez, and S. Oros-Ruiz, *Photophysical and photocatalytic properties of TiO_2-Cr sol–gel prepared semiconductors.* Catalysis Today, 2011. **166**(1): p. 159-165.

[18] Hajjaji, A., et al., *Cr-Doped TiO_2 Thin Films Prepared by Means of a Magnetron Co-Sputtering Process: Photocatalytic Application.* American Journal of Analytical Chemistry, 2014. **2014**.

[19] Jaimy, K.B., et al., *An aqueous sol–gel synthesis of chromium (III) doped mesoporous titanium dioxide for visible light photocatalysis.* Materials Research Bulletin, 2011. **46**(6): p. 914-921.

[20] Choudhury, B. and A. Choudhury, *Dopant induced changes in structural and optical properties of Cr^{3+} doped TiO_2 nanoparticles.* Materials Chemistry and Physics, 2012. **132**(2): p. 1112-1118.

[21] Radecka, M., et al., *Study of the TiO_2–Cr_2O_3 system for photoelectrolytic decomposition of water*. Solid State Ionics, 2003. **157**(1): p. 379-386.

[22] Dholam, R., et al., *Efficient indium tin oxide/Cr-doped-TiO_2 multilayer thin films for H_2 production by photocatalytic water-splitting.* International Journal of Hydrogen Energy, 2010. **35**(18): p. 9581-9590.

[23] Diaz-Uribe, C., W. Vallejo, and W. Ramos, *Methylene blue photocatalytic mineralization under visible irradiation on TiO_2 thin films doped with chromium.* Applied Surface Science, 2014. **319**: p. 121-127.

[24] Dholam, R., et al., *Hydrogen production by photocatalytic water-splitting using Cr- or Fe-doped TiO_2 composite thin films photocatalyst.* International Journal of Hydrogen Energy, 2009. **34**(13): p. 5337-5346.

[25] Michalow, K.A., et al., *Flame-made visible light active TiO_2:Cr photocatalysts: Correlation between structural, optical and photocatalytic properties.* Catalysis Today, 2013. **209**: p. 47-53.

[26] Kim, R., et al., *Charge and magnetic states of rutile TiO_2 doped with Cr ions.* Journal of Physics: Condensed Matter, 2014. **26**(14): p. 146003.

[27] Mardare, D., et al., *Chromium-doped titanium oxide thin films.* Materials Science and Engineering: B, 2005. **118**(1): p. 187-191.

[28] Zhang, S., et al., *Synthesis, characterization of Cr-doped TiO_2 nanotubes with high photocatalytic activity.* Journal of Nanoparticle Research, 2008. **10**(5): p. 871-875.

[29] Gong, J., et al., *A simple electrochemical oxidation method to prepare highly ordered Cr-doped titania nanotube arrays with promoted photoelectrochemical property.* Electrochimica Acta, 2012. **68**: p. 178-183.

[30] Momeni, M.M. and Y. Ghayeb, *Photoelectrochemical water splitting on chromium-doped titanium dioxide nanotube photoanodes prepared by single-step anodizing.* Journal of Alloys and Compounds, 2015. **637**: p. 393-400.

[31] Li, Y., et al., *Gas sensing properties of p-type semiconducting Cr-doped TiO_2 thin films.* Sensors and Actuators B: Chemical, 2002. **83**(1–3): p. 160-163.

[32] Sōmiya, S., S. Hirano, and S. Kamiya, *Phase relations of the Cr_2O_3-TiO_2 system.* Journal of Solid State Chemistry, 1978. **25**(3): p. 273-284.

[33] Choi, J., H. Park, and M.R. Hoffmann, *Effects of Single Metal-Ion Doping on the Visible-Light Photoreactivity of TiO_2.* The Journal of Physical Chemistry C, 2010. **114**(2): p. 783-792.

[34] Tian, B., C. Li, and J. Zhang, *One-step preparation, characterization and visible-light photocatalytic activity of Cr-doped TiO_2 with anatase and rutile bicrystalline phases.* Chemical Engineering Journal, 2012. **191**: p. 402-409.

[35] Trenczek-Zajac, A., et al., *Influence of Cr on structural and optical properties of TiO_2: Cr nanopowders prepared by flame spray synthesis.* Journal of Power Sources, 2009. **194**(1): p. 104-111.

[36] Koh, P.W., et al., *Photocatalytic degradation of photosensitizing and non-photosensitizing dyes over chromium doped titania photocatalysts under visible light.* Journal of Photochemistry and Photobiology A: Chemistry, 2017. **332**: p. 215-223.

[37] Li, W., et al., *Photocatalytic properties of TiO_2: Effect of niobium and oxygen activity on partial water oxidation.* Applied Catalysis B: Environmental, 2016. **198**: p. 243-253.

[38] Atanacio, A.J., T. Bak, and J. Nowotny, *Niobium segregation in niobium-doped titanium dioxide (rutile).* The Journal of Physical Chemistry C, 2014. **118**(21): p. 11174-11185.

[39] Jayamaha, U., et al., *Effect of oxygen activity on chromium segregation in Cr-doped TiO_2 single crystal.* Ionics, 2015. **21**(3): p. 785-790.

[40] Colmenares, J.C., et al., *Low-temperature ultrasound-promoted synthesis of Cr–TiO_2-supported photocatalysts for valorization of glucose and phenol degradation from liquid phase.* Applied Catalysis B: Environmental, 2013. **134**: p. 136-144.

[41] Mardare, D., et al., *Undoped and Cr-doped TiO_2 thin films obtained by spray pyrolysis.* Thin Solid Films, 2010. **518**(16): p. 4586-4589.

[42] Zhu, H., J. Tao, and X. Dong, *Preparation and photoelectrochemical activity of Cr-doped TiO_2 nanorods with nanocavities.* The Journal of Physical Chemistry C, 2010. **114**(7): p. 2873-2879.

[43] Li, X., Z. Guo, and T. He, *The doping mechanism of Cr into TiO_2 and its influence on the photocatalytic performance.* Physical Chemistry Chemical Physics, 2013. **15**(46): p. 20037-20045.

[44] Yin, J.B. and X.P. Zhao, *Preparation and enhanced electrorheological activity of TiO_2 doped with chromium ion.* Chemistry of Materials, 2004. **16**(2): p. 321-328.

[45] Kohler, K., et al., *Chromia Supported on Titania: I. An EPR Study of the Chemical and Structural Changes Occurring during Catalyst Genesis.* Journal of Catalysis, 1993. **143**(1): p. 201-214.

[46] Carpentier, J.-L., A. Lebrun, and F. Perdu, *Point defects and charge transport in pure and chromium-doped rutile at 1273 K.* Journal of Physics and Chemistry of Solids, 1989. **50**(2): p. 145-151.

[47] Radecka, M. and M. Rekas, *Defect structure and electrical properties of Cr-and Nb-doped TiO_2 thin films.* Solid State Phenomena, 1994. **39**: p. 135-138.

[48] Tani, E. and J.F. Baumard, *Electrical properties and defect structure of rutile slightly doped with Cr and Ta.* Journal of Solid State Chemistry, 1980. **32**(1): p. 105-113.

[49] Açıkgöz, M., *A study of the impurity structure for $3d^3$ (Cr^{3+} and Mn^{4+}) ions doped into rutile TiO_2 crystal.* Spectrochimica Acta Part A: Molecular and Biomolecular Spectroscopy, 2012. **86**: p. 417-422.

[50] Yang, K., Y. Dai, and B. Huang, *Density Functional Characterization of the Electronic Structure and Visible-Light Absorption of Cr-Doped Anatase TiO_2.* ChemPhysChem, 2009. **10**(13): p. 2327-2333.

[51] Sasaki, J., N. Peterson, and K. Hoshino, *Tracer impurity diffusion in single-crystal rutile (TiO_{2-x}).* Journal of Physics and Chemistry of Solids, 1985. **46**(11): p. 1267-1283.

[52] Atanacio, A.J., J. Nowotny, and K.E. Prince, *Effect of Oxygen Activity on Surface Composition of In-Doped TiO_2 at Elevated Temperatures.* The Journal of Physical Chemistry C, 2012. **116**(36): p. 19246-19251.

[53] Atanacio, A.J., et al., *Segregation in Titanium Dioxide Co-Doped with Indium and Niobium.* Journal of the American Ceramic Society, 2017. **100**(1): p. 419-428.

[54] Vieira, F.T.G., et al., *The influence of temperature on the color of TiO_2: Cr pigments.* Materials Research Bulletin, 2009. **44**(5): p. 1086-1092.

[55] Hamadanian, M., A. Reisi-Vanani, and A. Majedi, *Synthesis, characterization and effect of calcination temperature on phase transformation and photocatalytic activity of Cu, S-codoped TiO_2 nanoparticles.* Applied Surface Science, 2010. **256**(6): p. 1837-1844.

[56] He, J., et al., *Prediction of high-temperature point defect formation in TiO_2 from combined ab initio and thermodynamic calculations.* Acta Materialia, 2007. **55**(13): p. 4325-4337.

[57] Long, M., et al., *Preparation, characterization and photocatalytic activity of visible light driven chlorine-doped TiO_2.* Frontiers of Chemistry in China, 2007. **2**(3): p. 278-282.

Chapter 4
Segregation: Surface vs. Bulk Composition

The photocatalytic activity is determined by the local properties of the surface layer. Therefore, knowledge of the local surface composition, and the associated properties, is crucial in understanding and correctly interpreting the mechanism and kinetics of photocatalytic reactions. This chapter considers the effect of the phenomenon of the segregation of defects for Cr-doped TiO_2 and the associated concentration gradients.

4.1 Literature Overview

4.1.1 Surface vs. Bulk Properties

Segregation was first established for metal alloys [1], which are relatively easy for the determination of surface composition. The effect of segregation in metallic solids is represented in **Figure 4.1a** which shows the surface vs. bulk composition of nickel-copper alloy reported by Kuijers and Ponec [2]. As seen, the effect of segregation on the surface composition in metals is limited to 1-2 outermost atomic layers.

Surface studies of compounds, such as metal oxides, are more difficult. The collected experimental data for metal oxides indicate that the thickness of the segregation-induced surface layer, in this case, is much larger. As seen in **Figure 4.1b**, the thickness of the layer of Cr-doped CoO enriched in chromium is comparable to several hundred atomic layers [3].

It has been attested that the segregation-induced concentration gradients in oxide solid solutions are influenced by oxygen activity of the gas phase during annealing [4].

The effect of oxygen activity on segregation of chromium in Cr-doped TiO_2 is discussed below.

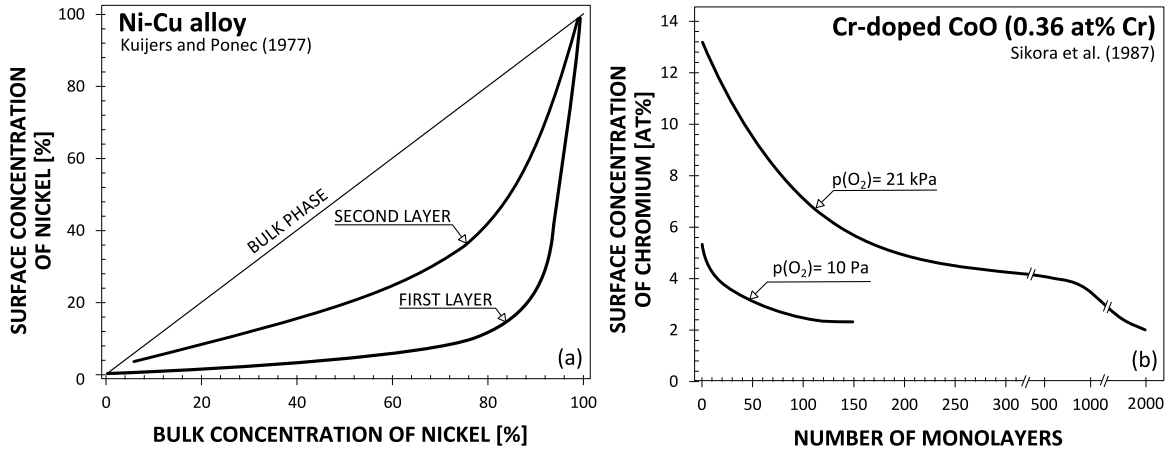

Figure 4.1. *The effect of segregation on surface vs. bulk composition of solids, including (a) Ni-Cu alloy [2]and (b) Cr-doped CoO [3].*

4.1.2 Literature Reports on Surface vs. Bulk Composition of Cr-doped TiO_2

There has been an accumulation of data on segregation in solid solutions of TiO_2 [4-6], including Cr-doped TiO_2 [7-14]. The studied systems, the related processing conditions, and the related segregation-induced enrichment factors are summarized in **Table 4.1**.

As evident, the scatter of data is substantial. The extent of the scatter in the reported data of segregation-induced surface versus bulk concentration of chromium seems related to the effect of processing conditions.

Table 4.1. *Literature reports on surface versus bulk concentration of chromium in Cr-doped TiO_2 (the notation T, A, R, s, b, and EF represent temperature, anatase, rutile, surface, bulk and enrichment factor, respectively).*

Authors	**Processing conditions**					**$[Cr]_b$** (at%)	**$[Cr]_s$** (at%)	**Approach**	**EF**
	Method	*T (K)*	*Time (h)*	*$p(O_2)$ (Pa)*	*Structure*				
Zhu et al., 2006 [8]	Sol-gel & hydro-thermal	473	8	21000	A	0.12	5.23	XPS	45.32
						0.24	5.89		24.34
Li et al., 2013 [9]	Hydro-thermal	673	1	-	A	1	5.48	XPS	5.48
						4	9.01		2.25
						7	10.87		1.55
						10	11.50		1.15
						13	15.54		1.20
Lopez et al., 2011 [10]	Sol-gel	773	4	21000	A	0.12	0.89	XPS	7.26
						0.61	3.57		5.82
						1.23	5.03		4.11
						6.07	12.59		2.07
Zhu et al., 2010 [11]	Facile hydro-thermal	923	1	21000	A	1	2.53	XPS	2.53
						3	7.66		2.55
						5	13.12		2.62
						10	18.63		1.86
Peng et al, 2012 [13]	Sol-gel	873	1	21000	A+R	-	11.40		-
Li et al., 2002 [14]	Sol-gel	873	1	21000	R	1	13.699	XPS	13.70
						2	19.608		9.80
						3	20.000		6.67
						4	17.544		4.39
						5	18.519		3.70
						6	20.833		3.47
						7	20.833		2.98
Chan et al., 2007 [12]	Cathodic arc plasma evaporation	723	3	-	A+R	10	33.33	AES	3.33
Jayamaha et al., 2015 [7]	Single crystal	1273	24	10^5	R	0.05	2.74	SIMS	54.84
				10^{-12}			0.002		0.03

Since the segregation-related experimental data for the specimens involving chromium content in excess of the solubility limit (approximately 8 at% Cr [15]) are not well defined, **Figure 4.2** represents only the data in **Table 4.1** corresponding to the solubility limit.

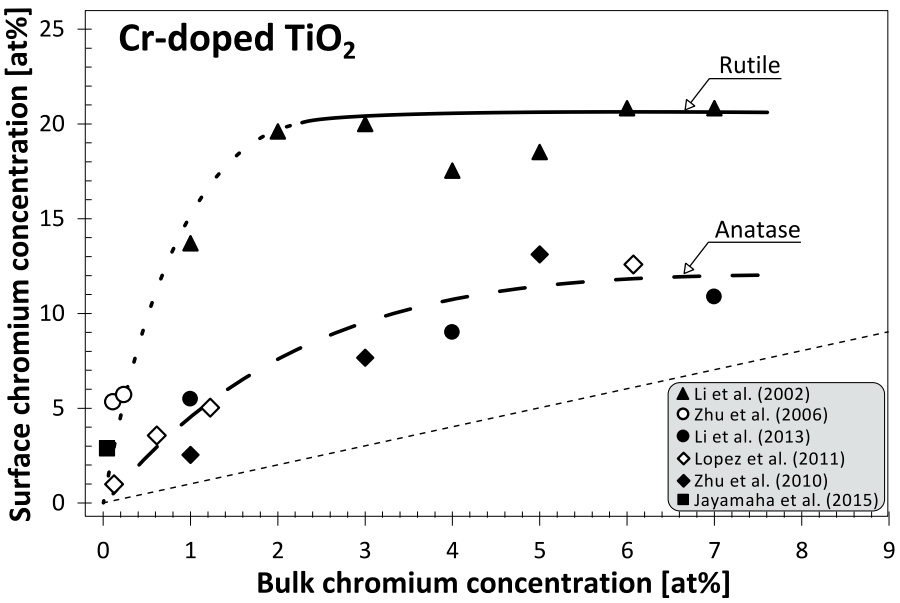

Figure 4.2. *The literature reported data on the surface versus bulk concentration and the related enrichment factor for chromium in Cr-doped TiO_2, including rutile and anatase [7-11, 14].*

As seen, the data on the segregation-induced surface chromium concentration for rutile is almost twice as large than that for the anatase structure. The data can be considered in terms of the following effects:

i) Dilute solid solutions (up to 2 at% Cr). The increase of bulk chromium concentration in this range results in increased surface concentration. The data in this range lined-up according to the curves for rutile and anatase.

ii) High concentrations (2-8 at% Cr). The segregation-induced surface concentrations of chromium in this regime follow the curves that are distinctively different:

a. Rutile. The extensive data of Li et al. [30] can be considered in this category. As seen, the segregation-induced surface concentration assumes a constant level of 20.5 at% Cr, which may be considered as corresponding to segregation equilibrium in the given experimental conditions of T = 873 K and $p(O_2)$ = 21 kPa.

b. Anatase. The segregation-induced surface concentration tends to assume 12.2 at% Cr [8-11].

With the exception of the work reported by Jayamaha et al. [7], all remaining data correspond to the polycrystalline specimens annealed in air. The study of Jayamaha et

al.[7], which is related to the single crystal of rutile, indicates that chromium segregation profoundly depends on oxygen activity during annealing. It has been documented that annealing at 1273 K in oxidizing conditions, $p(O_2) = 10^5$ Pa, and reducing conditions, $p(O_2) = 10^{-12}$ Pa, results in chromium enrichment factor of 55 and 0.03 (depletion), respectively.

The data related to the rutile structure (**Figure 4.2**) is expected to be well reproducible since this phase is thermodynamically stable. As also seen, the segregation-induced enrichment for the anatase structure (**Figure 4.2**) is substantially lower than that for the rutile phase.

The following section considers the experimental part concerning chromium segregation in Cr-doped TiO_2. The aim is to determine well defined experimental data free of the following effects:

i) *Kinetic Factor*. The annealing conditions for inducing segregation should correspond to segregation equilibrium. The estimated time required for equilibration of fast and slow defects within the studied specimen shown in Table 4.2.

ii) *Solubility*. The concentration of chromium in studied solid solutions should be within the solubility limit.

iii) *Structure*. The studies aim to form specimens with a rutile structure. This can be achieved by the prolonged annealing of the specimens.

iv) *Oxygen Activity*. Since segregation is affected by oxygen activity, the studies should be performed for the specimens annealed in the gas phase of the controlled oxygen activity.

Table 4.2. *The diffusion time required for penetration the distance of 2 μm in the TiO_2 lattice by different species in oxidizing conditions. The notation $D_{\parallel}$ and $D_{\perp}$ defines diffusion coefficient perpendicular and parallel to c-axis.*

Species		Temperature		Reference
		1073 K	1273 K	
Fast intrinsic defects[1]		1.67 min	0.5 min	[16]
Slow intrinsic defects[2]		3514 h	249 h	
Chromium[3]	$D_{\parallel}$	4.62 h	0.45 h	[17]
	$D_{\perp}$	7.94 h	0.74 h	

The selected diffusion distance of 2 μm is related to the average grain size of the studied polycrystalline specimen of TiO_2

1. Oxygen vacancies and titanium interstitials
2. Titanium vacancies
3. Diffusion of chromium isotope ^{51}Cr in TiO_2 single crystal

4.2 Experimental

4.2.1 Specimens Processing

The processing procedure of the studied specimens for the determination of segregation was the same as described in Chapter 3, section 3.1. The single crystal of Cr-doped TiO_2 was purchased from SurfaceNet Germany and its content of chromium was 0.05 at% [7].

4.2.2 Characterization

The bulk compositions of the studied specimens were determined by the proton-induced X-ray emission, PIXE (see Chapter 3, section 3.3). The surface properties were characterized using the secondary ion mass spectrometry (SIMS) and X-ray photoelectron spectroscopy (XPS).

4.2.2.1 X-ray Photoelectron Spectroscopy

X-ray Photoelectron Spectroscopy (XPS) is a widely used surface technique that is based on photoelectric effect which provides information on surface properties. An illustration of the basic working principle of the XPS technique is shown in **Figure 4.3**.

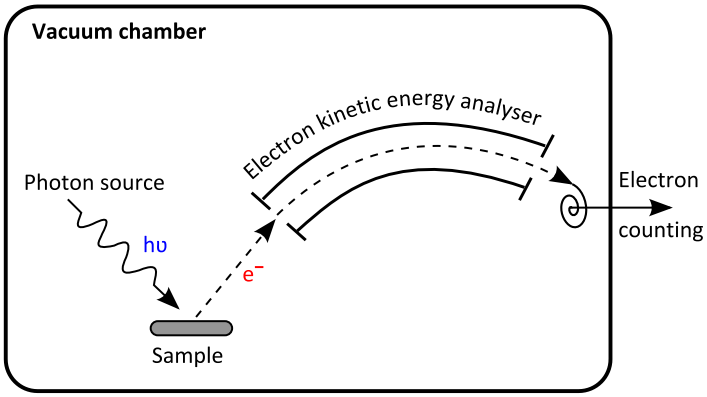

Figure 4.3. *Schematic representation of photoelectron spectrometer.*

The sample's surface, excited by a mono-energetic Al kα x-ray, causes the emission of free electrons from the surface. An electron energy analyzer measures the kinetic energy of the photoelectrons of:

$$KE = h\nu - (BE + \phi_s) \tag{4.1}$$

where $h\nu$ is the energy of the X-ray photon, BE is the binding energy of the electrons originating atomic orbital, and ϕ_s is the spectrometer work function, respectively.

The elemental identity, chemical state and the quantity of the detected electrons are determined from the binding energy and intensity of the photoelectron peak. The average depth measurement from the surface by XPS technique depends on the photoelectron take-off angle that varies between 4-6 nm [18].

The X-ray photoelectron spectroscopy, XPS, from Thermo Scientific, UK, equipped with a hemispherical analyzer, was used to determine the surface composition and the oxidation state of chromium in Cr-doped TiO_2. The XPS analysis was performed using the monochromated Al Kα source with $h\nu$= 1486.68 eV radiation in an ultra-high vacuum environment (<$2x10^{-9}$ mbar). The X-ray source was operated at 13.8 kV and 8.7 mA. A constant pass energy of 100 eV for survey scans or 20 eV for region scans was applied with the spectrometer to avoid the signal noise. A photoelectron take-off angle was set at 90° relative to the surface plane. The beam was focused to a spot size of 500 μm. The binding energy reference was set based on the C1s peak at 284.8 eV.

4.2.2.2 Secondary Ion Mass Spectrometry

Secondary Ion Mass Spectrometry (SIMS) is a technique with high elemental sensitivity (up to the ppb level) and high depth resolution (2-5 nm). This technique provides information on the chemical composition in the surface, near surface and in the bulk, respectively. The basic operation of SIMS is shown in **Figure 4.4**. It operates in an ultra-high vacuum environment ($<10^{-4}$ Pa). A focused primary ion beam, (e.g. cesium, oxygen) is used to sputter the surface of the studied specimen. The ejected secondary ions from the surface are detected by a mass spectrometer to determine the elemental, isotopic or molecular composition and its depth profile from the surface to the bulk as a function of time [19].

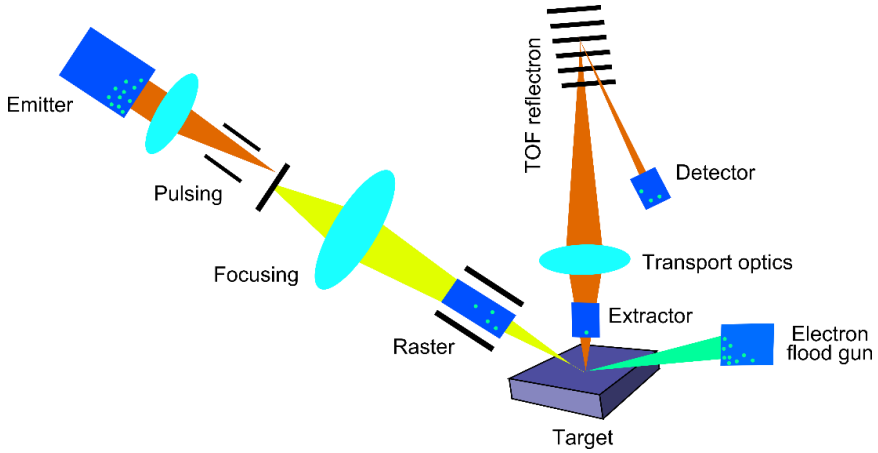

Figure 4.4. *Schematic representation of the experimental setup for SIMS technique [20].*

The concentration gradient of chromium from the surface was determined using secondary ion mass spectrometry, SIMS (Cameca IMS 5f). The analysis was performed on the surface area 180 x 180 μm rastered using O_2^+ primary ion beam of 30 nA current and 7.5 keV net impact energy. The crater depth was used for the determination of the average sputtering rate (0.2693 nm/s). In order to remove the surface charge that builds-up during sputtering, a thin surface layer of gold (10-15 nm) was deposited. The results of the SIMS analysis in ion yield (in term of counts) are proportional to absolute elemental concentrations. Therefore, relative concentrations can be obtained by normalizing the intensity of the analyzed species against the lattice species whose intensity throughout the specimen remains stable, such as the species of a selected isotope of titanium. The related intensity of Cr, between the level at the surface and in the bulk phase, were used to

determine the enrichment factor. The latter was applied in the determination of the effect of oxygen activity on the segregation-induced concentration profile.

4.2.2.3 Comparison of SIMS and XPS

In summary, the SIMS analysis, which is an invasive technique, allows scanning the chemical composition of the crystal lattice between the surface and the inward layers at the depth that depends on the time of sputtering. On the other hand, XPS analysis, which is not invasive, allows the determination of average chemical composition within the penetration depth that varies between 6 nm and 4 nm, depending on the incident angle. Both techniques provide a complementary picture of segregation.

4.3 Results and Discussion

This section reports the results on i) the effect of the bulk concentration of chromium on the segregation-induced enrichment of the surface layer with chromium after annealing in air as well as ii) the valence of the segregated chromium ions for polycrystalline specimens of Cr-doped TiO_2. This section also reports the effect of the oxygen activity in the gas phase during annealing on the chromium segregation in both single crystal and polycrystalline specimens of Cr-doped TiO_2.

4.3.1 Effect of Chromium Concentration

4.3.1.1 X-ray Photoelectron Spectroscopy

This section reports the results of XPS on the effect of bulk chromium concentration of the polycrystalline specimens of Cr-doped TiO_2 at 1373 K in artificial air on the segregation-induced surface chromium concentration and the related enrichment factor.

The XPS spectra are shown in **Figure 4.5** in terms of the intensity vs. binding energy, including (a-c) complete spectra for Cr-doped TiO_2 within a wide range of energy, (d) the Ti2p-related spectra and (e) Cr2p-related spectra for 0.04 at%, 0.116 at% and 1.365 at% Cr-doped TiO_2.

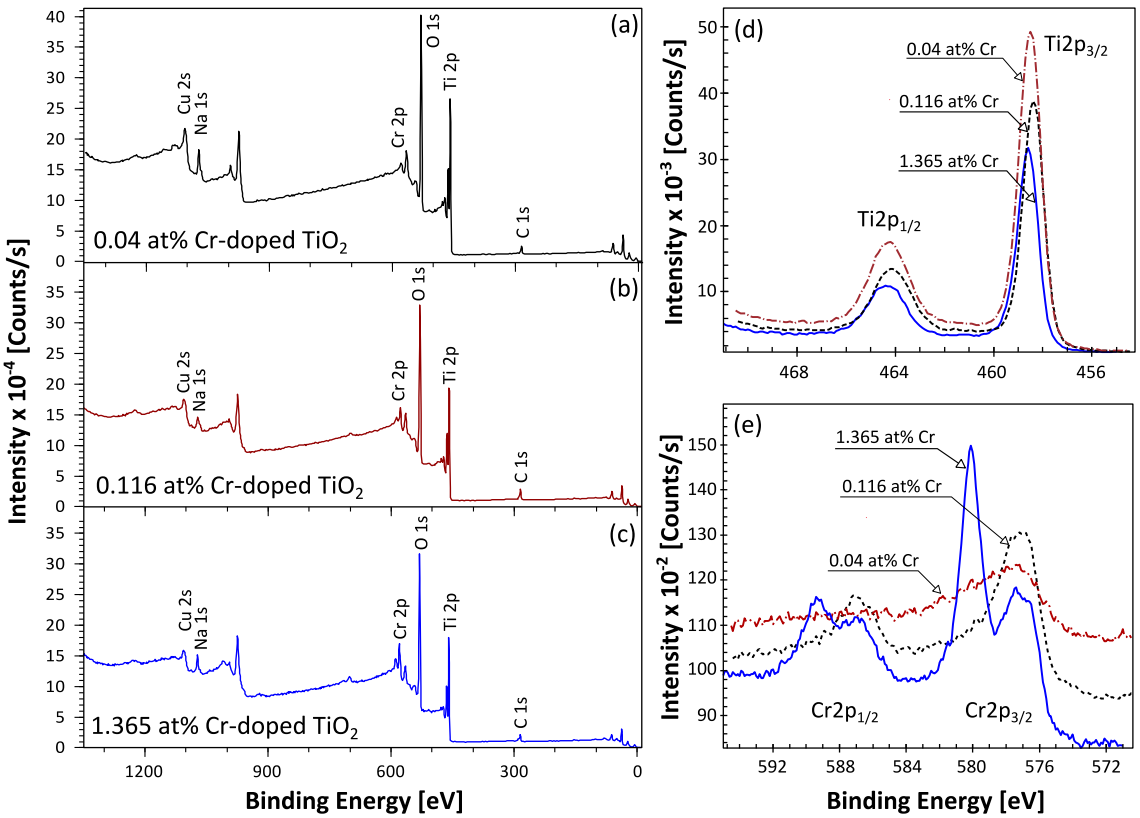

Figure 4.5. *The XPS survey spectra for (a-c) Cr-doped TiO_2 specimen annealed at 1373 K in artificial air, (d) the related Ti2p-related spectra and (e) Cr2p-related spectra for 0.04 at%, 0.116 at% and 1.365 at% Cr-doped TiO_2.*

As seen in **Figure 4.5d**, the intensity of the Ti2p-related peaks decreases with the increasing chromium concentration. This decrease is consistent with the increasing content of chromium in Cr-doped TiO_2. As also seen in **Figure 4.5e**, the Cr2p-related peaks increase with the increasing chromium content.

For evaluating the surface oxidation state of chromium, the chromium-related peaks (**Figure 4.5e**) were deconvoluted using the *casaXPS* software [21]. The Cr2p spectra of Cr-doped TiO_2, including the experimental XPS data (red dots), as well as the shape of the de-convoluted signals related to Cr^{3+} and Cr^{6+} ions, are shown in **Figure 4.6**.

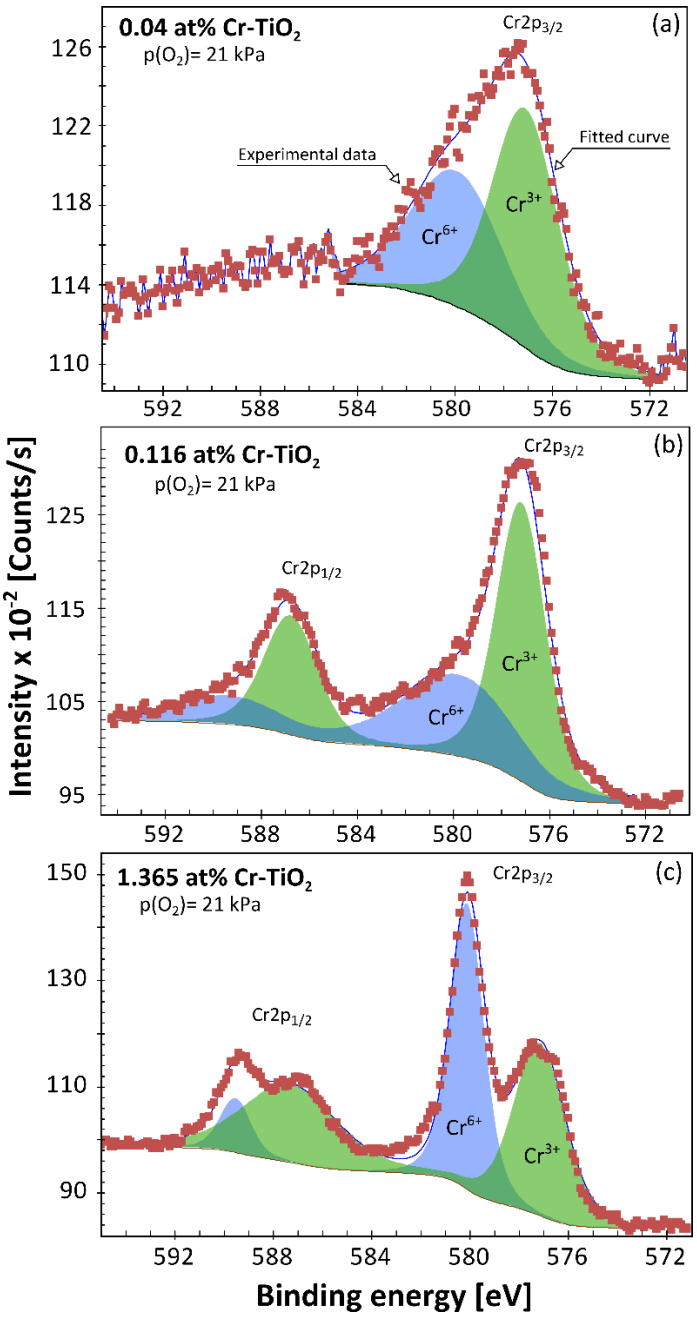

Figure 4.6. *The Cr2p-related spectra for Cr-doped TiO_2 processed at 1373 K in $p(O_2)$ = 21 kPa. (a) 0.04 at%, (b) 0.116 at% and (c) 1.365 at% Cr-doped TiO_2. The de-convoluted signals for the chromium oxidation state are shown within the spectra.*

The results of the investigations, including i) the binding energy of chromium species, ii) the relative amount of these species according to **Figure 4.6**, iii) the obtained surface chromium concentration and iv) the segregation-induced enrichment factor (EF), are presented in **Table 4.3**.

Table 4.3. *The binding energy of the predominant chromium species and their percentage within the surface layer for Cr-doped TiO_2 annealed in artificial air at 1373 K according to XPS.*

Specimen	Species	Percentage	Binding energy [eV]	Surface Cr/Ti	Surface Cr content [at%]	Enrichment factor
0.04 at% Cr	Cr^{3+} Cr^{6+}	56.15 43.85	577.08 579.90	*	*	*
0.116 at% Cr	Cr^{3+} Cr^{6+}	63.22 36.78	577.15 & 586.75 579.78 & 589.38	0.087	8.61	74.27
1.365 at% Cr	Cr^{3+} Cr^{6+}	58.55 41.45	577.15 & 587.28 580.11 & 589.52	0.213	18.81	13.78

*Lack of the data points is related to the sensitivity limit of the applied surface analysis technique, XPS

As seen, the trivalent oxidation state of chromium, Cr^{3+}, is the predominant species (approximately 60%) of the Cr-doped TiO_2 specimens annealed in air ($p(O_2)$ = 21 kPa). These results are consistent with the reports of Lopez et al. [10] and Mardare et al. [22]. The obtained results of the segregation-related surface chromium concentrations in **Table 4.5** may be considered in terms of the following points:

i) Dilute Solid Solution (0.04 at% Cr). The segregation-related data at this composition is below the level expected for segregation equilibrium since segregation of chromium in the dilute system is strongly affected by the kinetics factor. Moreover, the concentration of solute at this level is at the border of the XPS detectability limit.

ii) Medium Concentration (0.116 at% Cr). The data point related to this composition corresponds to segregation equilibrium or close to equilibrium.

iii) High Concentration (1.365 at% Cr). This data point corresponds to the equilibrium state of the entire system, involving the surface layer, the bulk phase, and the gas phase.

4.3.1.2 Secondary Ion Mass Spectrometry

The typical SIMS spectra for Cr-doped TiO_2 involving 0.116 at% Cr annealed at 1373 K in the gas phase of controlled oxygen activity, in terms of intensity profiles as a function of sputtering time, are presented in **Figure 4.7**. These spectra correspond to the specimens annealed in (a) oxidizing, imposed by artificial air, and (b) reducing conditions

imposed by the argon-hydrogen mixture. The related oxygen activities are reported in Chapter 3, section 3.2.3.

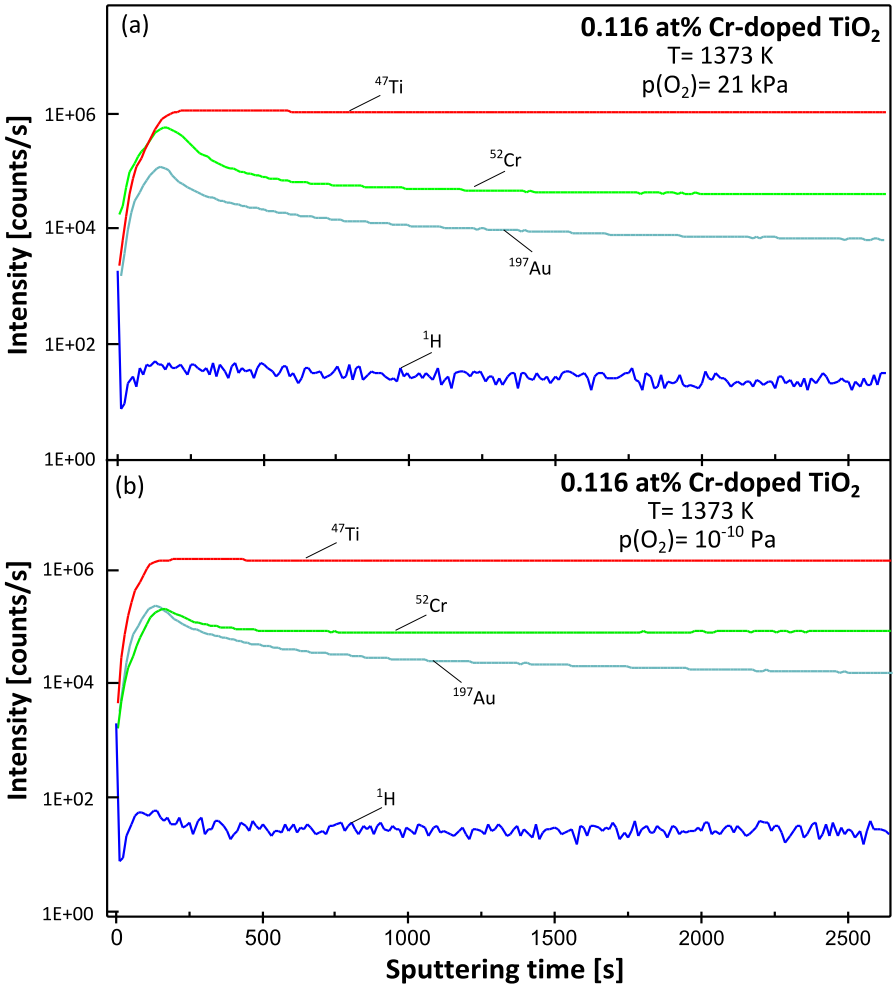

Figure 4.7. *The SIMS intensity data as a function of sputtering time for Cr-doped TiO_2 (0.116 at% Cr) for selected species in the secondary beam. The specimens were annealed at 1373 K in (a) artificial air and (b) in reducing gas mixture.*

As seen, the intensity profiles of both ^{52}Cr and ^{197}Au have a tendency to initially increase, reach a maximum and then decrease with the notable exception of hydrogen ions. In the latter case, the intensity sharply decreases, assumes minimum and then assumes a constant level that is slightly larger for the specimen annealed in reducing conditions. As also seen, the intensity profile of ^{47}Ti ions after the initial rise assumes a constant level. The latter will be used as a reference in considering the depth profiles of chromium in

terms of the intensity of ^{52}Cr. Therefore, the segregation-induced enrichment factor of chromium will be calculated using the following expression:

$$EF = \frac{(I_{Cr})_{surface}}{(I_{Cr})_{bulk}} \tag{4.2}$$

where the terms $(I_{Cr})_{surface}$ and $(I_{Cr})_{bulk}$ represent the intensity at the distance from the surface. Considering the depth of the crater, the time of sputtering was converted into the depth profile of I_{Cr} as a function of distance from the surface, as represented in **Figure 4.8**.

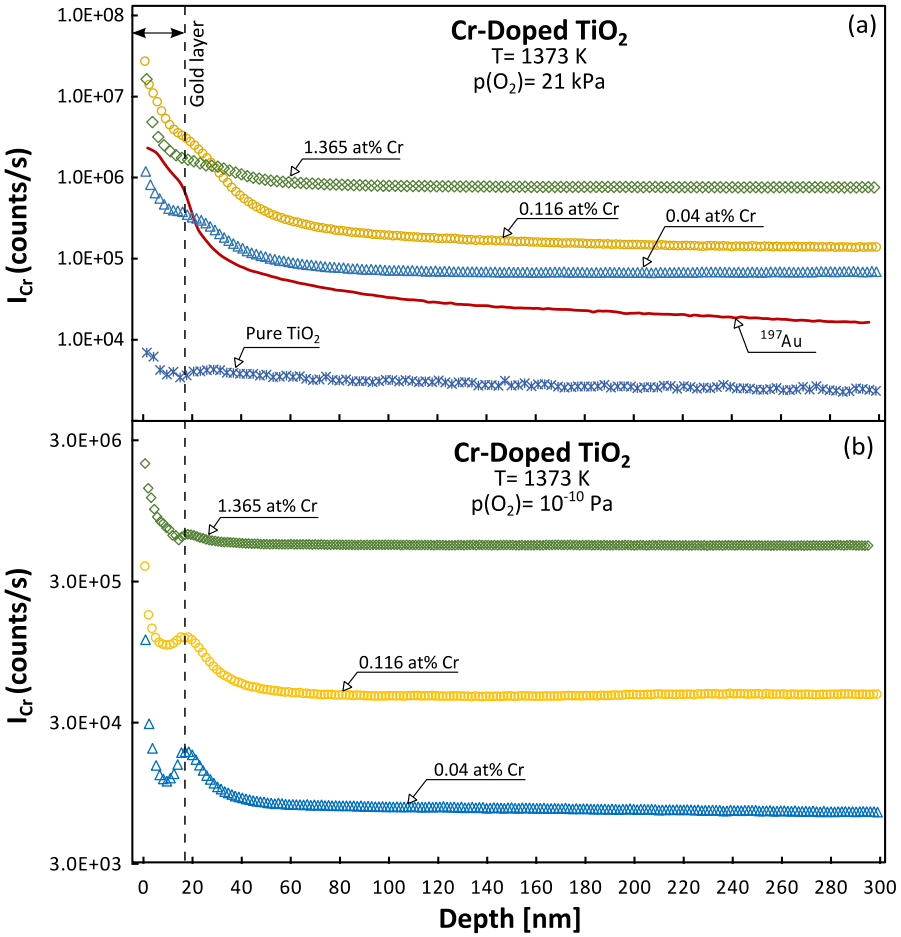

Figure 4.8. *The SIMS-related intensity of ^{52}Cr as a function of depth for Cr-doped TiO_2 after annealing (a) in artificial air and (b) in reducing gas mixture (the gold-related profile serves as a morphology-related tracer).*

As seen, the applied annealing conditions influence the shape of the intensity profiles as well as the related absolute values. To convert the intensity to concentration vs. depth profiles of solute, such as chromium, the following procedure can be applied:

i) *Determination of the morphology effect*. The thickness of the surface layer affected by the morphology is determined by the character of the intensity depth profile of tracer ions, such as gold. As seen in **Figure 4.8**, the initial 15 nm from the surface is considered as the gold layer. Due to the porosity of polycrystalline specimen, one might expect to get gold related spectra in the sub-surface layer, which is the phenomena in the presented study.

ii) *Determination of intensity-related enrichment factor*. The intensity depth profiles of the solute (chromium) after removing the gold layer are used for the determination of the related enrichment factor from equation (**4.2**), as illustrated in **Figure 4.9**.

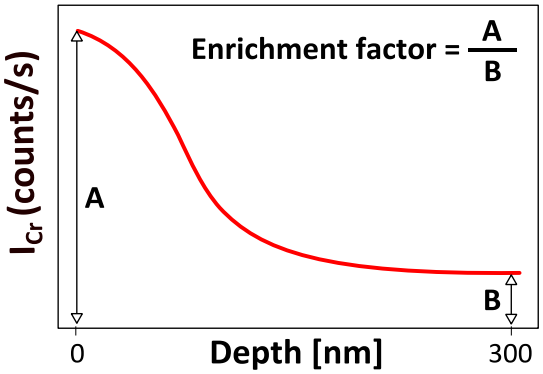

Figure 4.9. *Schematic representation of the determination of enrichment factor of chromium in Cr-doped TiO_2.*

iii) *Definition of the bulk level*. It is assumed that the intensity of the solute (chromium) at the distance of 300 nm from the surface corresponds to the bulk content as determined by the bulk-related technique, such as PIXE (**Table 3.3**). This level is assumed as a reference level.

iv) *Determination of concentration-related depth profile*. It is assumed that the concentration of the solute vs. depth is equal to the product of the enrichment factor determined by equation (**4.2**) and the bulk level concentration determined in point *(iii)*.

Following the above procedures, the segregation-induced enrichment factor and the related surface chromium concentration, as a function of bulk chromium concentration were determined from **Figure 4.8**. The results are shown in **Figure 4.10**.

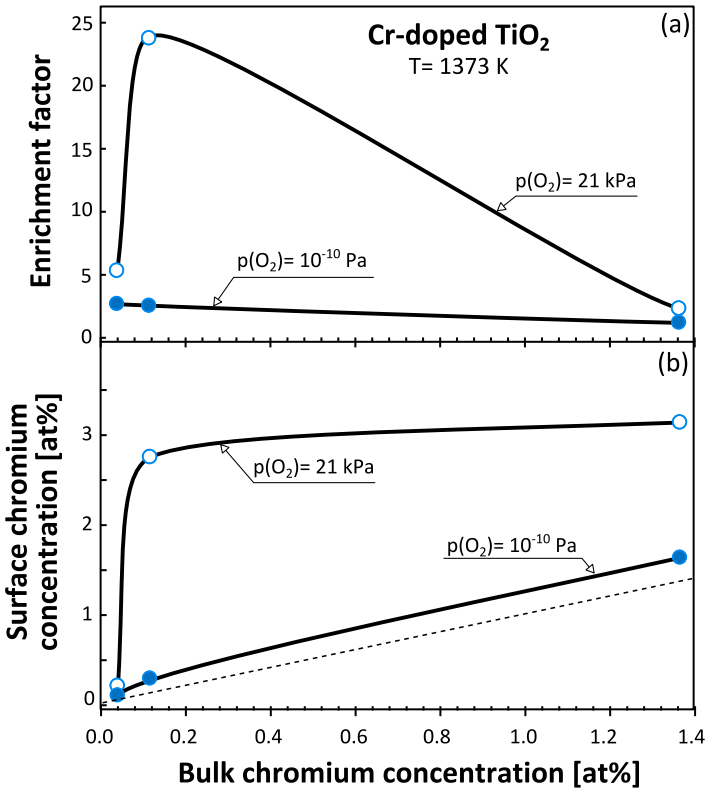

Figure 4.10. *Effect of bulk chromium concentration on (a) the segregation-induced enrichment factor and (b) the related surface chromium concentration for the specimens annealed in $p(O_2)$ = 21 kPa and 10^{-10} Pa.*

The effect of bulk chromium concentrations on the surface composition strongly depends on the oxygen activity during annealing. As seen in **Figure 4.10**, in reducing conditions, $p(O_2)$ = 10^{-10} Pa the effect of bulk chromium on the surface chromium concentration is insignificant (the related enrichment factor remains about 2). Whereas, the segregation-induced enrichment of the surface layer in chromium at $p(O_2)$ = 21 kPa is substantial. The related enrichment factor is 2.3 at 1.365 at% Cr and increases to 23.75 at 0.116 at% Cr (the observed decrease of the enrichment at 0.04 at% Cr is affected by the detectability of chromium at this dilution).

4.3.2 Effect of Oxygen Activity

4.3.2.1 X-ray Photoelectron Spectroscopy

The Cr2p-related spectra obtained from the XPS technique for 0.04 at% Cr-doped TiO_2 were deconvoluted in order to determine the surface chromium oxidation state. Such spectra are shown in **Figure 4.11**.

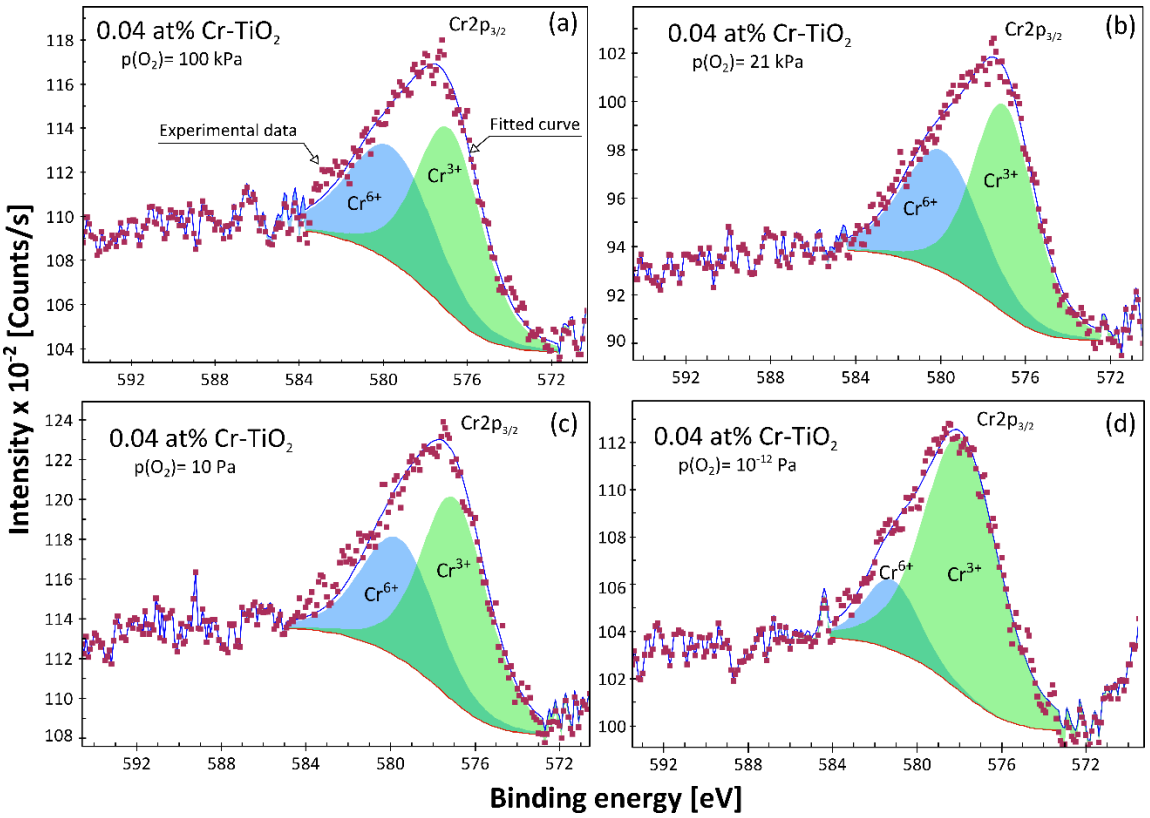

Figure 4.11. *Cr2p-related spectra for 0.04 at% Cr-doped TiO_2 annealed at 1273 K in the gas phase of controlled oxygen activity, including (a) $p(O_2)$ = 100 kPa, (b) 21 kPa, (c) 10 Pa and (d) 10^{-12} Pa. The de-convoluted spectra for both Cr^{3+} and Cr^{6+} species are marked by different shading intensity.*

The concentrations of the chromium species in the studied specimens of Cr-doped TiO_2, determined from the related surface area, are represented in **Figure 4.12** as a function of the oxygen activity.

As seen, the increase of oxygen activity results in a gradual transition from tri-valent chromium species, Cr^{3+}, as the predominant species in reduced conditions, to the mixture of the comparable concentration of both Cr^{3+} and Cr^{6+} species in oxidizing conditions.

The concentration of surface chromium for 0.04 at% Cr-doped TiO_2 specimens was undetectable due to the limitation of XPS technique. However, the surface concentration of chromium was able to be determined by the SIMS technique which is presented in the following section.

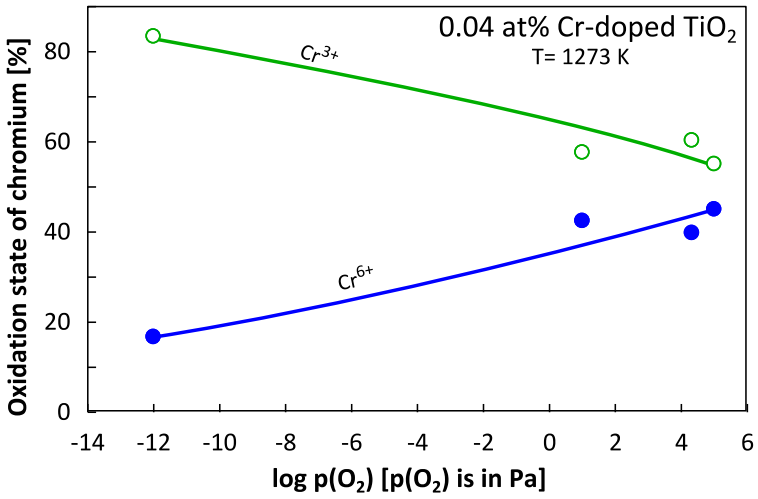

Figure 4.12. *Effect of oxygen activity on the concentration of chromium species at the surface of 0.04 at% Cr-doped TiO_2.*

4.3.2.2 Secondary Ion Mass Spectrometry

The results of the SIMS analysis, which reflect the effect of oxygen activity on the depth profiles of chromium in Cr-doped TiO_2, are represented in **Figure 4.13** in terms of the intensity of ^{52}Cr.

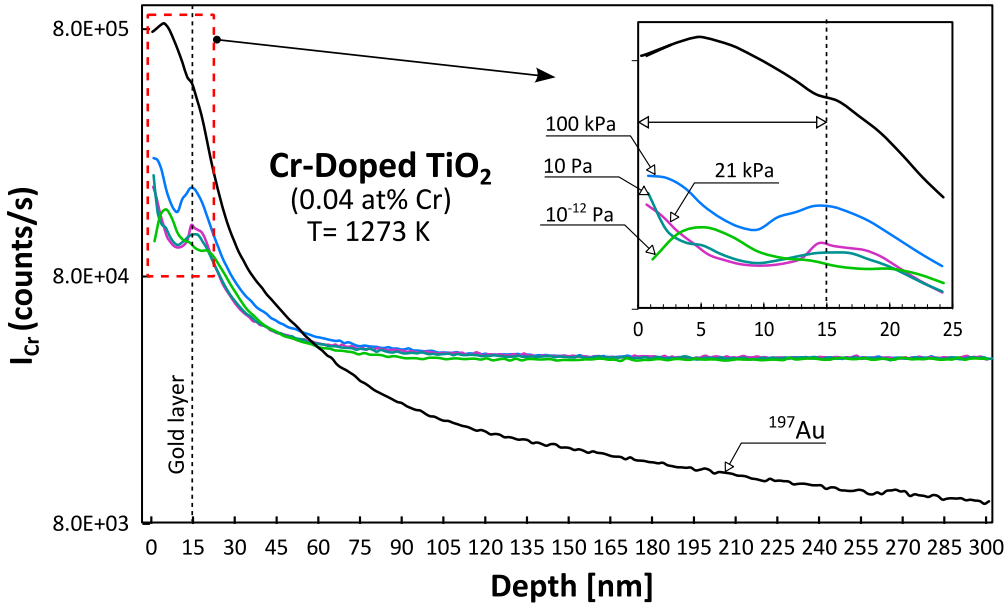

Figure 4.13. *The SIMS depth profiles of 0.04 at% Cr-doped TiO_2 annealed at 1273 K in different oxidizing conditions: $p(O_2)$ = 100 kPa, 21 kPa, 10 Pa, and 10^{-12} Pa as well as the gold-related tracer line. The insert shows the enlargement of the initial part of the depth profile related to 25 nm from the surface.*

The effect of the oxygen activity on the enrichment factor, EF, was determined as described in the previous section in equation (**4.2**). Then, the surface concentration of chromium, as a function of the oxygen activity, was determined by multiplying the bulk concentration. The resulting EF is shown in **Figure 4.14**.

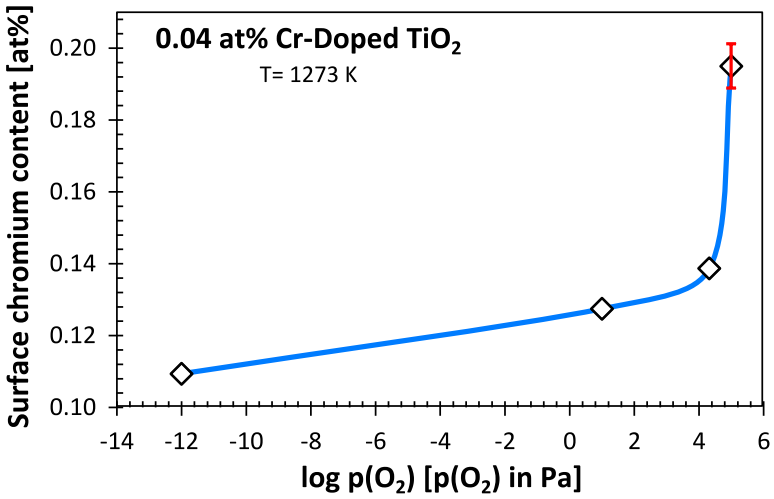

Figure 4.14. *The effect of oxygen activity on the surface chromium concentration for Cr-doped TiO_2. The error bar was calculated based on the measurements in seven different positions at the surface of a specimen annealed in $p(O_2)$ = 100 kPa.*

As seen, the surface chromium concentration increases with oxygen activity while the maximum of 0.19 at% is related to $p(O_2)$ = 100 kPa and the minimum of 0.11 at% is related to $p(O_2) = 10^{-12}$ Pa.

4.3.3 Theoretical Model

Derivation of the theoretical model that explains chromium segregation in polycrystalline Cr-doped TiO_2 in oxidizing and reducing conditions is based on the following assumptions:

i) The surface layer of TiO_2 in oxidizing conditions is enriched with titanium vacancies, which are formed at the surface and quenched within the surface layer due to an extremely low diffusion coefficient (**Table 4.2**). As such, the surface is charged negatively compared to the bulk phase.

ii) The surface layer is enriched with the mixture of both Cr^{3+} and Cr^{6+} species of comparable concentrations in oxidizing conditions (**Table 4.3** and **Figure 4.12**).

The charge of these species, compared to the lattice, depends on the mechanism of their incorporation that involves the following reactions:

a. The Cr^{3+} species may be introduced into the TiO_2 lattice according to either substitutional or interstitial mechanisms. The respective mechanisms for Cr^{3+} incorporation in reactions (**2.8**), (**2.10**) - (**2.12**). Reaction (**2.8**) leads to the formation of negatively charged chromium species, which in the electric field, induced by the surface layer, will have the tendency to be removed from the surface. Since the ionic mismatch between the chromium 3+ ions (r = 0.0615 nm [23, 24]) and titanium host ions (r = 0.0605 nm [23, 24]) is minimal, the related driving force of segregation can be ignored.

b. The Cr^{6+} species may be introduced into the TiO_2 lattice according to either substitutional or interstitial mechanisms, as represented in reaction (**2.20**) - (**2.22**). These reactions lead to the formation of positively charged chromium species, which in the electric field induced by the surface layer, will have the tendency to segregate to the surface. The predominant driving force of segregation is the electrostatic one.

iii) In reducing conditions, the predominant defect at the surface is oxygen vacancy. The XPS study shows that the predominant chromium species is Cr^{3+}, which incorporates following the mechanism (**2.6**). This reaction leads to the formation of negatively charged chromium species, which in the electric field, induced by the surface layer, will have the tendency to segregate to the surface.

iv) Considering that the predominant driving force in all cases is the electrostatic one, the theoretical model representing the surface vs. bulk concentration of chromium in Cr-doped TiO_2 may be considered in terms of the components related to the concentration gradients of different chromium species, as represented in **Figure 4.15**.

As seen, the proposed model indicates that the negatively charged surface layer enriched in titanium vacancies, V_{Ti}'''', attracts the transport of positively charged chromium ions ($Cr_i^{\bullet\bullet\bullet}, Cr_{Ti}^{\bullet\bullet}, Cr_i^{\bullet\bullet\bullet\bullet\bullet\bullet}$) from the bulk to the surface. The consequence of the transport is an accumulation of defects leading to the formation of larger defect aggregates within

the surface layer [25]. The formation of such defect aggregates is represented by equations (**4.3**) - (**4.5**).

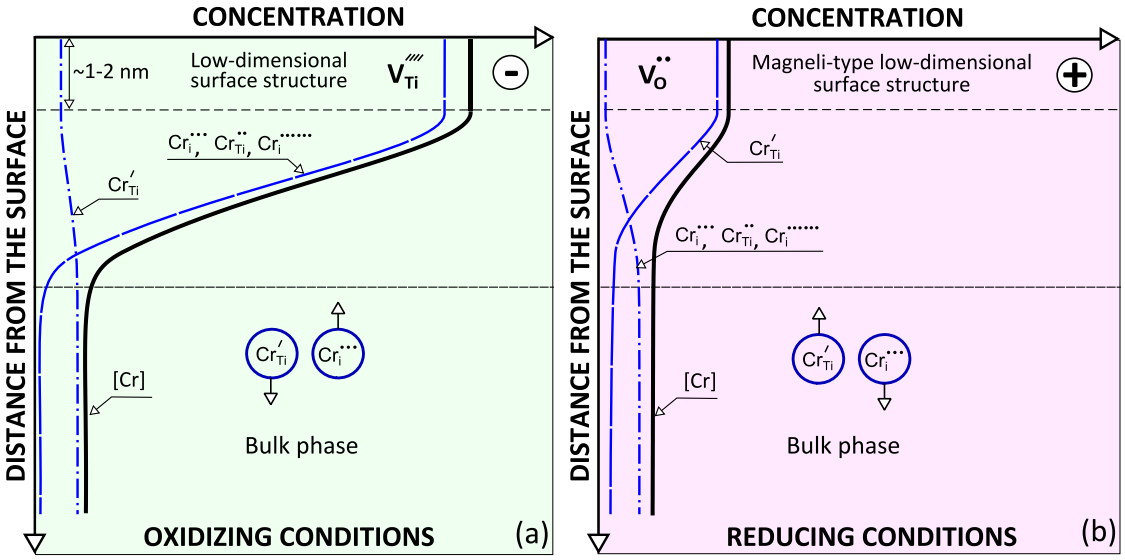

Figure 4.15. *The schematic representation of surface vs. bulk chromium concentration in Cr-doped TiO_2 in (a) oxidizing and (b) reducing conditions (the square bracket denotes total chromium concentration and arrows attached to the encircled chromium species indicate their diffusion direction).*

$$Cr_i^{\cdots} + V_{Ti}^{////} \rightarrow \left\{ Cr_i^{\cdots} V_{Ti}^{////} \right\}^{\prime} \tag{4.3}$$

$$Cr_{Ti}^{\cdot\cdot} + V_{Ti}^{////} \rightarrow \left\{ Cr_{Ti}^{\cdot\cdot} V_{Ti}^{////} \right\}^{\prime\prime} \tag{4.4}$$

$$Cr_i^{\cdot\cdot\cdot\cdot\cdot\cdot} + V_{Ti}^{////} \rightarrow \left\{ Cr_i^{\cdot\cdot\cdot\cdot\cdot\cdot} V_{Ti}^{////} \right\}^{\cdot\cdot} \tag{4.5}$$

As seen, these aggregates exhibit different effective valences. The reaction between these species is expected to form a local bi-dimensional surface structure. A better understanding of the related defect mechanisms, and of the properties of the local surface structure, is needed for the interpretation of the reactivity and light-induced reactivity of Cr-doped TiO_2.

4.3.4 Single Crystal vs. Polycrystalline Specimen

The SIMS depths profiles of the intensity of I_{Cr} for Cr-doped TiO_2 (0.05 at% Cr) single crystals annealed in both oxidizing and reducing conditions, as well as the as-polished specimen, are shown in **Figure 4.16**.

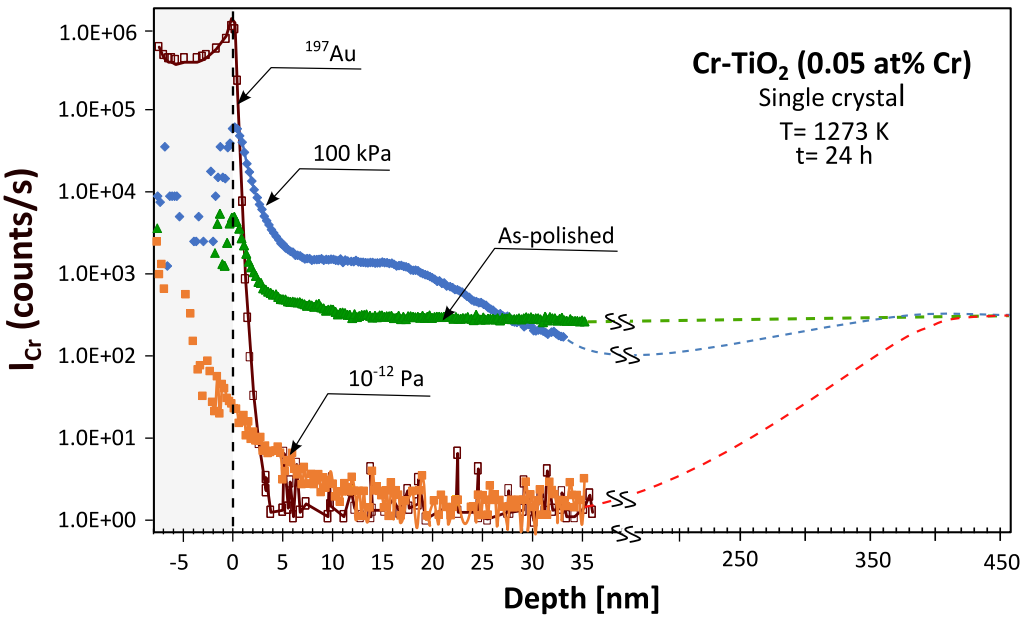

Figure 4.16. *SIMS intensity of chromium for Cr-doped TiO_2 single crystal annealed in oxidizing and reducing conditions as well as an as-polished specimen. The diagram also includes the intensity depth profile of gold. The shaded area indicates the thickness of the surface layer affected by gold.*

The diagram in **Figure 4.16** includes the profile of gold. The thin gold layer was deposited in order to remove the charge that build-up during sputtering. As seen, the surface layer affected by gold (its thickness is approximately 8 nm) exhibits a substantial scatter of data related to chromium. Therefore, the SIMS depth profile, taken above the 8 nm layer, was considered for quantitative analysis in the present work. The profile for the as-polished specimen was considered as the reference profile that below 15 nm corresponds to the bulk phase – the insignificant enrichment within the 15 nm thickness was induced by the process of polishing.

As seen, the specimen annealed in oxidizing conditions exhibits a substantial enrichment in chromium within the layer of 30 nm in thickness. As also seen, the specimen annealed in strongly reducing conditions exhibits a strong depletion of chromium. The intensity data related to chromium for the annealed specimens, which is still remote from the value expected for the bulk of the as-polished specimen, indicates that the bulk composition level is reached after prolonged sputtering leading to the removal of several hundreds of nanometers (compared to approximately 80 nm for polycrystalline specimens).

The resulting data of EF determined in oxidizing and reducing conditions for the TiO_2 single crystal, along with that for polycrystalline specimen (**Figure 4.13**), is shown in **Figure 4.17**.

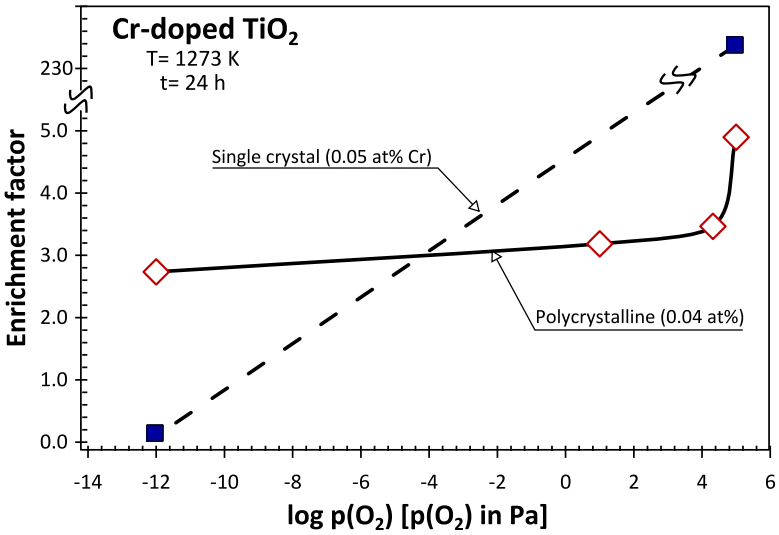

Figure 4.17. *The effect of oxygen activity on the enrichment factor, EF, for Cr-doped TiO_2 after annealing at 1273 K including single crystal and polycrystalline specimen.*

Knowledge of the bulk concentration of chromium, which is related to the results of the PIXE chemical analysis, and the enrichment factor shown in **Figure 4.17**, were used to determine the effect of oxygen activity on the surface vs. bulk concentration of chromium for both single crystal and polycrystalline specimens of Cr-doped TiO_2. The resulting comparative shapes of the concentration gradients are shown in **Figure 4.18**.

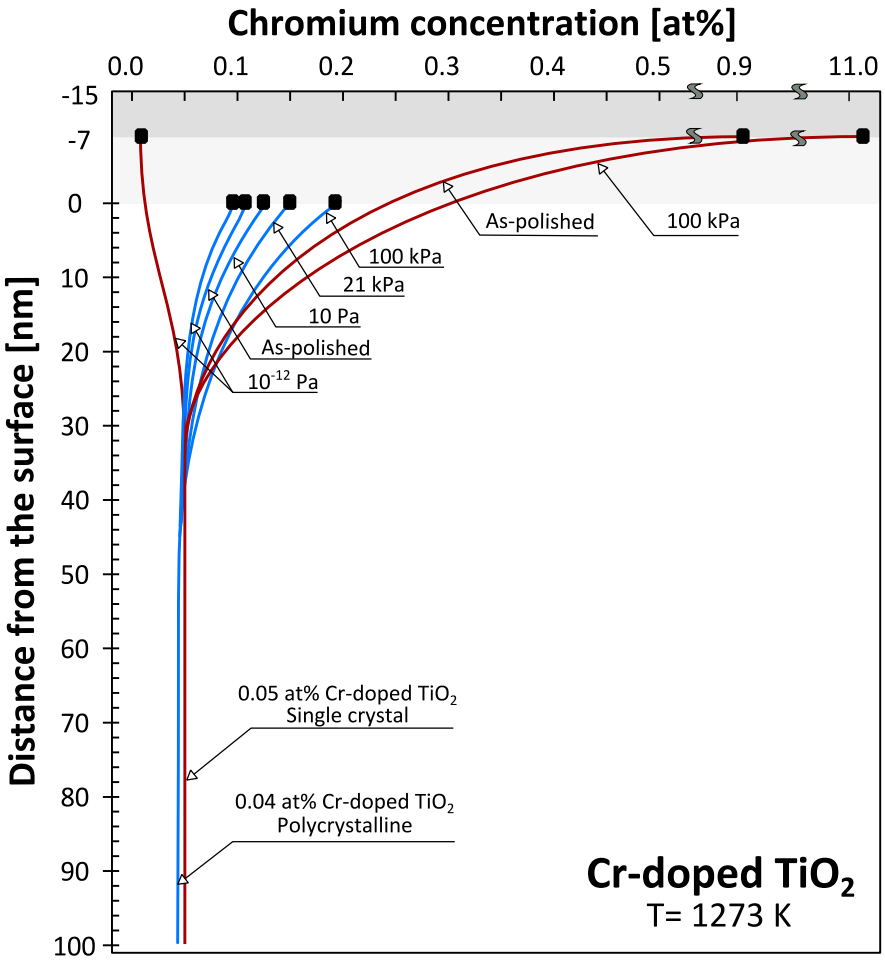

Figure 4.18. *The diagram representing the surface versus bulk concentration of chromium in both single crystal and polycrystalline specimens of Cr-doped TiO_2. The concentration gradient of chromium is shown after removing the gold layer of 8 nm for single crystal and 15 nm for polycrystalline specimen from the surface.*

On the top of the diagram in **Figure 4.18**, there are two shaded strips; the upper one is reflective of the 8 nm thick gold-affected layer for the single crystal, and the lower one corresponds to the 15 nm thick gold-affected layer for the polycrystalline specimen. Therefore, the concentration data for the layers beneath 15 nm are available for comparison of both specimens. These data points allow the following points to be made:

1. *Diffusion within the single crystal specimen free of linear defects*. The segregation-induced transport of chromium species is determined essentially by the crystal field of the periodic structure. This transport mechanism, which is induced by a well-defined homogeneous surface charge, allows the easy determination of the penetration distance.

2. *Diffusion in polycrystalline specimen*. The diffusion, in this case, should be considered in terms of the following complications;

   2.1. *The effect of the linear defects formed by intersections of grain boundaries with the external surface*. While the surface charge is of the same polarity, as is the case for the single crystal, the imposed electric field is reduced by the surface area of the linear defects, as characterized by the alternative defect disorder and voids. The schematic representation of the surface morphology of the polycrystalline specimens is shown in **Figure 4.19**.

   2.2. *The effect of grain boundaries*. In this case, the transport of charged chromium species towards the external surface is affected by the electrical potential gradient of the grain boundaries that exhibit an excess of electrons (**Figure 4.20**) [26].

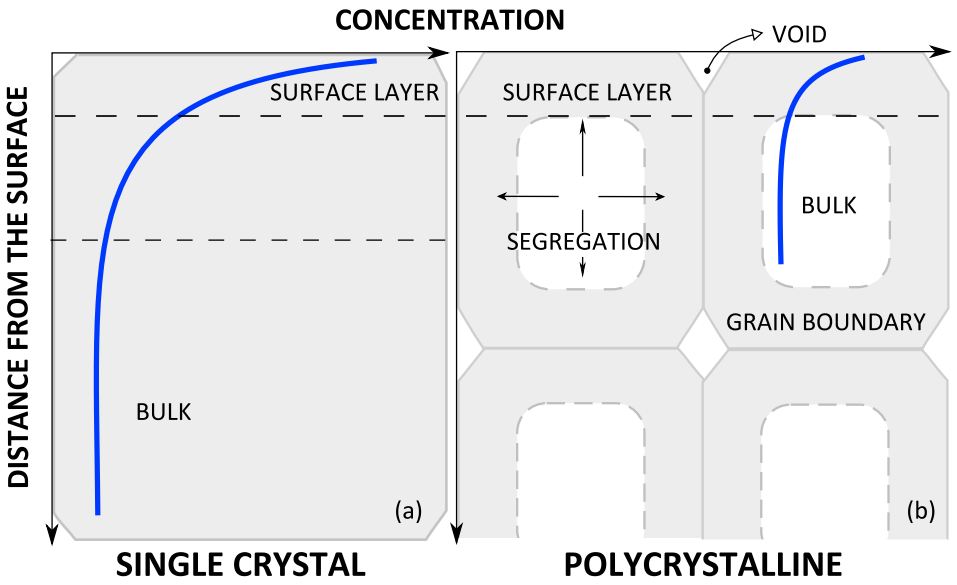

Figure 4.19. *Schematic representation of the morphology of the surface layer of (a) single crystal and the (b) polycrystalline specimen. The shaded area represents the grain boundary layer.*

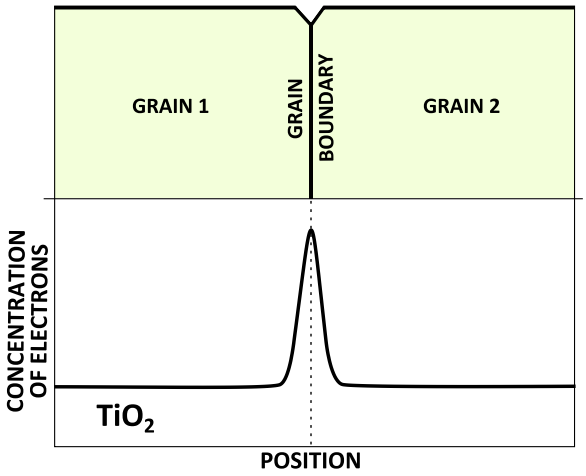

Figure 4.20. *Schematic representation of the concentration of electrons across grain boundaries [26].*

So far, the reported results on segregation in metal oxides are scarce and not reproducible. The main difficulty is the formation of systems with the reproducible morphology of polycrystalline specimens. In the case of single crystals, which are well-defined and free of macro-defects, the phenomenon of segregation may be considered mainly in terms of the temperature, the time of high-temperature treatment, the composition of the gas phase environment, the cooling procedure as well as the presence of contaminations, as detailed below.

i) *Impurities.* The segregation-induced concentration profile is well-defined when the specimen is free of impurities. It has been shown that attractive or repulsive interactions between two or more segregating species may have a substantial effect on both the kinetics and the segregation-induced enrichment [27].

ii) *Temperature.* The temperature treatment is critical for achieving segregation equilibrium in terms of the kinetic factor. While the increase of temperature favors the kinetics, the transport mechanism depends on the microstructure.

iii) *Time.* Time of annealing has a critical influence on the penetration distance.

iv) *Cooling.* The cooling process may lead to substantial changes in the segregation-induced concentration gradients. Therefore, fast cooling is the best approach to quench the segregation-related gradient corresponding to equilibrium.

v) *Oxygen activity.* The effect of oxygen activity in the gas phase environment on segregation may be considered in terms of the related gas/solid reactivity.

4.3.5 Effect of Segregation on the Formation of Low-dimensional Surface Structure

In order to better understanding of reactivity and performance in energy conversion of a semiconductor like TiO_2 knowledge of surface properties is crucial. A recent study shows that annealing of CoO at elevated temperatures a low-dimensional surface structure (LDSS) forms due to surface segregation, which is different from the bulk phase [28]. A schematic illustration is represented in **Figure 4.21**, showing the effect of segregation on the formation of structure in the bulk phase, near the surface and at the surface.

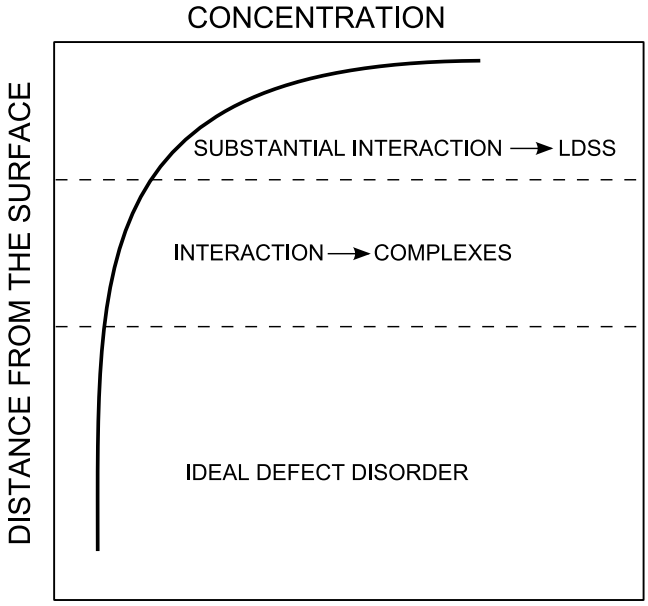

Figure 4.21. *Schematic representation of the formation of low-dimensional surface structure (LDSS) due to segregation.*

An ideal defect disorder for Cr-doped TiO_2 which has discussed in Chapter 2 is formed in the bulk phase after annealing at elevated temperature. A week interaction between the segregated defects leads to the formation of complexes in the near surface. A strong integration between the transported chromium species from bulk phase and the local defects leads larger aggregated defects (equations (**4.3**) - (**4.5**)) at the surface layer which forms a low-dimensional surface structure.

4.4 Chapter Summary

The obtained results allow the following general conclusions to be formulated:

i) The system of Cr-doped TiO_2 is a good templet for characterizing segregation in metal oxides and their solid solutions and the effect of segregation on properties. The matrix formed of TiO_2 is relatively well-defined in terms of its defect disorder and transport properties. The imposition of oxidizing conditions leads to the formation of the surface layer enriched with negatively charged titanium vacancies that, due to their low diffusivity, are quenched at the surface of the TiO_2 crystal. This surface charge is responsible for the electrostatic driving force of segregation, which is the predominant driving force of surface segregation for positively charged species in TiO_2 in oxidizing conditions. On the other hand, the imposition of reducing conditions results in the formation of a surface layer that is enriched in oxygen vacancies and related defect complexes and aggregates that are localized at the surface and charged positively. The related electric field is the predominant driving force of surface segregation for negatively charged species.

ii) In analogy to other oxide materials such as niobium-doped, indium-doped TiO_2, segregation in solid solutions of TiO_2 during annealing is sensitive to the oxygen activity of the gas phase during annealing [4, 29]. The sensitivity is related to the effect of oxygen on the defect disorder and the related surface charge that is determined by the segregation of intrinsic defects. It has been documented that the effect of oxygen activity in extreme cases may lead to either segregation-induced enrichment or depletion of the surface layer in chromium in oxidizing and reducing conditions, respectively. It is also shown that the charge of the segregated chromium species depends on the oxygen activity (see **Figure 4.12**).

iii) The properties of single crystals and polycrystalline specimens are entirely different. The differences between the two are determined by the microstructure of polycrystalline specimens. Therefore, the analysis of the effects associated with segregation in polycrystalline specimens requires knowledge of their microstructure.

4.5 References

[1] Marcus, H. and M. Fine, *Grain-Boundary Segregation in MgO-Doped Al_2O_3.* Journal of the American Ceramic Society, 1972. **55**(11): p. 568-570.

[2] Kuijers, F. and V. Ponec, *The surface composition of the nickel-copper alloy system as determined by Auger electron spectroscopy.* Surface Science, 1977. **68**: p. 294-304.

[3] Sikora, I., F. Stolze, and W. Hirschwald, *Segregation of chromium in CoO-Cr_2O_3 solid solutions and $CoCr_2O_4$ spinel phases studied by SIMS and ESCA.* Surface and Interface Analysis, 1987. **10**(8): p. 424-429.

[4] Atanacio, A.J., J. Nowotny, and K.E. Prince, *Effect of Oxygen Activity on Surface Composition of In-Doped TiO_2 at Elevated Temperatures.* The Journal of Physical Chemistry C, 2012. **116**(36): p. 19246-19251.

[5] Atanacio, A.J., T. Bak, and J. Nowotny, *Effect of Indium Segregation on the Surface versus Bulk Chemistry for Indium-Doped TiO_2.* ACS Applied Materials & Interfaces, 2012. **4**(12): p. 6626-6634.

[6] Atanacio, A.J., et al., *Segregation in Titanium Dioxide Co-Doped with Indium and Niobium.* Journal of the American Ceramic Society, 2017. **100**(1): p. 419-428.

[7] Jayamaha, U., et al., *Effect of oxygen activity on chromium segregation in Cr-doped TiO_2 single crystal.* Ionics, 2015. **21**(3): p. 785-790.

[8] Zhu, J., et al., *Hydrothermal doping method for preparation of Cr^{3+}-TiO_2 photocatalysts with concentration gradient distribution of Cr^{3+}*. Applied Catalysis B: Environmental, 2006. **62**(3–4): p. 329-335.

[9] Li, X., Z. Guo, and T. He, *The doping mechanism of Cr into TiO_2 and its influence on the photocatalytic performance.* Physical Chemistry Chemical Physics, 2013. **15**(46): p. 20037-20045.

[10] López, R., R. Gómez, and S. Oros-Ruiz, *Photophysical and photocatalytic properties of TiO_2-Cr sol–gel prepared semiconductors.* Catalysis Today, 2011. **166**(1): p. 159-165.

[11] Zhu, H., J. Tao, and X. Dong, *Preparation and photoelectrochemical activity of Cr-doped TiO_2 nanorods with nanocavities.* The Journal of Physical Chemistry C, 2010. **114**(7): p. 2873-2879.

[12] Chan, M.-H., et al., *Characterization of Cr-doped TiO_2 thin films prepared by cathodic arc plasma deposition.* Surface and Coatings Technology, 2007. **202**(4): p. 962-966.

[13] Peng, Y.-H., G.-F. Huang, and W.-Q. Huang, *Visible-light absorption and photocatalytic activity of Cr-doped TiO_2 nanocrystal films.* Advanced Powder Technology, 2012. **23**(1): p. 8-12.

[14] Li, Y., et al., *Gas sensing properties of p-type semiconducting Cr-doped TiO_2 thin films.* Sensors and Actuators B: Chemical, 2002. **83**(1–3): p. 160-163.

[15] Sōmiya, S., S. Hirano, and S. Kamiya, *Phase relations of the Cr_2O_3-TiO_2 system.* Journal of Solid State Chemistry, 1978. **25**(3): p. 273-284.

[16] Nowotny, M., T. Bak, and J. Nowotny, *Electrical properties and defect chemistry of TiO_2 single crystal. IV. Prolonged oxidation kinetics and chemical diffusion.* The Journal of Physical Chemistry B, 2006. **110**(33): p. 16302-16308.

[17] Sasaki, J., N. Peterson, and K. Hoshino, *Tracer impurity diffusion in single-crystal rutile (TiO_{2-x}).* Journal of Physics and Chemistry of Solids, 1985. **46**(11): p. 1267-1283.

[18] Zhang, Z., et al., *Surface cation nonstoichiometry in undoped $BaTiO_3$.* Journal of the Australasian Ceramic Society, 1998. **34**(1): p. 254-262.

[19] Sheppard, L., et al., *Application of secondary ion mass spectrometry in studies of niobium segregation in niobium-doped titanium dioxide.* 2007.

[20] Hofmann, J.P., M. Rohnke, and B.M. Weckhuysen, *Recent advances in secondary ion mass spectrometry of solid acid catalysts: large zeolite crystals under bombardment.* Physical Chemistry Chemical Physics, 2014. **16**(12): p. 5465-5474.

[21] Biesinger, M.C., et al., *Resolving surface chemical states in XPS analysis of first row transition metals, oxides and hydroxides: Cr, Mn, Fe, Co and Ni.* Applied Surface Science, 2011. **257**(7): p. 2717-2730.

[22] Mardare, D., et al., *Undoped and Cr-doped TiO_2 thin films obtained by spray pyrolysis.* Thin Solid Films, 2010. **518**(16): p. 4586-4589.

[23] Shannon, R.t., *Revised effective ionic radii and systematic studies of interatomic distances in halides and chalcogenides.* Acta Crystallographica Section A: Crystal Physics, Diffraction, Theoretical and General Crystallography, 1976. **32**(5): p. 751-767.

[24] Bechstein, R., et al., *Evidence for vacancy creation by chromium doping of rutile titanium dioxide (110).* The Journal of Physical Chemistry C, 2009. **113**(8): p. 3277-3280.

[25] Stoneham, A.M., *Theory of defect processes.* Physics Today, 1980. **33**(1): p. 34-37.

[26] Bak, T., et al., *Concentration of electrons at grain boundaries in TiO_2 (Rutile): Impact on charge transport and reactivity.* Catalysis Today, 2014. **224**: p. 200-208.

[27] Atanacio, A.J., et al., *Segregation in Titanium Dioxide Co-Doped with Indium and Niobium.* Journal of the American Ceramic Society, 2017. **100**(1): p. 419-428.

[28] Bak, T., et al., *Evidence of Low-Dimensional Surface Structures for Oxide Materials. Impact on Energy Conversion.* ACS Applied Energy Materials, 2018.

[29] Atanacio, A.J., T. Bak, and J. Nowotny, *Niobium segregation in niobium-doped titanium dioxide (rutile).* The Journal of Physical Chemistry C, 2014. **118**(21): p. 11174-11185.

Chapter 5
Photocatalytic Activity

This chapter reports the photocatalytic activity of Cr-doped TiO_2. The chapter considers several related effects, such as (i) the effect of chromium concentration on photocatalytic activity, (ii) the effect of oxygen activity in the lattice of Cr-doped TiO_2 on photocatalytic performance and (iii) the effect of electrochemical coupling of TiO_2 of different Fermi levels on photocatalytic properties. The reported experimental data result in the derivation of theoretical models that explain the mechanism of the photocatalytic process and allow a prediction of the effect of the defect disorder on photocatalytic performance and performance-related properties.

5.1 Literature Overview

5.1.1 Effect of Chromium on Photocatalytic Performance

The research project on photocatalysis of Cr-doped TiO_2 imposes the need to study the effect of chromium on the related properties, such as the electronic structure (reported in chapter 3) and surface-related properties (reported in chapter 4). In addition, the specific aim of the present project is to establish correlations between the photocatalytic properties and defect disorder of the photocatalytic system, which in this case, is based on Cr-doped TiO_2. The latter is discussed in chapter 2.

The reported data on the effect of chromium on the photocatalytic properties of TiO_2 (considered in terms of the rate constant of photocatalytic reaction) are represented in

Figure 5.1 and the results on alternative properties of Cr-doped TiO_2 are shown in Table 5.1 [1-14].

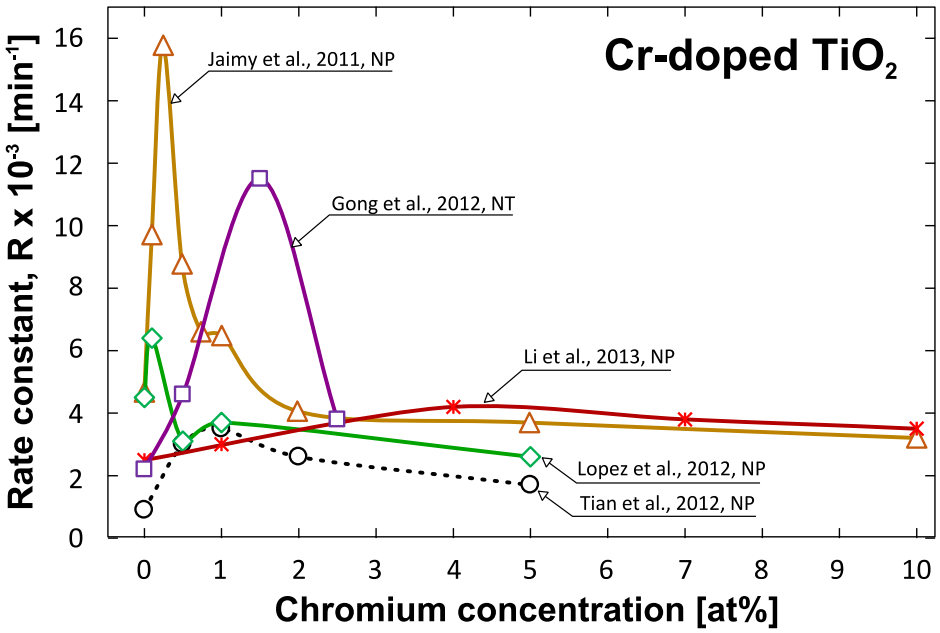

Figure 5.1. *The effect of chromium on the rate constant of photocatalytic removal for a range of organic compounds from water actions by Cr-doped TiO_2 (NP and NT correspond to nanoparticles and nanotube, respectively [1-5].*

As seen, the character of the reported dependences indicates that chromium enhances the performance for dilute solutions of chromium in TiO_2. However, at larger concentrations, the photocatalytic performance sharply decreases. This characteristic indicates that the mechanism and the kinetics of the photocatalytic reaction are different for dilute and concentrated solid solutions. As also seen, the reported data on photocatalytic performance exhibit a substantial scatter in terms of the compositions related to maximum performance, as well as absolute performance data. The conflicting data on the photocatalytic activity indicates that the effect of the applied processing procedure should be considered in terms of a range of alternative effects, including:

i) *Effect of electronic structure.* This point is related to the effect of chromium on the bandgap and the mid-gap levels.

ii) *Effect of segregation.* This point is related to the effect of segregation on surface vs. bulk properties.

iii) Effect of the incorporation mechanism. The reported data on chromium content involves chromium incorporated into the TiO_2 lattice as well as chromium introduced into grain boundaries. The effect of chromium in both cases is entirely different.

iv) Effect of phase composition. This effect takes into account that the studied TiO_2 specimens frequently involved the mixture of both anatase and rutile structures of unknown composition.

v) Effect of solubility. Chromium may enter the TiO_2 lattice only within the solubility limit. The data for Cr-doped TiO_2 in excess of this limit cannot be considered as a solid solution.

vi) Effect of gas phase composition. The effect of the gas phase composition, which can be considered in terms of its oxygen activity and humidity, is substantial.

vii) Effect of heterogeneous coupling. Frequently, the studied photocatalysts are activated by the deposition of islets of alternative phases of noble metals or oxides.

The effects related to electronic structure and segregation have been considered in chapters 3 and 4, respectively. The alternative effects are discussed below.

5.1.1.1 Effect of Chromium Incorporation Mechanism

Selected data on the effect of chromium on the mechanism of chromium incorporation into the TiO_2 lattice and the related electrical charge of chromium ions in the host lattice are shown in **Table 5.1**.

Table 5.1. *Selected data on the alternative properties of Cr-doped TiO_2.*

Authors	Determined properties	Conclusions
Jaimy et al. (2011) [1]	Incorporation of chromium into TiO_2 results in: • Decrease of bandgap in the range 0-10 at% Cr • Increase of photocatalytic activity up to 0.25 at% Cr.	• Reduction of the bandgap in the range 0.25 at% Cr leads to the reaction chain: ○ $Cr^{3+} \rightarrow Cr^{4+} + e^-$ ○ $e^- + O_2 \rightarrow O_2^-$ ○ $Cr^{4+} + OH^- \rightarrow OH^*$ • Interactions between lattice species in the range 0.25-10 at% Cr lead to less effective ionization of Cr-related acceptors
Gong et al. (2012) [2]	• Chromium results in enhanced photocatalytic activity up to 1.5 at% Cr • XPS shows the presence of Cr^{3+} ions only within the surface layer	• Cr^{3+} may be considered as either Cr'_{Ti} or $Cr_i^{\bullet\bullet\bullet}$ species or both • Positively charged Cr species leads to the formation of titanium vacancies
Li et al. (2013) [3]	• Chromium incorporation results in enhanced photocatalytic performance up to 4 at% Cr • Chromium results in bandgap reduction • Chromium leads to the formation of acceptor-type level • Surface area increases with chromium concentration	• Tri-valent chromium results in the formation of anodic sites up to 4 at% Cr • Interactions between chromium ions at high concentrations leads to decrease in photocatalytic observed above 4 at% Cr
Lopez et al. (2011) [4]	• Chromium leads to enhanced photocatalytic activity up to 0.16 at% Cr • Chromium incorporation leads to the formation of both Cr^{3+} (60%) and Cr^{6+} (40%) species at the surface (XPS analysis)	• Cr^{6+} forms either $Cr_{Ti}^{\bullet\bullet}$ or $Cr_i^{\bullet\bullet\bullet\bullet\bullet\bullet}$ species or both • Cr^{3+} forms either Cr'_{Ti} or $Cr_i^{\bullet\bullet\bullet}$ species or both • Positively charged Cr species can lead to the formation of titanium vacancies that form anodic surface sites
Tian et al. (2012) [5]	• Chromium results in enhanced photocatalytic performance up to 1at% Cr • The specimens involve both anatase and rutile phases • Chromium leads to the formation of Cr_2O_3 cluster at [Cr]>1at%	• The junction between rutile and anatase crystallites is the active reduction site that is responsible for photocatalytic activity • The Cr_2O_3 clusters are responsible for poor photocatalytic performance above 1 at% Cr
Mardare et al. (2010) [6]	• The XPS shows the presence of both Cr^{3+} (65%) and Cr^{6+} (35%) species at the surface • The water contact angle of 0.5 at% Cr-doped TiO_2 is lower than pure TiO_2	• Cr^{6+} forms either $Cr_{Ti}^{\bullet\bullet}$ or $Cr_i^{\bullet\bullet\bullet\bullet\bullet\bullet}$ species or both • Cr^{3+} forms either Cr'_{Ti} or $Cr_i^{\bullet\bullet\bullet}$ species or both
Diaz-Uribe et al. (2014) [7]	• The photocatalytic performance of Cr-doped TiO_2 (2.5 at% Cr) shows four times higher than undoped TiO_2 • Chromium incorporation results in the reduction of bandgap	The reduced bandgap of Cr-doped TiO_2 results enhanced light-induced ionization

Zhu et al. (2006) [8]	• Photocatalytic performance exhibits maximum at 0.25 at% Cr • Chromium results in bandgap reduction • XPS shows only Cr^{3+} species at the surface	• Cr^{3+} may be considered as either Cr'_{Ti} or $Cr_i^{\bullet\bullet\bullet}$ species or both • Positively charged Cr species leads to the formation of titanium vacancies • Defect interactions at > 0.25% Cr lead to less effective ionization of Cr-related acceptors
Peng et al. (2012) [9]	• Chromium incorporation (1.5 at%) results in an increase of the photocatalytic performance • The XPS shows Cr^{3+} species and the enhanced concentration of oxygen vacancy at the surface	Cr^{3+} may be considered as Cr'_{Ti} leading to the formation of oxygen vacancy
Choi et al. (2010) [10]	• Cr^{3+} doping (0.3 at%) results in enhanced of photocatalytic performance • Chromium leads to enhanced transition of anatase to rutile phase • Chromium incorporation results in the reduction of bandgap energy	The effect of chromium on the enhanced photocatalytic performance is related to increased light-induced bandgap ionization
Wilke and Breuer (1999) [11]	• Chromium doping (0.1-10 at%) leads to decrease photocatalytic performance • Chromium incorporation decreases the lifetime of photo-generated electron-hole	The reported data indicates that the photocatalytic performance is not related to the bandgap value
Ghasemi et al. (2009) [12]	• Chromium doping leads to enhanced photocatalytic performance • Chromium incorporation results in the reduction of bandgap	Reduced bandgap results in enhanced bandgap ionization
Jimmy et al. (2006) [13]	• The incorporation of chromium (2.5 at%) leads to enhanced photocatalytic performance • Chromium incorporation results in the reduction of bandgap	Reduction of bandgap results in enhanced photocatalytic activity
Koh et al. (2016) [14]	• Chromium doping up to 1 at% enhanced the photocatalytic performance • Bandgap decreases in the range of 0-4 at% Cr • XPS shows the presence of both Cr^{3+} and Cr^{6+} ions	• Cr^{6+} forms either $Cr_{Ti}^{\bullet\bullet}$ or $Cr_i^{\bullet\bullet\bullet\bullet\bullet\bullet}$ species or both • Cr^{3+} forms either Cr'_{Ti} or $Cr_i^{\bullet\bullet\bullet}$ species or both • Positively charged Cr species leads to the formation of titanium vacancies • Theoretical model (up to 1 at% Cr): ○ $Cr^{3+} \rightarrow Cr^{4+} + e^-$ ○ $Cr^{4+} + OH^- \rightarrow OH^*$ ○ $Cr^{6+} + e^- \rightarrow Cr^{5+}$ ○ $Cr^{5+} + O_{2(ads)} \rightarrow Cr^{6+} + O_2^-$

The data in **Table 5.1** may be summarized in the following points [1-14]:

i) It is a common perception that reduction of the bandgap results in enhanced photocatalytic performance [1-5]. However, the report of Wilke and Brauer [11] questions the impact of the bandgap on photocatalytic performance.

ii) The effect of chromium on performance has been considered in terms of its electrical charge [4, 6, 14]. Reports supporting this claim are conflicting.

iii) There has been an accumulation of reports indicating that the mechanism of chromium incorporation into the TiO_2 lattice is different in the bulk and at the surface. Specifically, it has been proposed that the bulk mechanism leads to the formation of predominantly acceptor-type ions, $Cr_{Ti}^{'}$, while the surface mechanisms involve the formation of donor-type ions, $Cr_{Ti}^{\bullet\bullet}$ [4, 6].

iv) The conflicting data are also considered in terms of the effect of the phase composition of the studied specimens. The related effects are considered in the following sections.

5.1.1.2 Phase Composition

It has been shown that chromium incorporation into the anatase phase results in its phase transition into rutile. The observed phase transition is facilitated by the amount of chromium and the temperature of the process.

The effect of chromium on the phase transition is represented in **Figure 5.2** in terms of the percentage of the anatase/rutile mixture as a function of chromium content [5, 10, 14-16].

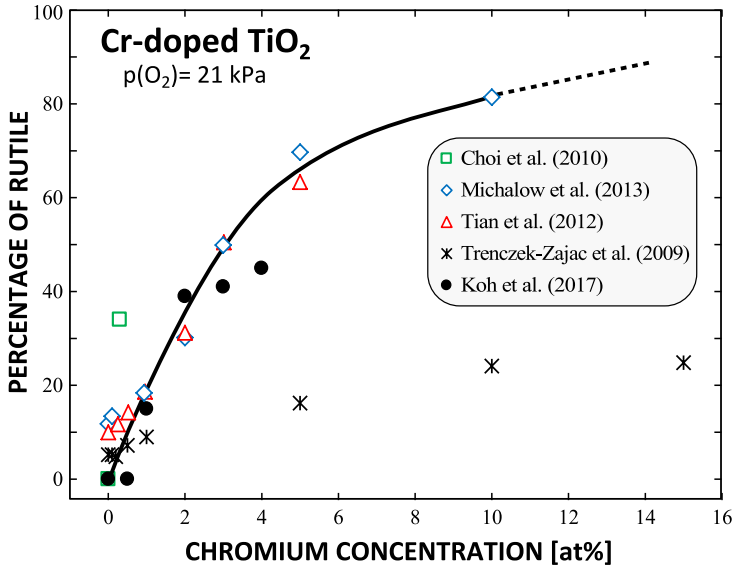

Figure 5.2. *Effect of chromium content in Cr-doped TiO_2 on phase composition of the rutile/anatase phase mixture [5, 10, 14-16].*

As seen, the increased chromium concentration results in an increased content of the rutile phase in the anatase/rutile phase mixture. These results indicate that chromium acts as a catalyst for the anatase-to-rutile phase transition. This effect results in the main complication in the interpretation of the effect of chromium on photocatalytic properties.

The effect of temperature on the phase transition of Cr-doped TiO_2, taking place in the gas phase of different oxygen activity is represented in **Figure 5.3**.

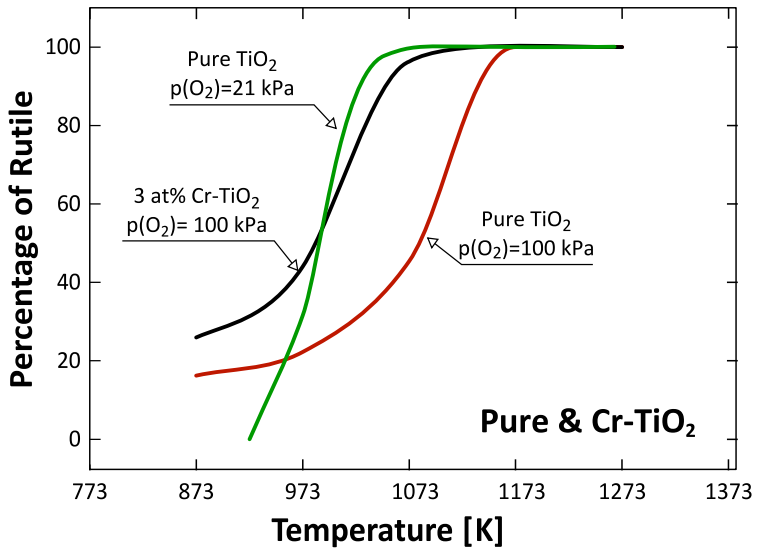

Figure 5.3. *Effect of temperature on the percentage of phase transition from anatase to rutile [17, 18].*

As seen, heating of the anatase phase in air and pure oxygen results in complete phase transitions of anatase into rutile at 1073 K and 1173 K respectively. A similar effect is observed for Cr-doped TiO_2 heated in oxygen [17, 18].

5.1.1.3 Solubility of Chromium in Titanium Dioxide

The effect of temperature on the solubility limit of chromium in TiO_2 in air is shown in **Figure 5.4**.

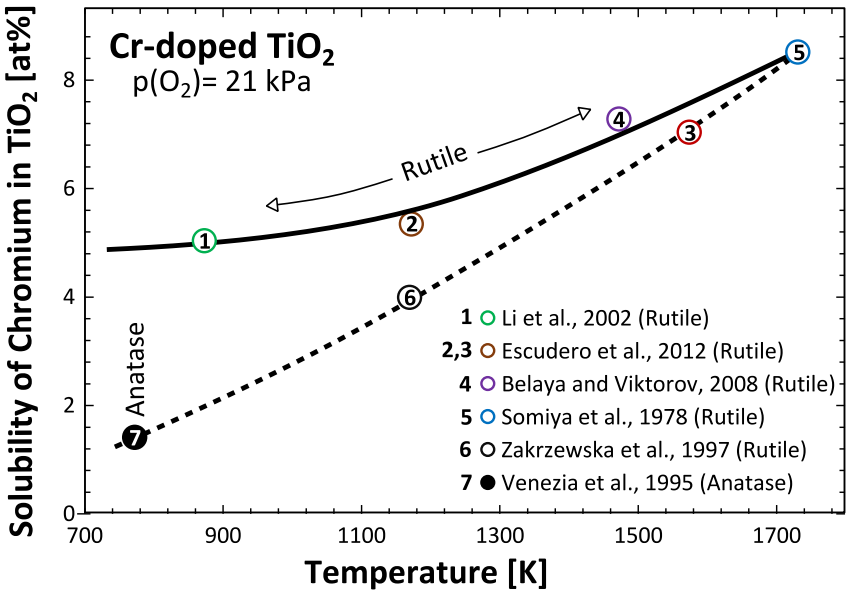

Figure 5.4. *Changes of solubility limit of chromium in TiO_2 with temperature at atmospheric pressure [19-24].*

As seen, the solubility limit of chromium in rutile (solid line) in air increases from 5 at 773 K to 8.5 at% at 1723 K. As also seen, the solubility of chromium in anatase (dashed line) is 1.6 at% at 773 K and increases with the temperature. The two solubility lines converge at 1723 K.

5.1.1.4 Effect of Oxygen in Gas Phase

Data summary of the literature on the effect of oxygen activity on the charge of chromium ions in the TiO_2 lattice is listed in **Table 5.2**.

As seen, the surface layer contains both tri- and hexavalent chromium incorporated into both substitutional and interstitial sites [4, 6, 25-27]. However, the effect of these defects on surface properties depends on charge compensation.

Table 5.2. *Literature reports on the effect of oxygen activity on the oxidation state of chromium in Cr-doped TiO_2 specimen (subscripts s and b correspond to the surface layer and the bulk phase respectively).*

Authors	Oxygen activity	Approach	Reported outcome	Plausible chromium incorporation mechanisms
Kohler et al. (1993) [28]	100 kPa	EPR	• $(Cr^{6+})_s$ when [Cr]≤ 0.61 at% • $(Cr^{6+})_s$ & $(Cr^{3+})_s$ when [Cr] ≥ 0.61 at%	• Cr^{6+} corresponds to either $Cr_{Ti}^{\bullet\bullet}$ or $Cr_i^{\bullet\bullet\bullet\bullet}$ species • Cr^{3+} corresponds to either $Cr_{Ti}^{\prime}$ or $Cr_i^{\bullet\bullet\bullet}$ species
Venezia et al. (1994) [29]	100 kPa	FT-IR	• $(Cr^{6+})_s$ • $(Cr^{3+})_b$	• Cr^{6+} forms either $Cr_{Ti}^{\bullet\bullet}$ or $Cr_i^{\bullet\bullet\bullet\bullet}$ species or both at the surface • Cr^{3+} forms either $Cr_{Ti}^{\prime}$ or $Cr_i^{\bullet\bullet\bullet}$ species or both in the bulk
Kohler et al. (1995) [30]	100 kPa	EPR	$(Cr^{6+})_s$	Cr^{6+} forms either $Cr_{Ti}^{\bullet\bullet}$ or $Cr_i^{\bullet\bullet\bullet\bullet}$ species or both
	H_2		$(Cr^{3+})_s$	Cr^{3+} forms either $Cr_{Ti}^{\prime}$ or $Cr_i^{\bullet\bullet\bullet}$ species
Kim et al (2014) [31]	100 kPa	DFT	Cr^{4+}	Cr^{4+} forms either Cr_{Ti} or $Cr_i^{\bullet\bullet\bullet\bullet}$ species or both
	10 Pa		Cr^{3+}	Cr^{3+} forms either $Cr_{Ti}^{\prime}$ or $Cr_i^{\bullet\bullet\bullet}$ species
Koh et al. (2017) [14]	21 kPa	XPS	$(Cr^{3+})_s$ & $(Cr^{6+})_s$	Cr^{3+} forms either $Cr_{Ti}^{\prime}$ or $Cr_i^{\bullet\bullet\bullet}$ species or both with $Cr_{Ti}^{\bullet\bullet}$ or $Cr_i^{\bullet\bullet\bullet\bullet}$ species or both
Lopez et al. (2011) [4]	21 kPa	XPS	60% $(Cr^{3+})_s$ & 40% $(Cr^{6+})_s$	Cr^{3+} forms either $Cr_{Ti}^{\prime}$ or $Cr_i^{\bullet\bullet\bullet}$ species or both with $Cr_{Ti}^{\bullet\bullet}$ or $Cr_i^{\bullet\bullet\bullet\bullet}$ species or both
Mardare et al. (2010) [6]	21 kPa	XPS	65% $(Cr^{3+})_s$ & 35% $(Cr^{6+})_s$	Cr^{3+} forms either $Cr_{Ti}^{\prime}$ or $Cr_i^{\bullet\bullet\bullet}$ species or both with $Cr_{Ti}^{\bullet\bullet}$ or $Cr_i^{\bullet\bullet\bullet\bullet}$ species or both
Santara et al. (2016) [32]	21 kPa	XPS	$(Cr^{3+})_s$ & $(Cr^{6+})_s$	Cr^{3+} forms either $Cr_{Ti}^{\prime}$ or $Cr_i^{\bullet\bullet\bullet}$ species or both with $Cr_{Ti}^{\bullet\bullet}$ or $Cr_i^{\bullet\bullet\bullet\bullet}$ species or both
Wang and Egerton (2013) [33]	21 kPa	XPS	19.8% $(Cr^{3+})_s$ & 81.2% $(Cr^{6+})_s$	Cr^{3+} forms either $Cr_{Ti}^{\prime}$ or $Cr_i^{\bullet\bullet\bullet}$ species or both with $Cr_{Ti}^{\bullet\bullet}$ or $Cr_i^{\bullet\bullet\bullet\bullet}$ species or both
Belaya and Viktorov (2008) [21]	21 kPa	Photocolorimetry	$(Cr^{6+})_s$	Cr^{6+} forms either $Cr_{Ti}^{\bullet\bullet}$ or $Cr_i^{\bullet\bullet\bullet\bullet}$ species or both
	10 Pa		$(Cr^{3+})_s$	Cr^{3+} forms either $Cr_{Ti}^{\prime}$ or $Cr_i^{\bullet\bullet\bullet}$ species or both
Osterwalder et al. (2005) [34]	2.67×10^{-3} Pa	XPS	$(Cr^{3+})_s$	Cr^{3+} forms either $Cr_{Ti}^{\prime}$ or $Cr_i^{\bullet\bullet\bullet}$ species or both

The effect of chromium on the properties of TiO_2 at room temperature depends on the effect of the applied cooling procedure and the associated change of defect equilibria within the outermost surface layer. So far, little is known on this matter.

5.1.2 Electrochemical Couples

The electrochemical coupling consists in bringing two or more phases into galvanic connection. As a result, the coupling leads to the formation of a functional electrochemical chain. Heterogeneous systems, involving the coupling of different phases, are defined in Chapter 2.

The present section considers the effect of metal islets on the photocatalytic performance of TiO_2. The results on the effect of the heterogeneous couples are presented in **Tables 5.3 and 5.4** [35-46].

Table 5.3. *Selected reports on photocatalytic activity of the couples formed of noble metals and TiO_2.*

Authors	Studied system	Reported outcome
Chandrasekharan & Kamat (2000) [35]	Au/TiO_2/glass plate (Au diameter: 5nm), TF	• Apparent flat-band potential become more negative for Au/TiO_2 • The incident photon to charge carrier generation efficiency (IPCE) for Au/TiO_2 is higher than TiO_2 film
Subramanian et al. (2004) [36]	Au/TiO_2 (Au diameter: 3-8 nm), TF	• Apparent flat-band potential is more negative at 3 nm diameter of Au • The maximum photocatalytic performance is at 3 nm diameter Au/TiO_2 sample
Li et al. (2007)[37]	Au/TiO_2 (0.1-5mol% Au), PC	• Photocatalytic activity of TiO_2 depends on the size of Au islet. Maximum photocatalytic performance is at 5 nm diameter of Au (0.5mol% Au) • The large diameter Au islet block the pore channel of TiO_2 inhibits charge transport
Wang et al. (2005) [38]	Pt/TiO_2, (Pt diameter: 5 nm) TF	Mesoporous Pt/TiO_2 film shows highest photocatalytic activity compared to pure TiO_2
Chen et al. (2007) [39]	Pt/TiO_2 (0.02-1wt% Pt), PC	• Photocatalytic activity depends on the ratio of Pt to TiO_2. Maximum performance is at 0.2 wt% Pt • The high concentration of Pt blocks the surface-active site, which was confirmed by the adsorption of CH_3OH
Zou et al. (2007) [40]	Pt/TiO_2 (0.1-2wt% Pt), PC	▪ H_2 evolution depends on the Pt to TiO_2 ratio ▪ Effect of Pt concentration depends on the synthesis method ▪ Effect of Pt concentration depends on the type of electrolyte
Ranjit et al. (1995) [41]	Ru/TiO_2 (0.1-2% Ru), PC	Photocatalytic activity depends on the ratio of Ru to TiO_2. Maximum performance is at 1% Ru
Zhang & Chen (2009) [42]	Ag/TiO_2 (7.4wt% Ag), PC	Ag/TiO_2 shows maximum photocatalytic activity than pure TiO_2 sample

Zhong et al. (2009) [43]	Pd/TiO_2 (0.2-0.75wt% Pd), PC	• Photocatalytic activity depends on the ratio of Pd to TiO_2. Maximum performance is at 0.25 wt% Pd. • It was interpreted that the high content of Pd at the TiO_2 surface reduces the charges transfer
Chen et al. (2012) [44]	Ir/TiO_2 (0.5-5wt% Ir), PC	• Photocatalytic activity depends on the surface acidity • The large surface acid site observed for 3 wt% Ir/TiO_2 leads maximum photocatalytic performance
Pan & Xu (2013) [45]	Ag/TiO_2 (2.23wt% Ag), Pt/TiO_2 (1.98wt% Pt), Pd/TiO_2 (1.96wt% Pd), PC	Maximum photocatalytic performance attributed as Pd/TiO_2> Pt/TiO_2> Ag/TiO_2> TiO_2.
Wu et al. (2007) [46]	Rh/TiO_2, Pt/TiO_2, Ru/TiO_2, Au/TiO_2, Cu/TiO_2, Ni/TiO_2 (0.3wt% metal), PC	Maximum photocatalytic performance attributed as Rh/TiO_2> Pt/TiO_2=Cu/TiO_2=Ni/TiO_2>Au/TiO_2>Ru/TiO_2> Ir/TiO_2>TiO_2.
Notation: NSF- nano-size film, PC-polycrystalline, TF – thin film		

As seen, the deposition of the metal islets, forming the metal/TiO_2 couples, results in higher photocatalytic performance compared to pure TiO_2, however, the effect exhibits a maximum. This effect indicates that the beneficial activity of the islets corresponds to their critical concentration, above which their effect on performance decreases.

A summary of the literature on the effect of TiO_2 coupling with alternative oxide phases is shown in **Table 5.4**.

Table 5.4. *Literature reports on the photocatalytic performance of the electrochemical couples formed of TiO_2 and alternative oxide phases.*

Authors	**Studied system**	**Reported outcome**
Bessekhouad et al. (2006) [47]	CdS/TiO_2 (5-50 wt% CdS), PC	Photocatalytic activity of CdS/TiO_2 depends on the CdS to TiO_2 ratio. $CdS(h^{\bullet}, e') + TiO_2 \xrightarrow{h\nu} CdS(h^{\bullet}) + TiO_2(e')$
Tristao et al. (2006) [48]	CdS/TiO_2 (1-20 mol% CdS), PC	Photocatalytic activity depends on the ratio of CdS to TiO_2. Maximum photocatalytic performance is at 5 mol% CdS
Wu et al. (2006) [49]	CdS/TiO_2 (1-5 mol% CdS), PC	The increase of the CdS to TiO_2 ratio results in increased photocatalytic activity of the CdS/TiO_2 couple
Yu et al. (2014) [50]	Ag_2CO_3/TiO_2 (0.5-4 wt% Ag_2CO_3), PC	Photocatalytic activity depends on the Ag_2CO_3 to TiO_2 ratio. The maximum performance is at 1 wt% of Ag_2CO_3

Dohčević-Mitrović (2016) [51]	WO_3/TiO_2, TF	The photocatalytic activity depends on the composition of WO_3/TiO_2 couple
Kim et al. (2015) [52]	▪ WO_3/TiO_2, TF ▪ $TiO_2/SiO_2/WO_3$, TF	The WO_3/TiO_2 couple shows lower contact angle of water. $WO_3(h^{\bullet}, e') + TiO_2 \xrightarrow{h\nu} WO_3(e') + TiO_2(h^{\bullet})$
Momeni &Ghayed (2015) [53]	ZnO/TiO_2 (1-5 wt% ZnO), NT	The photocatalytic activity of ZnO/TiO_2 couple depends on the ratio of ZnO to TiO_2. Maximum performance is observed at 3 wt% of ZnO
Hao et al. (2013) [54]	SiC/TiO_2, PC	The photocatalytic activity of couple SiC/TiO_2 depends on the processing condition of SiC.
Zhang et al. (2012) [55]	Cr_2O_3–SiC–TiO_2, PC	The photocatalytic performance increases with the concentration of Cr_2O_3. The maximum performance is at 0.75 wt% of Cr_2O_3.
Hattori et al. (2000) [56]	TiO_2/SnO_2, TF	The photocatalytic performance of TiO_2/SnO_2 increases comparing to TiO_2 film $SnO_2(h^{\bullet}, e') + TiO_2 \xrightarrow{h\nu} SnO_2(e') + TiO_2(h^{\bullet})$
Cao et al. (2000) [57]	TiO_2/SnO_2, TF	The photocatalytic activity of TiO_2/SnO_2 couple depends on the ratio of TiO_2 to SnO_2
Jun et al. (2012) [58]	TiO_2/Cr-TiO_2(1.6-4.8 at% Cr), TF	Increase of Cr content in TiO_2 results decrease of contact angle for the TiO_2/Cr-TiO_2 couple
Notation: NT – nanotube; PC – polycrystalline; TF-Thin film		

As seen in Table 5.4, the electrochemical couples formed of TiO_2 with alternative oxide semiconductors results in an increased efficiency of photocatalytic performance which is commonly considered in terms of enhanced charge separation.

5.1.3 Literature Summary

The literature on the effect of chromium on the properties of TiO_2, including photocatalytic properties, indicates that the data reported so far are conflicting. The conflicting reports are essentially caused by the applied experimental procedures, which are not uniform. Awareness is growing that to progress of research aiming at the development of photocatalysts with enhanced performance requires that the experimental data are reproducible and free of side effects (discussed in section 5.1.1) that are reflective of the applied processing procedures. This project aims at addressing this objective.

5.2 Experimental

This section reports the experimental approach in the determination of the following effects:

i) The effect of chromium on photocatalytic performance of chromium doped TiO_2 annealed on the gas phase of controlled oxygen activity, including (i) artificial air, forming oxidizing conditions, $p(O_2)$ =21 kPa, and (ii) argon (99%) - hydrogen (1%) mixture, forming reducing conditions, $p(O_2) = 10^{-10}$ Pa.

ii) The effect of oxygen activity on the photocatalytic performance of pure and Cr-doped TiO_2.

iii) The effect of electrochemical coupling on the photocatalytic properties of the systems formed of pure and Cr-doped TiO_2 annealed in the gas phase of different oxygen activity:

   a) Pure TiO_2 specimens annealed in pure oxygen, forming strongly oxidizing conditions, $p(O_2)$ = 100 kPa, and reducing conditions, $p(O_2) = 10^{-10}$ Pa.

   b) Cr-doped TiO_2 (0.04 at% Cr) annealed in pure oxygen, forming strongly oxidizing conditions, $p(O_2)$ = 100 kPa, and reducing conditions, $p(O_2) = 10^{-10}$ Pa.

   c) Cr-doped TiO_2 (0.376 at% Cr) annealed in in pure oxygen, forming strongly oxidizing conditions, $p(O_2)$ = 100 kPa, and reducing conditions, $p(O_2) = 10^{-10}$ Pa.

5.2.1 Specimen Processing

The specimens of pure and Cr-doped TiO_2 for the photocatalytic experiments were processed following the same procedures as those are reported in Chapter 3. The processing procedure of the formation of the electrochemical couples is reported below.

Formation of Electrochemical Couples. The couples of TiO_2 specimens were annealed at different oxygen activities; the TiO_2/Cr-TiO_2 specimens were of different compositions and annealing conditions. The formation procedure involved: (i) mixing the powders of two couple components in proportion 50:50, (ii) heating the mixture for one hour at 343 to 353 K in air, (iii) pressing the mixture uniaxially into cylindrical pellets using hardened stainless-steel die, (iv) subsequent heating in a tube furnace for 10 hours at 873 K in air - for binder (wax) removal – and (v) densification into a polycrystalline solid by sintering at 1373 K for 5 hours in either oxygen or the argon-hydrogen mixture.

The specimens were polished and then annealed at 1373 K for 1 h under a 100 ml/min controlled gas flow system of controlled oxygen activity, including the following gases:

i) Pure oxygen, $p(O_2)$ = 100 kPa.
ii) The argon + 1% hydrogen mixture [$p(O_2) = 10^{-10}$ Pa at 1373 K].

In summary, the applied processing procedure resulted in the formation of a reproducible effect for the following reasons:

i) The applied sintering procedure (1373 K) was high enough to secure phase transition of the anatase phase, if any, to the rutile phase. Consequently, the system can be considered as homogeneous in terms of its structure.
ii) The selected chromium concentrations were within the solubility limit.
iii) The complex surface morphology was removed by polishing and reannealing. The latter process aimed at removing the effect of polishing.
iv) The time of annealing was sufficient for the system to reach chromium segregation equilibrium.
v) The final processing step of annealing in the gas phase of the controlled oxygen activity resulted in the imposition of well-defined oxygen activity in the oxide lattice and the related defect disorder.

5.2.2 Characterization

The characterization techniques of the specimens involved (i) PIXE analysis of bulk composition, (ii) SEM studies in the determination of surface morphology, (iii) XPS and SIMS analysis for the determination of surface composition and (iv) the application of UV−vis−NIR spectrophotometry for the determination of both optical and photocatalytic properties. The details of the experimental procedures of PIXE, XPS and SIMS techniques have been reported in chapters 3 and 4.

5.2.2.1 Scanning Electron Microscope

The scanning electron microscope (SEM) provides high-resolution images of the studied sample. The precisely focused beam of electrons in SEM technique produces high-resolution images with a three-dimensional appearance and provides topographical,

morphological and compositional information. A schematic illustration of SEM technique is presented in **Figure 5.5**, which is required to be in a vacuum chamber during operation.

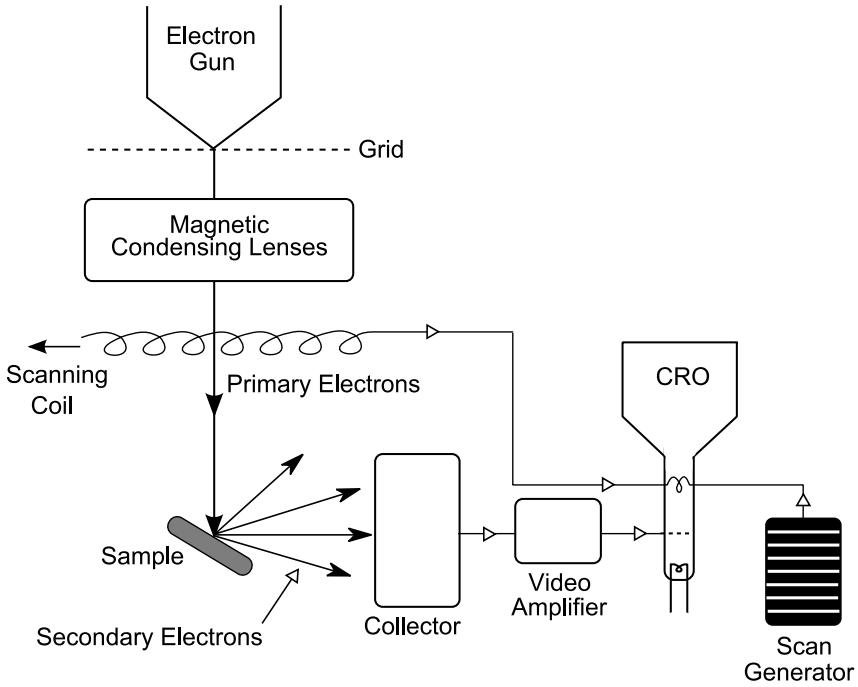

Figure 5.5. *Schematic representation of the experimental setup of the scanning electron microscope.*

An electron gun produces the high energy electron beam (λ ~0.0025nm at 200kV). The diameter of the beam is controlled by a magnetic condensing lens. A scanning coil is located in-between the magnetic condensing lens and the sample to maintain a parallel electron beam. The primary electrons from the electron gun strike the surface of the sample and produce secondary ions which are collected by a positively charged electron detector and converted into electrical signals. These signals are fed into a conversion rate optimizer (CRO) through a video amplifier.

In this research, the specimens were mounted with a conductive carbon adhesive and approximately 5 nm of carbon was evaporated onto the surfaces under vacuum to avoid the effect of charging. A Zeiss Ultra Plus with an attached Oxford Instruments X-ray microanalysis system was used to obtain the SEM micrographs, and all images were captured using an in-lens secondary electron detector. The average grain size of the specimen was calculated considering 15 grains randomly.

5.2.2.2 Photocatalytic Performance

The decomposition of the aqueous solution of MB was determined under simulated solar irradiation. A schematic representation of the experimental setup is illustrated in **Figure 5.6**.

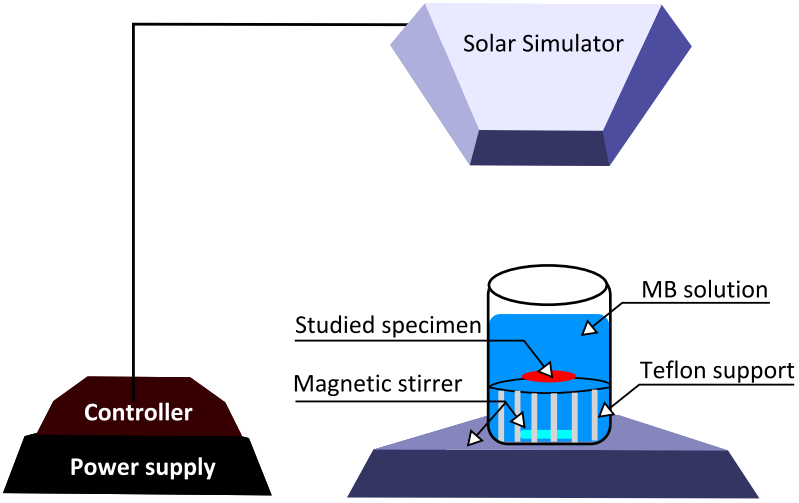

Figure 5.6. *Schematic representation of photocatalytic experimental setup.*

The Oriel Sol3A solar simulator (model 94043A with 450 W lamp) was applied. The working distance between the lamp and the solution was 10 cm. The light spectrum matched the solar spectrum within 98.75%. The studied samples were immersed in the beaker with 9 ml water solution of MB and placed on a Teflon plate. A stirrer was used to dissolve any concentration of gradients in the solution. Initially, a reference experiment was performed for 2 hours in the dark. Afterward, light was imposed, and the concentration of MB was determined as a function of irradiation time.

The concentration of MB in the aqueous solution was determined using the Agilent Cary 5000 UV−vis−NIR spectrophotometer in the absorption mode of operation. The typical absorbance spectrum for MB in a water solution as a function of wavelength is shown in **Figure 5.7**.

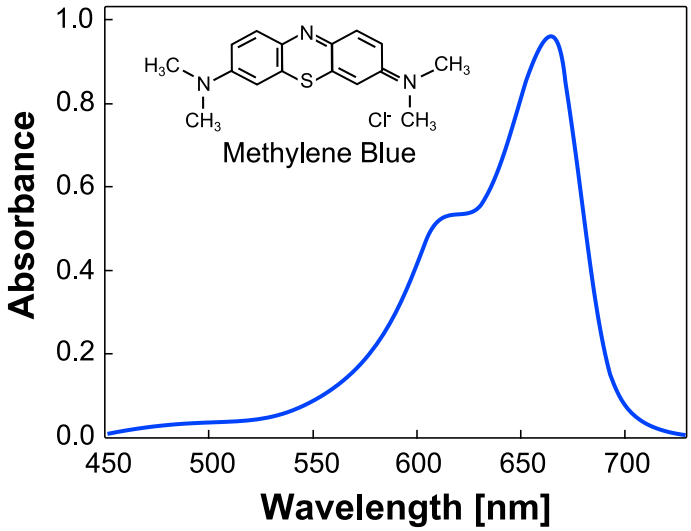

Figure 5.7. *Absorbance versus wavelength spectrum of methylene blue in aqueous solution and its structure.*

The efficiency of MB degradation, η is calculated by the following equation:

$$\eta = \frac{C_0 - C_t}{C_0} \times 100 \tag{5.1}$$

where C_0 is the initial solution concentration of dye and C_t is the solution concentration of dye after t minutes since the light was switched on.

The apparent first-order reaction rate constant (R) of MB degradation can be calculated using the expression (5.2) as shown in **Figure 5.8**.

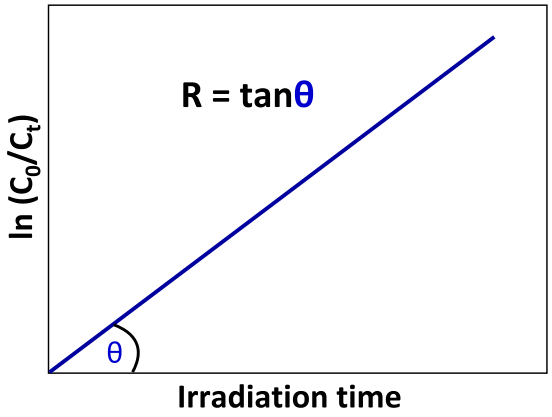

Figure 5.8. *Schematic representation of the determination of rate constant, R of photocatalytic reaction.*

Consequently:

$$\ln\left(\frac{C_0}{C_t}\right) = Rt \tag{5.2}$$

The photocatalytic activity, considered in terms of the rate constant R, was used in assessing the photocatalytic performance of the studied specimens.

5.3 Results and Discussion

The results reported in this section are focused on surface morphology of the specimens forming the couples, as well as the associated optical properties. The results of the bulk and the surface composition of chromium of the studied specimens, as determined by PIXE and XPS techniques are reported in chapters 3 and 4.

5.3.1 Surface Morphology

5.3.1.1 Effect of Chromium Concentration

The micrographs of the scanning electron microscope, SEM, for pure and Cr-doped TiO_2 are shown in **Figure 5.9**.

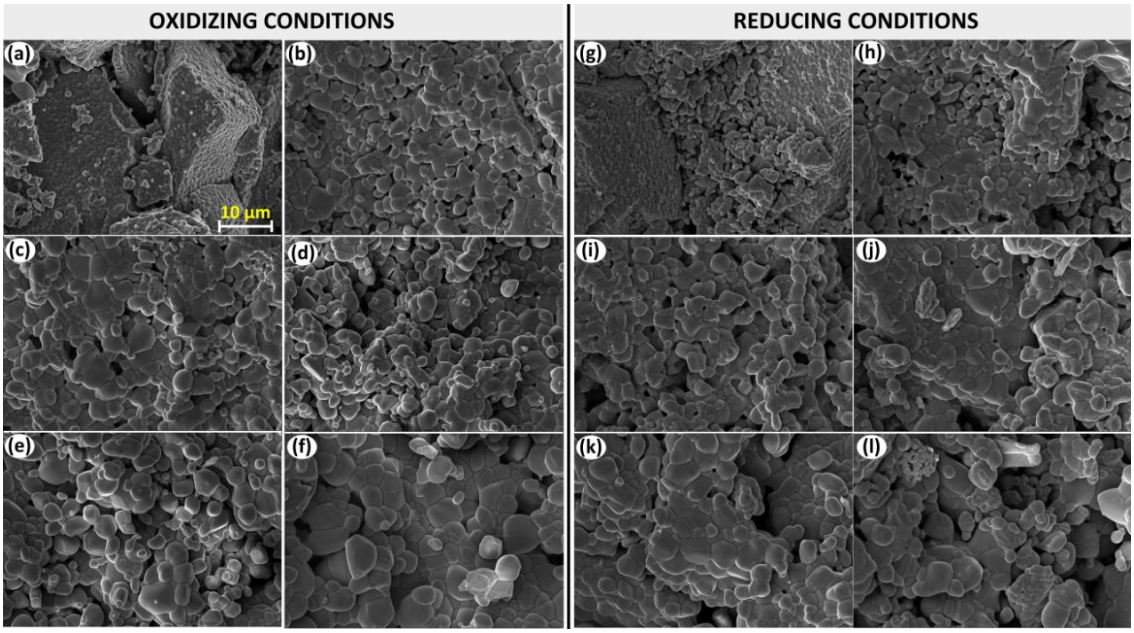

Figure 5.9. *SEM micrographs for the specimens of (a) pure and Cr-doped TiO_2, including (b) 0.04 at%, (c) 0.043 at%, (d) 0.116 at%, (e) 0.376 at% and (f) 1.365 at% Cr.*

As seen, the average grain size of the specimens annealed in both oxidizing and reducing conditions increased with chromium concentration from approximately 1.6 μm to 4.3 μm. However, the individual grains were better shaped after annealing in oxidizing conditions. As also seen, the morphology of pure TiO_2 was entirely different from that of Cr-doped TiO_2.

5.3.1.2 Effect of Oxygen Activity

The SEM images of studied specimens after annealing in the gas phase of different oxygen activity are presented in **Figure 5.10**.

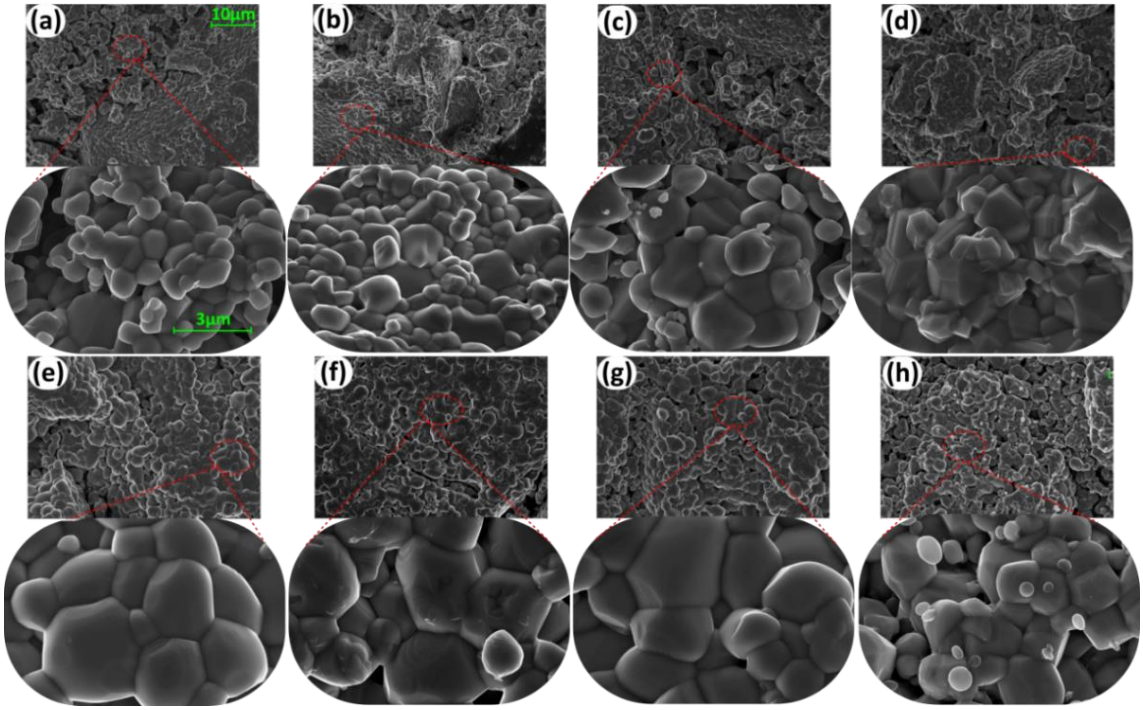

Figure 5.10. *SEM micrograph for (a-d) pure and (e-h) 0.04 at% Cr-doped TiO_2 specimens. The specimens were annealed at 1273 K in different oxygen activity, such as (a) & (e) in 100 kPa, (b) & (f) in 21 kPa, (c) & (d) in 10 Pa and (d) & (h) in 10^{-12} Pa respectively.*

The effect of the oxygen activity on the morphology of both pure and Cr-doped TiO_2 can be summarized as follows:

- The average grain size of pure TiO_2 at $p(O_2)$>10 Pa remains between 1 and 1.6 μm (a-c). The imposition of reducing conditions, $p(O_2)=10^{-12}$ Pa (d), results in the aggregation of grains.

- Average grain size for Cr-doped TiO_2 remains between 2.7-3.2 μm. The largest and the smallest grain sizes (3.22 μm and 2.77 μm) correspond to at $p(O_2)$=21 kPa and $p(O_2)=10^{-12}$ Pa respectively.

5.3.1.3 Electrochemical Couple

The SEM micrographs of the oxidized and reduced TiO_2 and TiO_2/Cr-TiO_2 couple pellets are shown in **Figure 5.11.**

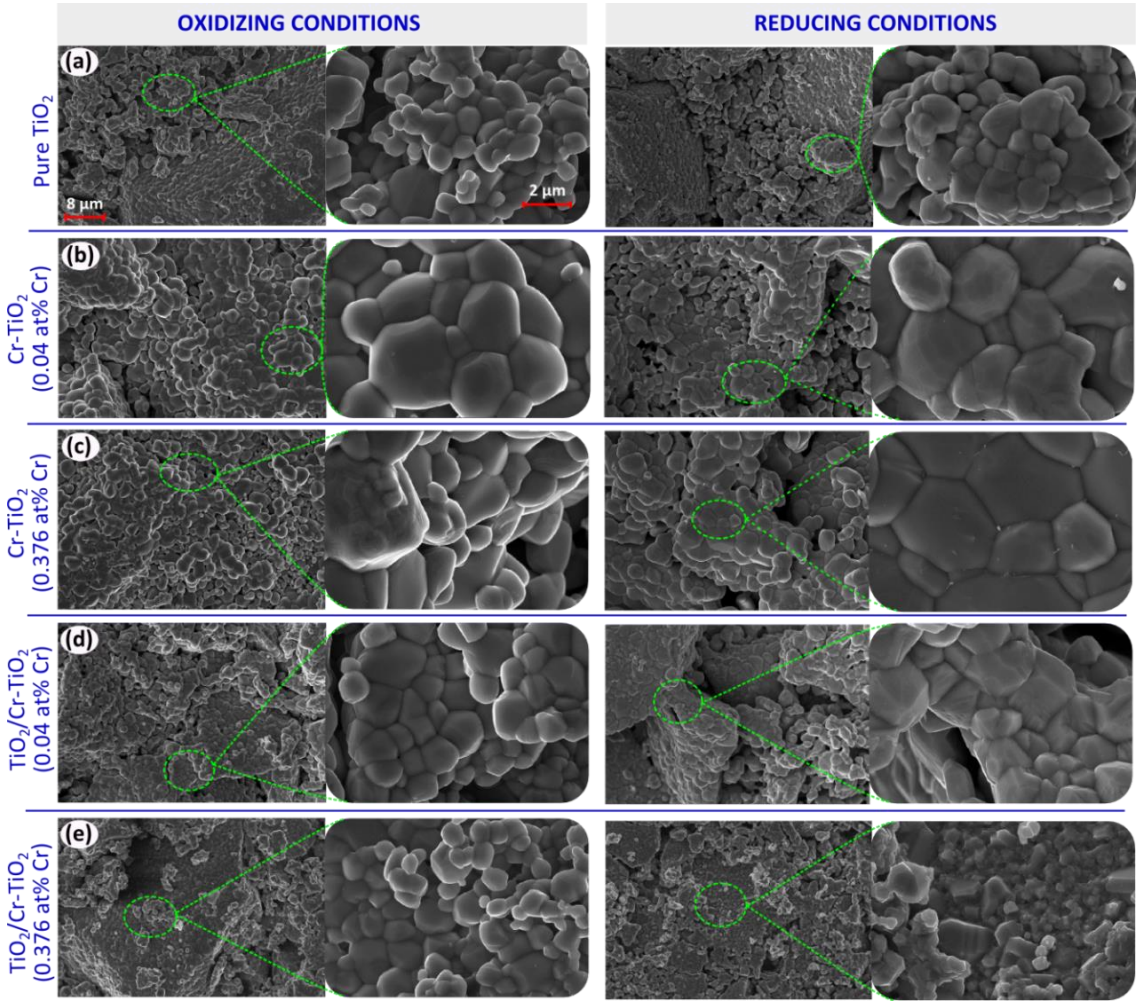

Figure 5.11. *SEM micrograph for pure and Cr-doped TiO_2 as well as the electrochemical couples annealed at 1373 K in oxidizing, $p(O_2)$ = 100 kPa, and reducing conditions, $p(O_2) = 10^{-10}$ Pa.*

The SEM images indicate that the annealing of the couple results in the formation of larger grain aggregates including both pure and Cr-doped TiO_2 components. It appears

that the aggregates annealed in reducing conditions are slightly larger and the individual grains are well shaped. On the other hand, annealing in oxidizing conditions leads to the formation of rounded grains. The assembly including 0.04 at% Cr is relatively well integrated while those involving 0.376 at% are looser.

5.3.2 Optical Properties

The effect of chromium concentration and oxygen activity on optical properties has been reported in **Chapter 3**.

Electrochemical Couple. The reflectance plotted as a function of the wavelength of the mono-phase and coupled systems are shown in **Figure 5.12**.

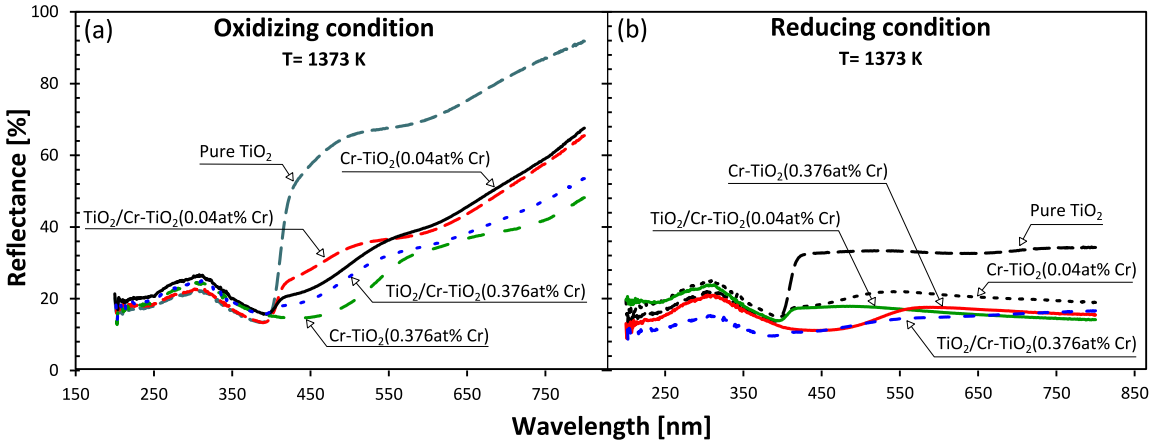

Figure 5.12. *Reflectance spectra for pure TiO_2, Cr-doped TiO_2 and the couples of TiO_2/Cr-TiO_2 annealed in oxidizing and reducing conditions corresponding to $p(O_2) = 10^5$ Pa and $p(O_2) = 10^{-10}$ Pa respectively.*

These spectra indicate that light absorption for the specimens annealed in reducing conditions is much larger than that for oxidizing conditions.

5.3.3 Light Induced Partial Water Oxidation

5.3.3.1 Effect of chromium concentration

The effect of irradiation time on the concentration of MB in the aqueous solution was determined spectrophotometrically by measuring the height of the absorption peak at 665 nm wavelength. As an example, the typical evolution of this peak, after different radiation times for pure and Cr-doped TiO_2 involving 0.04 at% Cr, is shown in **Figure 5.13**.

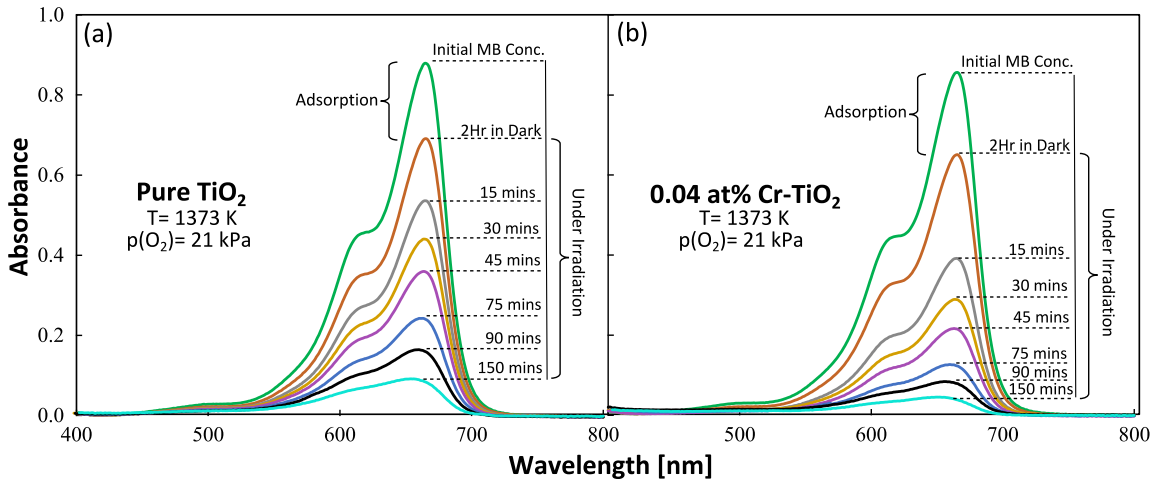

Figure 5.13. *Changes of UV-vis absorbance spectra related to MB solution in dark and under light at different irradiation time for (a) pure and (b) Cr-doped TiO_2.*

The light-induced time dependence of MB concentration in the solution for Cr-doped TiO_2 annealed in both oxidizing and reducing conditions, commencing from the dark experiment, is shown in **Figure 5.14**.

The effect of light on the decomposition of MB is shown in **Figure 5.15** in terms of the dependence that is normalized at the time corresponding to the imposition of light.

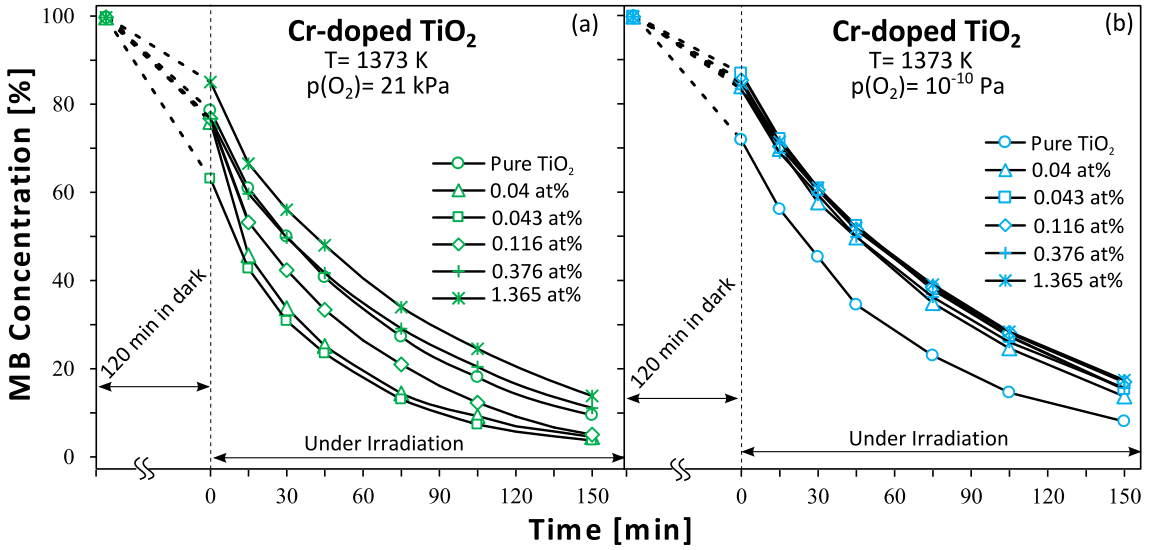

Figure 5.14. *Changes of MB concentration as a function of time for Cr-doped TiO_2 annealed in (a) oxidizing and (b) reducing conditions, related to $p(O_2)$=21 kPa and 10^{-10} Pa.*

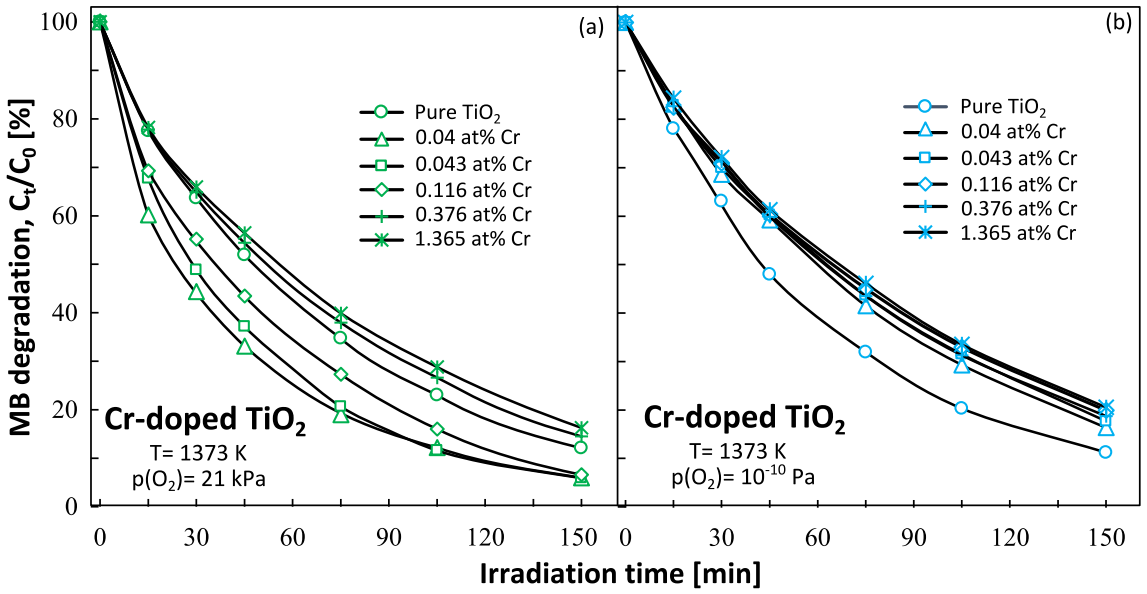

Figure 5.15. *Effect of chromium concentration on the degradation of MB concentration with irradiation time for Cr-doped TiO_2 annealed in oxidizing and reducing conditions (C_o and C_t denote the concentration of MB at t=0 and time t, respectively).*

In order to assess the effect of chromium on photocatalytic activity in terms of uniform quantities related to chromium concentration, the dependencies in **Figure 5.15** were converted into linear dependences of $\ln(C_0/C_t)$ as a function of irradiation time. The related linear plots are shown in **Figure 5.16**.

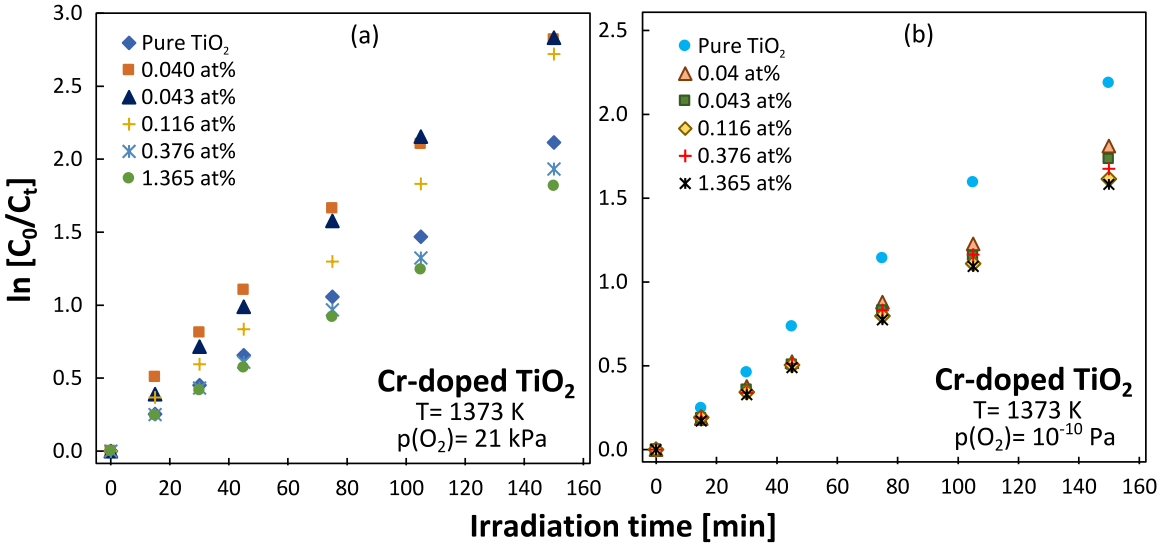

Figure 5.16. *Changes of $\ln(C_0/C_t)$ with irradiation time for different composite of Cr-doped TiO_2 annealed in (a) oxidizing and (b) reducing conditions, respectively.*

The slope of the linear dependencies in **Figure 5.16** (termed as the rate constant of the light-induced decomposition of MB, R) was calculated following the method presented in **Figure 5.8** and is subsequently plotted as a function of chromium concentration. The effect of chromium concentration on the rate constant, R, of Cr-doped TiO_2 annealed in oxidizing and reducing conditions is shown in **Figure 5.17**.

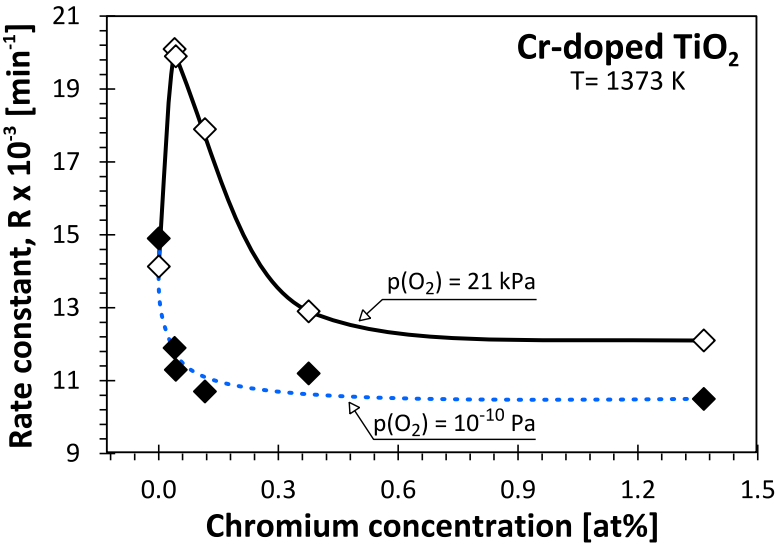

Figure 5.17. *Effect of composition on the rate constant, R, for Cr-doped TiO_2, annealed in both oxidizing and reducing conditions, respectively.*

As seen, the increase of chromium concentration for the specimens annealed in oxidizing conditions results in a sharp increase in photocatalytic activity up to 0.04 at%. When the chromium content exceeds 0.04 at%, the photocatalytic activity drops below the level observed for pure TiO_2. As also seen in **Figure 5.17**, the incorporation of chromium in reducing conditions results in reduced photocatalytic performance within the entire range of chromium content.

The effect of chromium on photocatalytic activity, which is represented in **Figure 5.17**, may be considered in terms of a competitive influence of all KPPs, as discussed in the following section. Considering the character of the dependence in oxidizing conditions, the discussion on the effect of the KPPs (defined in chapter 2) may be considered in terms of two regimes:

I. The regime corresponding to low chromium concentrations (up to 0.04 at%).
II. The regime corresponding to high chromium concentrations (> 0.04 at%).

Specimens Annealed in Oxidizing Conditions

The sharp rise of the rate constant in the regime I (**Figure 5.17**) can be considered in terms of the following KPP-related effects:

i) *Bandgap (KPP-1).* The observed effect of chromium on the reduction of the bandgap is expected to have a favorable effect on photocatalytic activity in **regimes I** and **II**. However, the decrease of photocatalytic activity in **regime II**, despite the still strong decrease of the bandgap, indicates that the related KPP has little effect on photocatalytic performance. (See the related bandgap vs. chromium concentration reported in **Figure 3.17b**)

ii) *The concentration of surface active sites (KPP-2).* It is shown that the defect disorder of TiO_2 in the bulk and at the surface is different [59]. The XPS data (**Table 4.2**) has also shown that chromium incorporation into the surface layer leads to the formation of both acceptor and donor-type species (Cr^{3+}, Cr^{6+}), which are associated with the formation of titanium vacancies at the surface following the mechanisms **(5.3)** to **(5.6)**. Therefore, the observed increase of photocatalytic performance in the range 0-0.04 at% Cr seems to be profoundly influenced by the concentration of surface active sites. The obtained results indicate, however, that these active sites are dis-activated at [Cr]>0.04 at%.

iii) *Fermi level (KPP-3).* The mechanisms **(5.3)** to **(5.6)** lead to the formation of strong donors. However, if the anodic process is critical for the reaction progress, the donor-type mechanisms, leading to an increase of the Fermi level, are expected to have a negative effect on performance in **regimes I** and **II**.

iv) *Charge transport (KPP-4).* It has been shown that incorporation of chromium leads to a shift of n-p transition in TiO_2 towards lower oxygen activity [60]. Since the concentration of electronic charge carriers in the vicinity of the n-p transition drops to a minimum level, the related charge transport is diminished or blocked. The latter seems to have a critical effect on low performance in **regime II**.

Based on the discussion in points (i) – (iv), one may assume the following mechanisms of chromium incorporation in regimes I and II:

I. Up to 0.04 at% Cr:

$$\frac{1}{2}O_2 + Cr_2O_3 \leftrightarrow 2Cr_i^{\bullet\bullet\bullet} + 2V_{Ti}'''' + 2h^{\bullet} + 4O_O^x \tag{5.3}$$

$$2Cr_2O_3 \rightarrow 4Cr_i^{\bullet\bullet\bullet} + 3V_{Ti}'''' + 6O_O^x \tag{5.4}$$

$$2CrO_3 \rightarrow 2Cr_{Ti}^{\bullet\bullet} + V_{Ti}'''' + 6O_O^x \tag{5.5}$$

$$\frac{1}{2}O_2 + CrO_3 \rightarrow Cr_i^{\bullet\bullet\bullet\bullet\bullet\bullet} + 2V_{Ti}'''' + 2h^{\bullet} + 4O_O^x \tag{5.6}$$

II. Above 0.04 at% Cr:

$$Cr_i^{\bullet\bullet\bullet} + V_{Ti}'''' \rightarrow \left\{Cr_i^{\bullet\bullet\bullet}V_{Ti}''''\right\}' \tag{5.7}$$

$$Cr_{Ti}^{\bullet\bullet} + V_{Ti}'''' \rightarrow \left\{Cr_{Ti}^{\bullet\bullet}V_{Ti}''''\right\}'' \tag{5.8}$$

$$Cr_i^{\bullet\bullet\bullet\bullet\bullet\bullet} + V_{Ti}'''' \rightarrow \left\{Cr_i^{\bullet\bullet\bullet\bullet\bullet\bullet}V_{Ti}''''\right\}^{\bullet\bullet} \tag{5.9}$$

In summary, the anodic active sites (KPP-2) are critical for the light-induced reactivity of Cr-doped TiO_2 with water. However, the performance requires an efficient charge transport (KPP-4) that is dropped in **regime II** [60].

Specimens Annealed in Reducing Conditions

As seen in **Figure 5.17**, the incorporation of chromium in reduced conditions results in a decrease of photocatalytic activity within the entire range of chromium concentrations. The negative effect of chromium on the performance of Cr-doped TiO_2 annealed in reduced conditions may be considered in terms of either the predominant influence of the intrinsic ionic defects or a change in valence of chromium:

i) *Intrinsic ionic defects*. Annealing in reducing conditions results in the generation of positively charged ionic defects (oxygen vacancies and titanium interstitials) leading to the formation of cathodic active sites and a decrease in the concentration of titanium vacancies that are anodic sites. Consequently, the concentrations of anodic sites (KPP-2), which are critical for the reaction progress, are reduced. Independently, ionization of the increased concentration of donor-type intrinsic

defects leads to the formation of electrons and an increase of the Fermi level (KPP-3). This has a negative effect on the anodic reactivity of water.

ii) *Extrinsic defects.* Chromium incorporation in reducing conditions results in the formation of cathodic sites rather than the anodic sites that are required for the reactivity with water. Based on the points (i) – (iii) the following mechanisms of chromium incorporation can be proposed:

$$Cr_2O_3 \leftrightarrow 2Cr'_{Ti} + V_O^{\bullet\bullet} + 3O_O^x \tag{5.10}$$

$$Cr_2O_3 \leftrightarrow 2Cr_i^{\bullet\bullet\bullet} + 6e' + \frac{3}{2}O_2 \tag{5.11}$$

$$CrO_3 \leftrightarrow Cr_i^{\bullet\bullet\bullet\bullet\bullet\bullet} + 6e' + \frac{3}{2}O_2 \tag{5.12}$$

The picture is much simpler for the solid solutions of TiO_2 donor-type ions, such as niobium [61] and tantalum [62]. The aim of the following section is to provide a brief comparison of the effects related to these two donor-type elements on one side and chromium on the other side.

Effect of Chromium vs. Tantalum and Niobium on Properties of TiO_2

The effect of chromium, niobium, and tantalum on the bandgap and photocatalytic activity is shown in **Figure 5.18**.

As seen, unlike chromium that leads to a bandgap reduction, the incorporation of both niobium and tantalum results in an increase in the bandgap. However, the increase of the bandgap, which is counterproductive to photocatalytic performance, is probably out-weighed by their associated effect on the formation of titanium vacancies that are formed according to the following reactions:

$$2\,Ta_2O_5 \rightarrow 4Ta_{Ti}^{\bullet} + V_{Ti}'''' + 10\,O_O^x \tag{5.13}$$

$$2Nb_2O_5 \rightarrow 4Nb_{Ti}^{\bullet} + V_{Ti}'''' + 10\,O_O^x \tag{5.14}$$

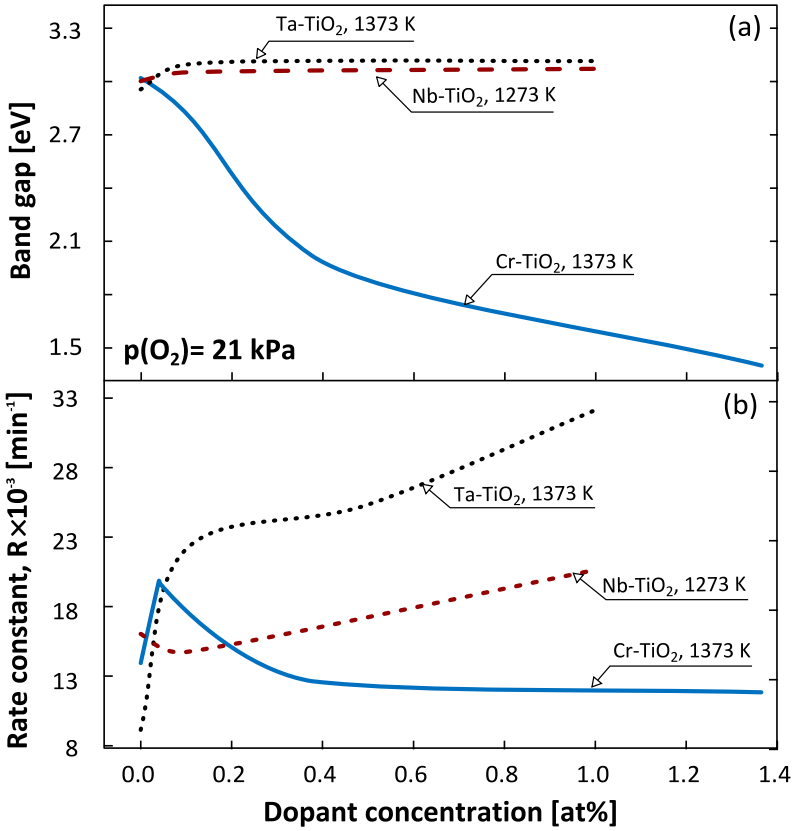

Figure 5.18. *Effect of chromium, niobium, and tantalum on photocatalytic activity of TiO_2 annealed in oxidizing conditions, $p(O_2)$ = 21 kPa*

It appears that the effects of both niobium and tantalum on the increase of the bandgap have a minor effect on photocatalytic performance, which is determined by the concentration of the active sites formed by titanium vacancies.

This comparison provides strong experimental evidence that the commonly assumed research strategy in the formation of high-performance TiO_2-based photocatalysts through a reduction of the bandgap requires revision.

In summary, while it is reasonable to expect that all KPPs, including the bandgap, the concentration of titanium vacancies, Fermi level, and charge transport, have an effect on performance, the effect of KPP-2 has the dominant role in partial water oxidation by TiO_2-based photocatalysts.

5.3.3.2 Effect of Oxygen Activity

While chromium results in a substantial reduction of the bandgap of TiO_2, the former section shows that the effect of chromium on photocatalytic performance is limited

to diluted solid solutions (**Figure 5.17**). It also shows that the photocatalytic activity of TiO_2 is affected by a range of key performance-related properties, KPPs, which are associated with defect disorder. The present section aims at the determination of the effect of intrinsic defects (oxygen vacancies, titanium vacancies, titanium interstitials and electronic defects), imposed by variable oxygen activity on photocatalytic activity of both pure and Cr-doped TiO_2.

The reaction progress, represented by the decomposition rate of MB, is illustrated in **Figure 5.19**.

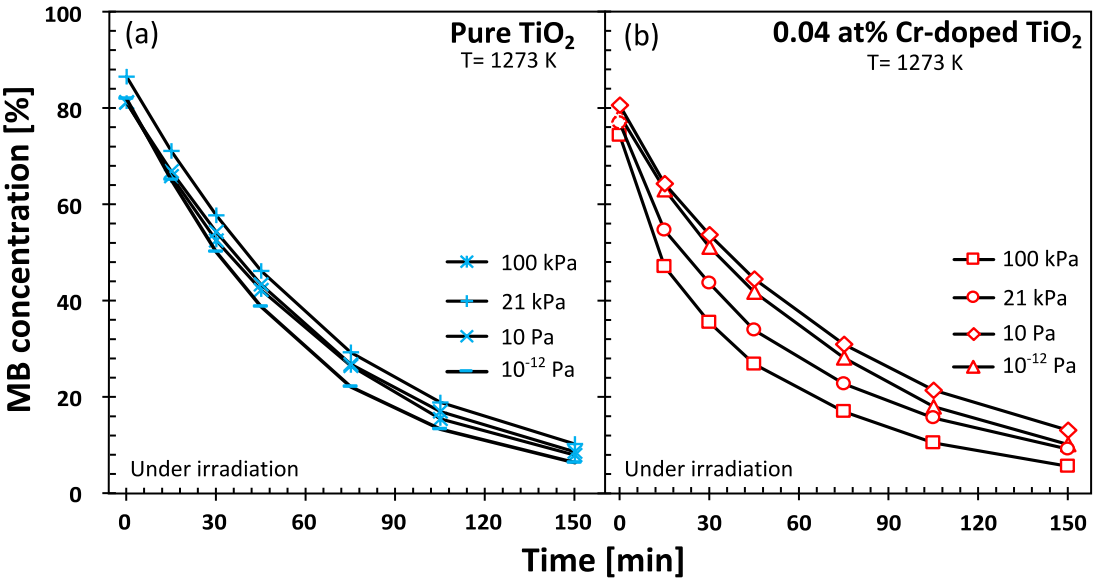

Figure 5.19. *Effect of light on the changes of MB concentration in water solution with time for (a) pure and (b) Cr-doped TiO_2, involving 0.04 at% Cr.*

As seen, the MB concentration levels at t=0 in **Figure 5.19** correspond to the values determined at the end of the dark experiment. In order to determine the photocatalytic activity, the concentration of MB after the dark experiment was normalized at the time t=0 corresponding to the beginning of light exposure. The changes of MB concentration, as the function of irradiation time for TiO_2 specimens annealed in the gas phase of different oxygen activity, are presented in **Figure 5.20** (the effect of oxygen activity on MB degradation efficiency - calculated using equation **4.2** - under different irradiation time for pure and Cr-doped TiO_2 is shown insert of **Figure 5.20)**.

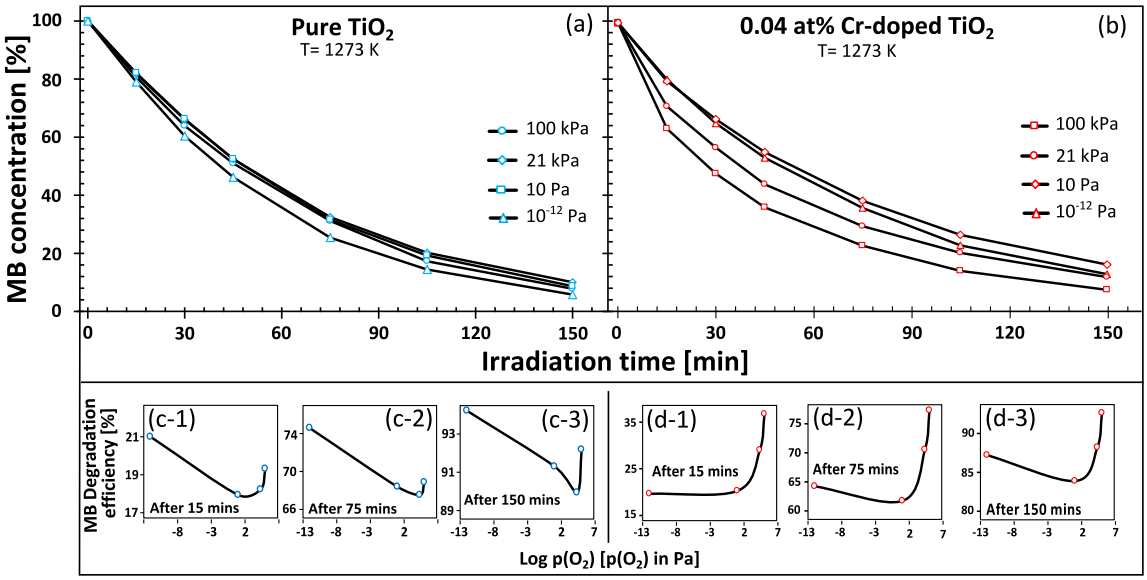

Figure 5.20. *Effect of light on normalized changes of MB concentration in water for pure and 0.04 at% Cr-doped TiO_2 (represented in a and b, respectively) specimens. The related oxidation efficiency is represented in c-1, c-2 and c-3 for pure TiO_2 and d-1, d-2 and d-3 for Cr-doped TiO_2.*

Following the procedure reported in Section 5.2.2.2, the MB degradation is considered in terms of linear relationships, as represented in **Figure 5.21**.

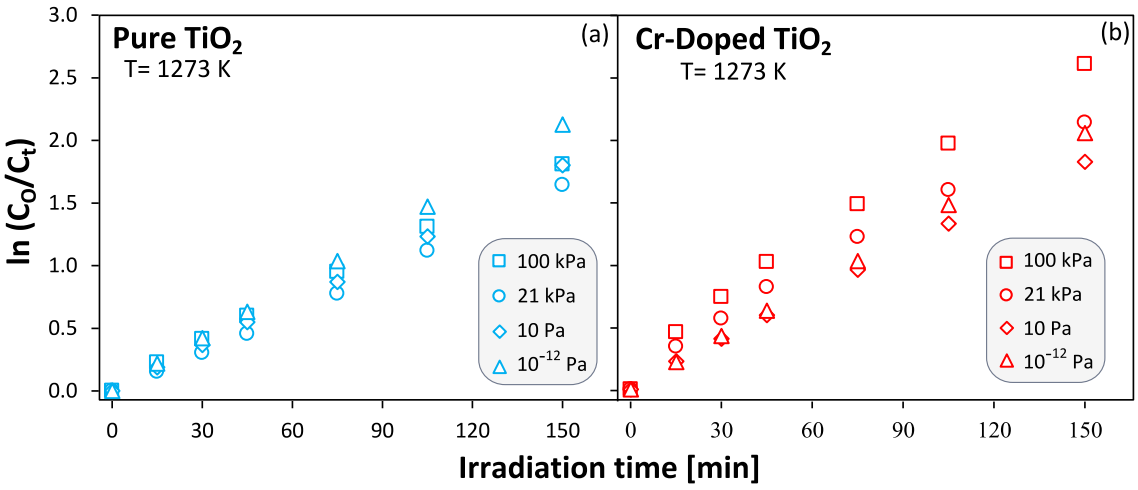

Figure 5.21. *The change of ln (C_0/C_t) with irradiation time for the specimens of (a) pure and (b) Cr-doped TiO_2 prepared at different oxygen activity in order to determine the photocatalytic rate constant using equation (**5.2**).*

The resulting effect of oxygen activity on the reaction rate constant R for the specimens annealed at 1273 K is represented in **Figure 5.22**, along with the bandgap. (The details of bandgap determination are reported in section 3.4.2).

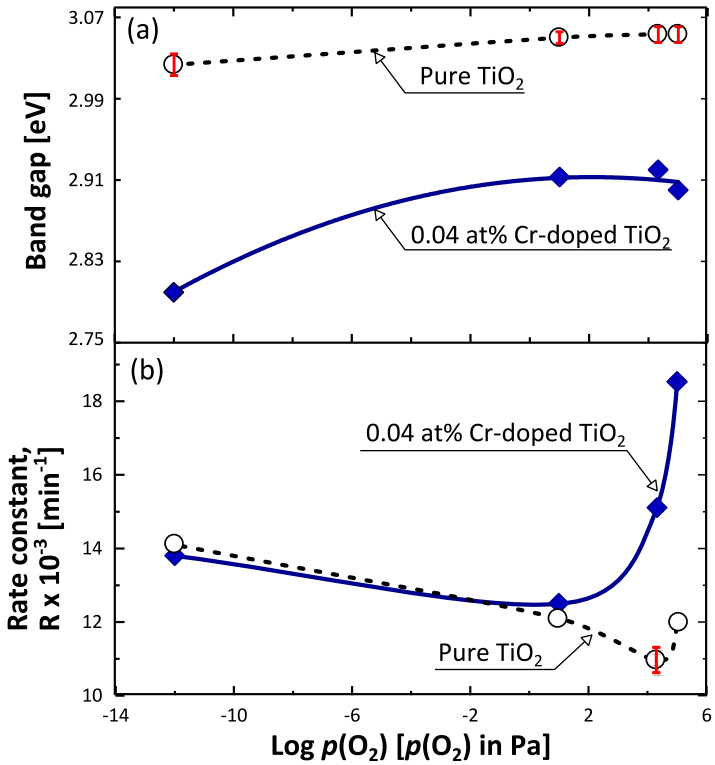

Figure 5.22. *Effect of oxygen activity on (a) bandgap and (b) photocatalytic performance for pure and Cr-doped TiO_2 (0.04 at% Cr) annealed at 1273 K in the gas phase of variable oxygen activity. The represented error bars for pure TiO_2 specimens were calculated based on four individual experiments.*

As seen, the photocatalytic activity, represented by the parameter R, for both pure and Cr-doped TiO_2 annealed at 1273 K, exhibits a minimum at the oxygen activity corresponding to the n-p transition point. A similar effect can be observed for the specimens annealed at 1373 K (Figure 5.23):

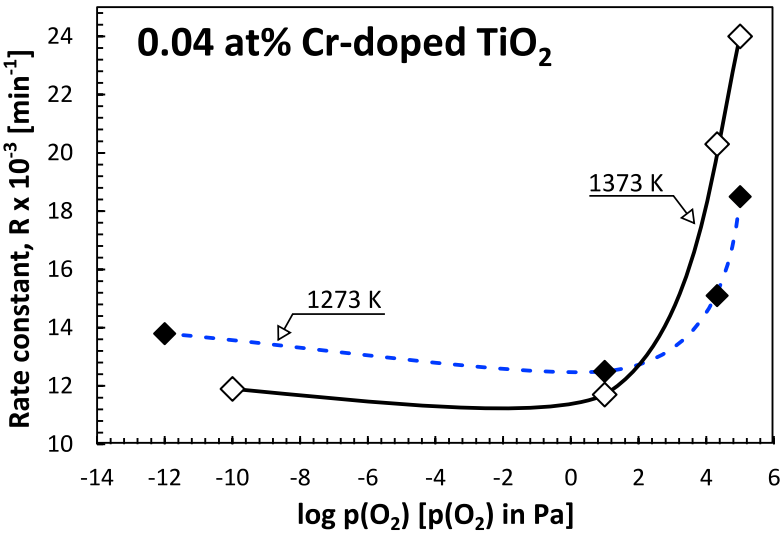

Figure 5.23. *Comparison of the effect of oxygen on the photocatalytic activity of Cr-doped TiO_2 (0.04 at% Cr) at 1273 K and 1373 K.*

The observed minimum performance at the n-p transition point, when the charge transport assumes minimum value, indicates the charge transport may exhibit a predominant – although negative – effect on performance as determined by the transport of the electronic charge carriers from the sites of their generation to the reaction sites at the surface.

5.3.3.3 Electrochemical Couples

This section considers the photocatalytic properties of the electrochemical couples formed by the TiO_2 specimens of different Fermi levels and imposed by different concentration of either intrinsic defects or chromium. It shows that the couples exhibit an enhanced effect when coupling leads to the desired change of the KPP as required for reactivity. For example:

i) Coupling results in an enhanced performance (positive synergy) when (i) the concentration of anodic active sites increases, or (ii) the Fermi level decreases, or the (iii) charge transport increases, or (iv) the bandgap decreases.

ii) Coupling results in a negative synergy when the KPPs are changed in undesired directions (alternative to the changes mentioned above).

The determination of the effect of coupling on performance first requires the determination of photocatalytic activity of the couple components, as shown in **Figure 5.24.**

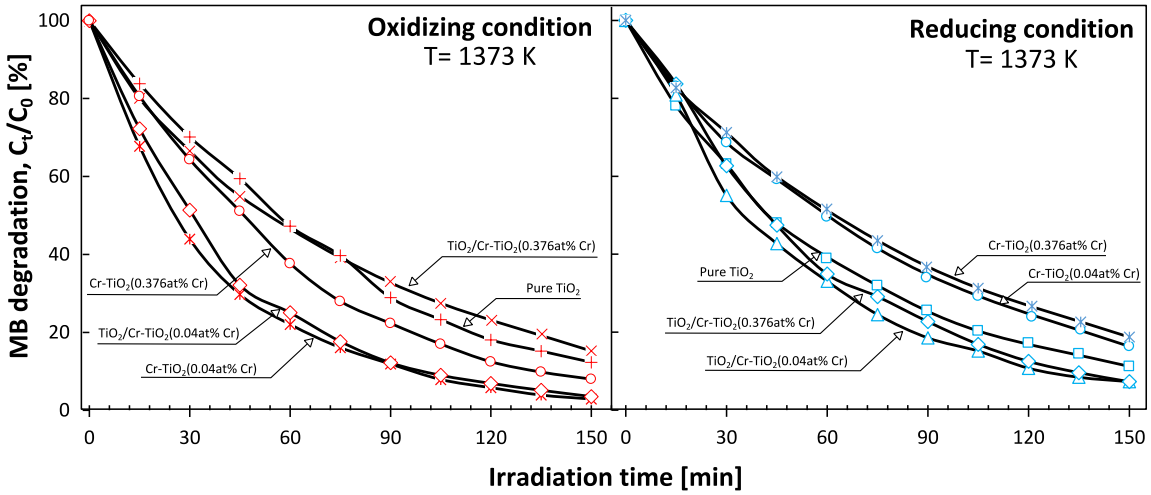

Figure 5.24. *The degradation of MB concentration with irradiation time for mono-phase and coupled of pure and Cr-doped TiO_2 systems annealed in oxidizing and reducing conditions (C_o and C_t denote the concentration of MB at t=0 and time t, respectively).*

The reaction progress of MB oxidation in terms of $\ln(C_o/C_t)$ as a function of the time of light exposure, calculated from **Figure 5.24**, is shown in **Figure 5.25**.

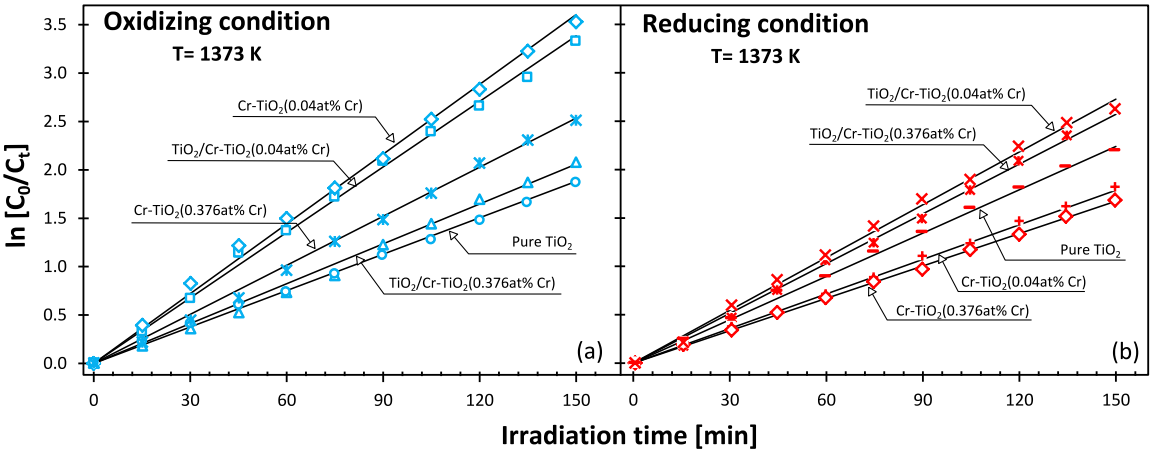

Figure 5.25. *The reaction progress of light-induced MB oxidation as a function of time for mono-phase systems of pure and Cr-doped TiO_2 as well as the electrochemical couples annealed at 1373 K in (a) oxidising and (b) reducing conditions corresponding to $p(O_2) = 10^5$ Pa and $p(O_2) = 10^{-10}$ Pa, respectively.*

The photocatalytic rate constant of the individual components, as well as the couples, was determined from **Figure 5.25** using equation (**5.2**), as represented by the columns in **Figure 5.26**.

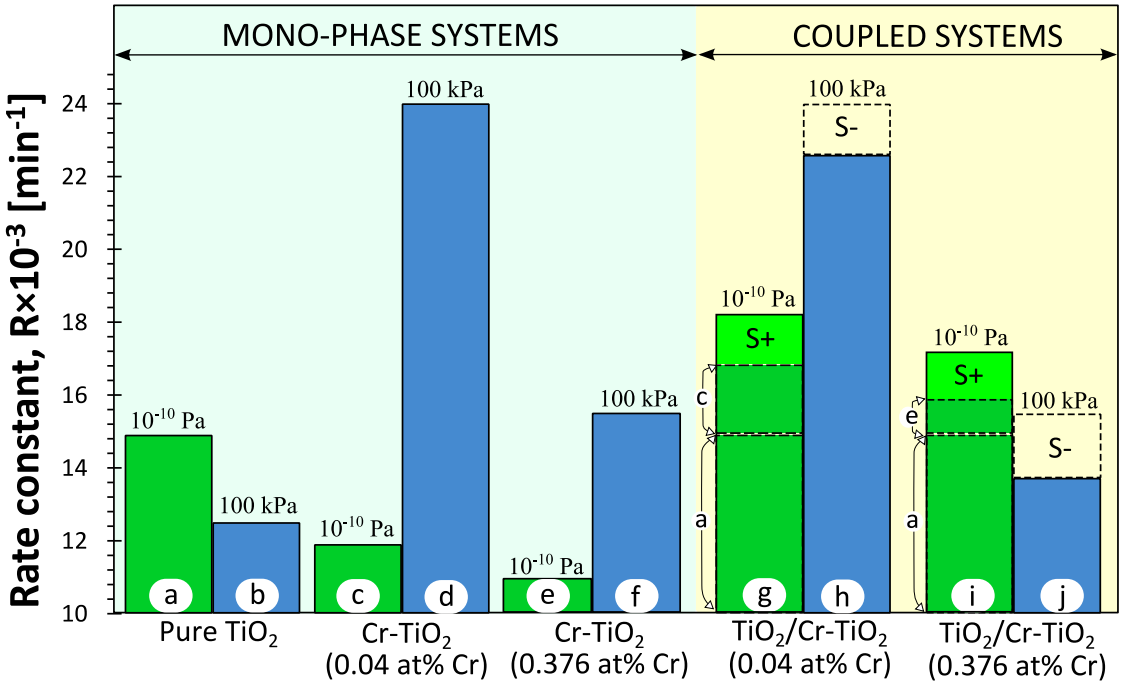

Figure 5.26. *Rate constant of the light-induced reaction progress for MB decomposition for pure TiO_2, Cr-doped TiO_2 as well as the couples after annealing on oxidizing and reducing conditions corresponding to $p(O_2) = 10^5$ Pa and $p(O_2) = 10^{-10}$ Pa, respectively. The numbers above the columns correspond to the oxygen activity of the gas phase during annealing, and S+ and S- denote positive and negative synergy.*

The couples are formed of the following components:

a) Pure TiO_2 annealed at $p(O_2) = 10^{-10}$ Pa
b) Pure TiO_2 annealed at $p(O_2) = 10^5$ Pa
c) Cr-doped TiO_2 (0.04 at% Cr) annealed at $p(O_2) = 10^{-10}$ Pa
d) Cr-doped TiO_2 (0.04 at% Cr) annealed at $p(O_2) = 10^5$ Pa
e) Cr-doped TiO_2 (0.376 at% Cr) annealed at $p(O_2) = 10^{-10}$ Pa
f) Cr-doped TiO_2 (0.376 at% Cr) annealed at $p(O_2) = 10^5$ Pa

The effects of composition and oxygen activity on the photocatalytic activity of mono-phase systems have been considered in **sections 5.3.3.1 and 5.3.3.2**. The coupled systems include the following compositions:

g) TiO_2+Cr-doped TiO_2 (0.04 at% Cr) annealed at $p(O_2) = 10^{-10}$ Pa
h) TiO_2+Cr-doped TiO_2 (0.04 at% Cr) annealed at $p(O_2) = 10^{5}$ Pa
i) TiO_2+Cr-doped TiO_2 (0.376 at% Cr) annealed at $p(O_2) = 10^{-10}$ Pa
j) TiO_2+Cr-doped TiO_2 (0.376 at% Cr) annealed at $p(O_2) = 10^{5}$ Pa

In considering the results, the following points should be made:

i) The columns in **Figure 5.26**, representing the performance of the couple components and the coupled systems are not additive as their value is a complex function of four variables related to different properties reflective of KPPs.
ii) The synergy represented in **Figure 5.26** is only a simplified approach to compare the performance of the couples with that of the individual components.
iii) The effect of the electrical potential barrier between the couple components on the charge transfer can be considered only for the charge carriers formed by light-induced ionization (described in Chapter 2, **Figure 2.4**).
iv) The results indicate that the photocatalytic performance of the couple systems formed of pure and Cr-doped TiO_2 is substantially larger after annealing in oxidizing conditions, even if the synergy is not observed.

The observed effects of coupling indicate that the specimens annealed in reducing conditions exhibit a synergy of the performance while the specimens annealed in oxidizing conditions display a negative synergy.

5.3.4 Effect of Segregation on Photocatalytic Performance

The key feature of the photocatalytic activity is the presence of a build-in electric field. Due to the surface segregation of chromium (discussed in Chapter 4) in Cr-doped TiO_2 a potential difference formed in the gradient at the surface which is responsible for the efficient separation of the photogenerated electrons and holes, thereby preventing recombination (as shown in **Figure 5.27**). In **Figure 5.27a**, shows the energy loses due to the recombination of photogenerated electron and hole in the absence of a segregation-induced electric field. On the other hand, in **Figure 5.27b**, shows the efficient charge separation at the surface because of the presence of the segregation-induced electric field, which increases the photocatalytic activity.

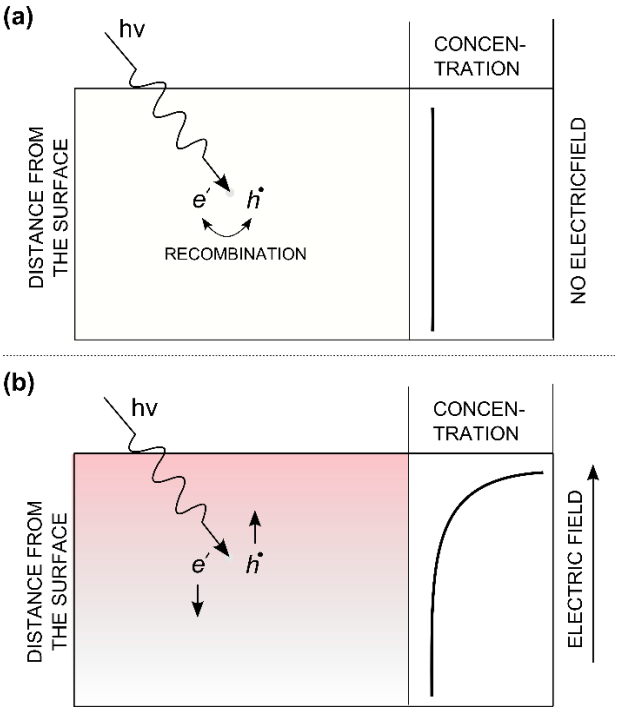

Figure 5.27. *Schematic representation of the effect of the electric field formed due to segregation on photogenerated charge separation.*

5.3.5 Mechanism of Photocatalytic Water Oxidation

The results obtained in this work allow derivation of a theoretical model on the mechanism of photocatalytic water oxidation by the mono-phase system of Cr-doped TiO_2 processed in oxidizing conditions and the related charge transfer (**Figure 5.28**).

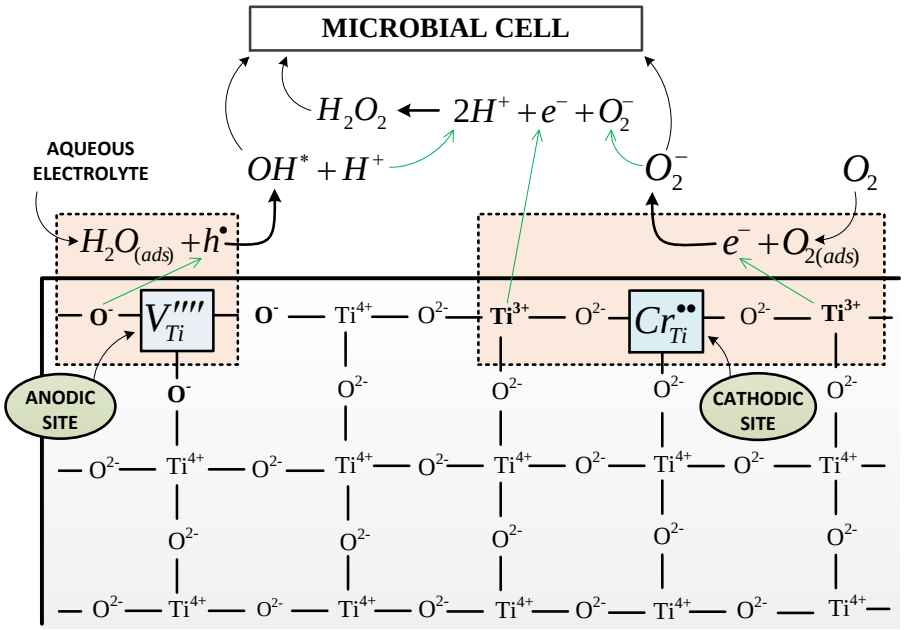

Figure 5.28. *Schematic representation of the reaction mechanisms between the surface-active sites (anodic and cathodic) for Cr-doped TiO_2 (involving low chromium concentration [Cr]<0.04 at%) and the adsorbed molecules of water and oxygen, respectively, leading to the formation of reactive radicals, such as hydroxyl radical and superoxide species.*

The most critical step in water oxidation is the anodic charge transfer of water molecule(s) adsorbed at titanium vacancies. This reaction, which is associated the with removal of electron holes from TiO_2, leads to the formation of hydroxyl radicals and protons. Assuming the lowest valence of the functional ions, the related anodic and cathodic reactions are represented by the following reactions:

Anodic Reactions[1]

(i) Formation of anodic active complex:

$$H_2O + V_{Ti}^x \rightarrow \{H_2O - V_{Ti}^x\}^* \tag{5.15}$$

(ii) Charge transfer:

$$\{H_2O - V_{Ti}^x\} \rightarrow \{H_2O^+ - V_{Ti}^{'}\}^* \tag{5.16}$$

(iii) Complex decomposition:

$$\{H_2O^+ - V_{Ti}^{'}\}^* \rightarrow HO^* + H^+ + V_{Ti}^{'} \tag{5.17}$$

[1] The species in the solid phase are represented according to the Kröger-Vink notation

(iv) Light-induced bandgap ionization:

$$O_O^x + Ti_{Ti}^x \rightarrow O_O^{\bullet} + Ti_{Ti}^{'} \tag{5.18}$$

(v) Light-induced oxidation of titanium vacancies:

$$O_O^{\bullet} + V_{Ti}^{'} \rightarrow O_O^x + V_{Ti}^x \tag{5.19}$$

Cathodic Reactions

(i) Formation of cathodic active complex:

$$O_2 + Cr_{Ti}^x \rightarrow \{O_2 - Cr_{Ti}^x\}^* \tag{5.20}$$

(ii) Charge transfer:

$$\{O_2 - Cr_{Ti}^x\}^* \rightarrow \{O_2^- - Cr_{Ti}^{\bullet}\}^* \tag{5.21}$$

(iii) Complex decomposition:

$$\{O_2^- - Cr_{Ti}^{\bullet}\}^* \rightarrow Cr_{Ti}^{\bullet} + O_2^- \tag{5.22}$$

(iv) Light-induced reduction of chromium ions:

$$Ti_{Ti}^{'} + Cr_{Ti}^{\bullet} \rightarrow Ti_{Ti}^x + Cr_{Ti}^x \tag{5.23}$$

The maximum performance, observed at 0.04 at% in oxidizing conditions, corresponds to the maximum activity of the titanium vacancies, formed according to the reactions represented by **equations (5.3)** to **(5.6)**, which are critical for initiating of anodic reactions.

This suggests the maximum activity of these defects corresponds to the dilute solution of chromium in TiO_2. While the increase of chromium content above 0.04 at% still results in the formation of titanium vacancies, the surface chromium concentration increases (**Table 4.3**). Therefore, the titanium vacancies at higher concentrations lead to the formation of complexes [63] such as equations **(5.7)** to **(5.9)** that are less active as anodic sites. As an example, a schematic representation of one of the associated defects in Cr-doped TiO_2 is shown in **Figure 5.29**.

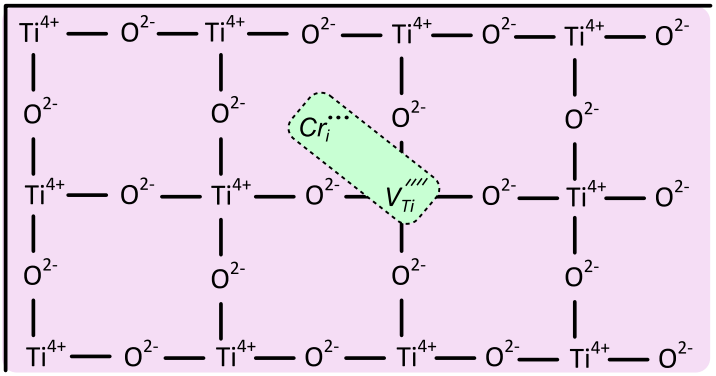

Figure 5.29. *Schematic representation of the associated defect forms at higher concentration of chromium in Cr-doped TiO_2.*

Alternatively, the observed decrease of performance at high chromium concentration, at [Cr]>0.04 at%, may be considered in terms of the mechanism leading to the formation of less active tri-valent chromium ions in titanium sites:

$$2Cr_2O_3 + V_{Ti}'''' + 2O_O^x \leftrightarrow 4Cr_{Ti}' + 8O_O^x \qquad (5.24)$$

The observed effect of chromium on photocatalytic properties is complex since its activity depends on the mechanism of its incorporation into the TiO_2 lattice. As shown, chromium may act either as acceptor or donor depending on the mechanisms of its incorporation and the related defect disorder. The complexity, however, helps to better understand the effect of defect disorder on performance.

5.4 Chapter Summary

The present work investigates the effect of chromium on photocatalytic properties of TiO_2. One may expect that the incorporation of chromium into the TiO_2 lattice results in the formation of acceptor-type levels that are related to commonly recognized chromium incorporation mechanism involving tri-valent chromium in titanium lattice site. The present work indicates that the mechanism of the incorporation of chromium, which in the case of photocatalytic performance must be considered in terms of the surface layer, is entirely different than that in the bulk phase. As a consequence, chromium results in enhanced photocatalytic performance only within very diluted solutions of chromium in the TiO_2 lattice. The related mechanism of chromium incorporation results in the

formation of titanium vacancies that are outstanding anodic active sites for water oxidation.

The important technical outcomes can be summarized as following:

i) Annealing in oxidizing conditions indicates that the effect of chromium on performance should be considered in terms of two compositional regimes:
   a) *Dilute Cr-doped TiO_2 involving the concentration below 0.04 at% Cr*. In this regime, chromium enhances the photocatalytic performance of TiO_2. This effect indicates that chromium incorporation in this concentration regime results in the formation of isolated titanium vacancies forming strong anodic sites, which have a controlling effect on performance.
   b) *Cr-doped TiO_2 involving high chromium content (above 0.04 at% Cr).* The results related to this regime indicate that either (i) incorporation of chromium results in the formation of titanium vacancies involved in defect complexes, or (ii) chromium incorporation results in the formation of negatively charged species forming weak anodic sites.

ii) Annealing of Cr-doped TiO_2 in reducing conditions results in a decrease of photocatalytic performance below the level of pure TiO_2. This is because the incorporation of chromium, in this case, does not lead to the formation of titanium vacancies, which are the anodic active sites.

iii) Annealing of pure TiO_2 and Cr-doped TiO_2 in controlled oxygen activity results in minimum of performance in $p(O_2)$ = 21 kPa and $p(O_2)$ = 10 Pa respectively. These minima, which correspond to the n-p transition [60], indicate that the performance is affected when the charge transfer is blocked.

iv) The studies of the electrochemical couples indicate that the couples formed in reducing conditions exhibit a synergy effect on photocatalytic performance. The synergy effect is absent for the couples formed in oxidizing conditions as a result of the negative effect of the charge transport.

The present work confirms the crucial role of defect chemistry in the interpretation of photocatalytic properties of TiO_2.

5.5 References

[1] Jaimy, K.B., et al., *An aqueous sol–gel synthesis of chromium (III) doped mesoporous titanium dioxide for visible light photocatalysis.* Materials Research Bulletin, 2011. **46**(6): p. 914-921.

[2] Gong, J., et al., *A simple electrochemical oxidation method to prepare highly ordered Cr-doped titania nanotube arrays with promoted photoelectrochemical property.* Electrochimica Acta, 2012. **68**: p. 178-183.

[3] Li, X., Z. Guo, and T. He, *The doping mechanism of Cr into TiO_2 and its influence on the photocatalytic performance.* Physical Chemistry Chemical Physics, 2013. **15**(46): p. 20037-20045.

[4] López, R., R. Gómez, and S. Oros-Ruiz, *Photophysical and photocatalytic properties of TiO_2-Cr sol–gel prepared semiconductors.* Catalysis Today, 2011. **166**(1): p. 159-165.

[5] Tian, B., C. Li, and J. Zhang, *One-step preparation, characterization and visible-light photocatalytic activity of Cr-doped TiO_2 with anatase and rutile bicrystalline phases.* Chemical Engineering Journal, 2012. **191**: p. 402-409.

[6] Mardare, D., et al., *Undoped and Cr-doped TiO_2 thin films obtained by spray pyrolysis.* Thin Solid Films, 2010. **518**(16): p. 4586-4589.

[7] Diaz-Uribe, C., W. Vallejo, and W. Ramos, *Methylene blue photocatalytic mineralization under visible irradiation on TiO_2 thin films doped with chromium.* Applied Surface Science, 2014. **319**: p. 121-127.

[8] Zhu, J., et al., *Hydrothermal doping method for preparation of Cr^{3+}-TiO_2 photocatalysts with concentration gradient distribution of Cr^{3+}*. Applied Catalysis B: Environmental, 2006. **62**(3–4): p. 329-335.

[9] Peng, Y.-H., G.-F. Huang, and W.-Q. Huang, *Visible-light absorption and photocatalytic activity of Cr-doped TiO_2 nanocrystal films.* Advanced Powder Technology, 2012. **23**(1): p. 8-12.

[10] Choi, J., H. Park, and M.R. Hoffmann, *Effects of Single Metal-Ion Doping on the Visible-Light Photoreactivity of TiO_2.* The Journal of Physical Chemistry C, 2010. **114**(2): p. 783-792.

[11] Wilke, K. and H. Breuer, *The influence of transition metal doping on the physical and photocatalytic properties of titania.* Journal of Photochemistry and Photobiology A: Chemistry, 1999. **121**(1): p. 49-53.

[12] Ghasemi, S., et al., *Transition metal ions effect on the properties and photocatalytic activity of nanocrystalline TiO_2 prepared in an ionic liquid.* Journal of hazardous materials, 2009. **172**(2): p. 1573-1578.

[13] Jimmy, C.Y., et al., *An ordered cubic Im3m mesoporous Cr–TiO_2 visible light photocatalyst.* Chemical communications, 2006(25): p. 2717-2719.

[14] Koh, P.W., et al., *Photocatalytic degradation of photosensitizing and non-photosensitizing dyes over chromium doped titania photocatalysts under visible light.* Journal of Photochemistry and Photobiology A: Chemistry, 2017. **332**: p. 215-223.

[15] Michalow, K.A., et al., *Flame-made visible light active TiO_2:Cr photocatalysts: Correlation between structural, optical and photocatalytic properties.* Catalysis Today, 2013. **209**: p. 47-53.

[16] Trenczek-Zajac, A., et al., *Influence of Cr on structural and optical properties of TiO_2: Cr nanopowders prepared by flame spray synthesis.* Journal of Power Sources, 2009. **194**(1): p. 104-111.

[17] Vieira, F.T.G., et al., *The influence of temperature on the color of TiO_2: Cr pigments.* Materials Research Bulletin, 2009. **44**(5): p. 1086-1092.

[18] Hamadanian, M., A. Reisi-Vanani, and A. Majedi, *Synthesis, characterization and effect of calcination temperature on phase transformation and photocatalytic activity of Cu, S-codoped TiO_2 nanoparticles.* Applied Surface Science, 2010. **256**(6): p. 1837-1844.

[19] Li, Y., et al., *Gas sensing properties of p-type semiconducting Cr-doped TiO_2 thin films.* Sensors and Actuators B: Chemical, 2002. **83**(1–3): p. 160-163.

[20] Escudero, A. and F. Langenhorst, *Chromium incorporation into TiO_2 at high pressure.* Journal of Solid State Chemistry, 2012. **190**(0): p. 61-67.

[21] Belaya, E. and V. Viktorov, *Formation of solid solutions in the TiO_2-Cr_2O_3 system.* Inorganic Materials, 2008. **44**(1): p. 62-66.

[22] Sōmiya, S., S. Hirano, and S. Kamiya, *Phase relations of the Cr_2O_3-TiO_2 system.* Journal of Solid State Chemistry, 1978. **25**(3): p. 273-284.

[23] Zakrzewska, K., M. Radecka, and M. Rekas, *Effect of Nb, Cr, Sn additions on gas sensing properties of TiO_2 thin films.* Thin Solid Films, 1997. **310**(1–2): p. 161-166.

[24] Venezia, A.M., L. Palmisano, and M. Schiavello, *Structural Changes of Titanium Oxide Induced by Chromium Addition as Determined by an X-Ray Diffraction Study.* Journal of Solid State Chemistry, 1995. **114**(2): p. 364-368.

[25] Choudhury, B. and A. Choudhury, *Dopant induced changes in structural and optical properties of Cr^{3+} doped TiO_2 nanoparticles.* Materials Chemistry and Physics, 2012. **132**(2): p. 1112-1118.

[26] Açıkgöz, M., *A study of the impurity structure for $3d^3$ (Cr^{3+} and Mn^{4+}) ions doped into rutile TiO_2 crystal.* Spectrochimica Acta Part A: Molecular and Biomolecular Spectroscopy, 2012. **86**: p. 417-422.

[27] Sasaki, J., N. Peterson, and K. Hoshino, *Tracer impurity diffusion in single-crystal rutile (TiO_{2-x}).* Journal of Physics and Chemistry of Solids, 1985. **46**(11): p. 1267-1283.

[28] Kohler, K., et al., *Chromia Supported on Titania: I. An EPR Study of the Chemical and Structural Changes Occurring during Catalyst Genesis.* Journal of Catalysis, 1993. **143**(1): p. 201-214.

[29] Venezia, A., et al., *Characterization of chromium ion-doped titania by FTIR and XPS.* Journal of Catalysis, 1994. **147**(1): p. 115-122.

[30] Köhler, K., et al., *Chromium oxide supported on titania: Preparation of highly dispersed Cr (III) systems by grafting.* Langmuir, 1995. **11**(9): p. 3423-3430.

[31] Kim, R., et al., *Charge and magnetic states of rutile TiO_2 doped with Cr ions.* Journal of Physics: Condensed Matter, 2014. **26**(14): p. 146003.

[32] Santara, B., et al., *Mechanism of defect induced ferromagnetism in undoped and Cr doped TiO_2 nanorods/nanoribbons.* Journal of Alloys and Compounds, 2016. **661**: p. 331-344.

[33] Wang, L. and T.A. Egerton, *The influence of chromium on photocatalysis of propane-2-ol and octadecanoic acid oxidation by rutile TiO_2.* Journal of Photochemistry and Photobiology A: Chemistry, 2013. **252**: p. 211-215.

[34] Osterwalder, J., et al., *Growth of Cr-doped TiO_2 films in the rutile and anatase structures by oxygen plasma assisted molecular beam epitaxy.* Thin Solid Films, 2005. **484**(1): p. 289-298.

[35] Chandrasekharan, N. and P.V. Kamat, *Improving the photoelectrochemical performance of nanostructured TiO_2 films by adsorption of gold nanoparticles.* The Journal of Physical Chemistry B, 2000. **104**(46): p. 10851-10857.

[36] Subramanian, V., E.E. Wolf, and P.V. Kamat, *Catalysis with TiO_2/gold nanocomposites. Effect of metal particle size on the Fermi level equilibration.* Journal of the American Chemical Society, 2004. **126**(15): p. 4943-4950.

[37] Li, H., et al., *Mesoporous Au/TiO_2 nanocomposites with enhanced photocatalytic activity.* Journal of the American Chemical Society, 2007. **129**(15): p. 4538-4539.

[38] Wang, X., et al., *A mesoporous Pt/TiO_2 nanoarchitecture with catalytic and photocatalytic functions.* Chemistry-A European Journal, 2005. **11**(10): p. 2997-3004.

[39] Chen, T., et al., *Mechanistic studies of photocatalytic reaction of methanol for hydrogen production on Pt/TiO_2 by in situ Fourier transform IR and time-resolved IR spectroscopy.* The Journal of Physical Chemistry C, 2007. **111**(22): p. 8005-8014.

[40] Zou, J.-J., et al., *Highly efficient Pt/TiO_2 photocatalyst for hydrogen generation prepared by a cold plasma method.* International Journal of Hydrogen Energy, 2007. **32**(12): p. 1762-1770.

[41] Ranjit, K., T.K. Varadarajan, and B. Viswanathan, *Photocatalytic reduction of nitrite and nitrate ions to ammonia on Ru/TiO_2 catalysts.* Journal of Photochemistry and Photobiology A: Chemistry, 1995. **89**(1): p. 67-68.

[42] Zhang, H. and G. Chen, *Potent antibacterial activities of Ag/TiO_2 nanocomposite powders synthesized by a one-pot sol-gel method.* Environmental Science & Technology, 2009. **43**(8): p. 2905-2910.

[43] Zhong, J.B., et al., *Characterization and photocatalytic property of Pd/TiO_2 with the oxidation of gaseous benzene.* Journal of Hazardous Materials, 2009. **168**(2): p. 1632-1635.

[44] Chen, P., et al., *Characterizations of Ir/TiO_2 catalysts with different Ir contents for selective hydrogenation of crotonaldehyde.* Reaction Kinetics, Mechanisms and Catalysis, 2012. **106**(2): p. 419-434.

[45] Pan, X. and Y.-J. Xu, *Defect-mediated growth of noble-metal (Ag, Pt, and Pd) nanoparticles on TiO_2 with oxygen vacancies for photocatalytic redox reactions under visible light.* The Journal of Physical Chemistry C, 2013. **117**(35): p. 17996-18005.

[46] Wu, G., et al., *H_2 production with low CO selectivity from photocatalytic reforming of glucose on metal/TiO_2 catalysts.* Science in China Series B: Chemistry, 2008. **51**(2): p. 97-100.

[47] Bessekhouad, Y., et al., *UV–vis versus visible degradation of Acid Orange II in a coupled CdS/TiO_2 semiconductors suspension.* Journal of Photochemistry and Photobiology A: Chemistry, 2006. **183**(1): p. 218-224.

[48] Tristão, J.C., et al., *Electronic characterization and photocatalytic properties of CdS/TiO_2 semiconductor composite.* Journal of Photochemistry and Photobiology A: Chemistry, 2006. **181**(2): p. 152-157.

[49] Wu, L., C.Y. Jimmy, and X. Fu, *Characterization and photocatalytic mechanism of nanosized CdS coupled TiO_2 nanocrystals under visible light irradiation.* Journal of Molecular Catalysis A: Chemical, 2006. **244**(1): p. 25-32.

[50] Yu, C., et al., *Enhancing the photocatalytic performance of commercial TiO_2 crystals by coupling with trace narrow-band-gap Ag_2CO_3.* Industrial & Engineering Chemistry Research, 2014. **53**(14): p. 5759-5766.

[51] DohĿeviĿ-MitroviĿ, Z., et al., *WO_3/TiO_2 composite coatings: Structural, optical and photocatalytic properties.* Materials Research Bulletin, 2016. **83**: p. 217-224.

[52] Kim, H.-M., D. Kim, and B. Kim, *Photoinduced hydrophilicity of TiO_2/WO_3 double layer films.* Surface and Coatings Technology, 2015. **271**: p. 18-21.

[53] Momeni, M.M. and Y. Ghayeb, *Visible light-driven photoelectrochemical water splitting on ZnO–TiO_2 heterogeneous nanotube photoanodes.* Journal of Applied Electrochemistry, 2015. **45**(6): p. 557-566.

[54] Hao, D., et al., *Photocatalytic Activities of TiO_2 Coated on Different Semiconductive SiC Foam Supports.* Journal of Materials Science & Technology, 2013. **29**(11): p. 1074-1078.

[55] Zhang, Y., et al., *Preparation of ternary Cr_2O_3–SiC–TiO_2 composites for the photocatalytic production of hydrogen.* Particuology, 2012. **10**(1): p. 46-50.

[56] Hattori, A., et al., *Acceleration of Oxidations and Retardation of Reductions in Photocatalysis of a TiO_2/SnO_2 Bilayer-Type Catalyst.* Journal of the Electrochemical Society, 2000. **147**(6): p. 2279-2283.

[57] Cao, Y., et al., *A bicomponent TiO_2/SnO_2 particulate film for photocatalysis.* Chemistry of Materials, 2000. **12**(11): p. 3445-3448.

[58] Jun, T.H., K.-S. Lee, and H.S. Song, *Hydrophilicity of anatase TiO_2/Cr-doped TiO_2 thin films with different band gaps.* Thin Solid Films, 2012. **520**(7): p. 2609-2612.

[59] Bak, T., et al., *Effect of crystal imperfections on reactivity and photoreactivity of TiO_2 (Rutile) with oxygen, water, and bacteria.* The Journal of Physical Chemistry C, 2011. **115**(32): p. 15711-15738.

[60] Nowotny, J., et al., *Effect of Oxygen Activity on the n–p Transition for Pure and Cr-Doped TiO_2.* The Journal of Physical Chemistry C, 2016. **120**(6): p. 3221-3228.

[61] Li, W., et al., *Photocatalytic properties of TiO_2: Effect of niobium and oxygen activity on partial water oxidation.* Applied Catalysis B: Environmental, 2016. **198**: p. 243-253.

[62] Alim, M.A., et al., *Photocatalytic properties of Ta-doped TiO_2.* Ionics, 2017: p. 1-15.

[63] Stoneham, A.M., *Theory of defect processes.* Physics Today, 1980. **33**(1): p. 34-37.

Chapter 6
Brief Summary

Research Strategy

This PhD research project performed comprehensive studies on the effect of processing of Cr-doped TiO_2-based systems on the light-induced partial water oxidation. The analysis of the results is based on the assumption that the photocatalytic performance, tested by the decomposition of methylene blue (MB), is determined by defect disorder of the studied system and the associated defect-related properties. The established effects of defect disorder on the performance are fully consistent with the postulate of the thesis that the performance of TiO_2-based system in solar-to-chemical energy conversion is determined by point defects and defect-related properties.

Surface vs. bulk properties

This research project has shown that annealing Cr-doped TiO_2 at elevated temperatures in the gas phase of controlled oxygen activity results in surface segregation of chromium leading, in consequence, to a substantial difference between surface and bulk composition. The latter has a substantial impact on solar-to-chemical energy conversion. It has been attested that the segregation-induced enrichment factor of chromium, as well as the valence of segregating chromium ions, are profoundly influenced by oxygen activity. This finding indicates that oxygen activity is an important factor in defect engineering in general and surface processing in particular.

Defect-related properties

The established effects of point defects on photocatalytic performance provide the information about the competition between the defect-related KPPs, including (i) the concentration of surface active sites, (ii) Fermi level, (iii) band gap and (iv) charge transport. The most significant discovery of this project is that the substantial reduction of the bandgap of TiO_2 has only an insignificant effect on photocatalytic performance that can be ignored for the system under present studies. This observation contradicts the literature reports that the band gap is the most critical KPP [1-13]. It has been attested that the photocatalytic performance of Cr-doped TiO_2 is determined by the remaining KPPs, including the concentration of anodic surface sites, which are mainly titanium vacancies, and the related Fermi level. It has also been shown that the charge transport has a critical effect on photocatalytic performance of TiO_2 when the system becomes insulating.

Defect Engineering

The effects of the KPPs on performance established in this project, pave the way for the development of defect engineering as a new approach in processing of energy materials in general and solar materials in particular. It has been documented the approach of *defect engineering* should be applied to both the bulk phase and the surface layer.

Key Findings

The key findings of this PhD projects have been outlined in the Abstract (page 2).

6.1 References

[1] Hajjaji, A., et al., *Cr-Doped TiO_2 Thin Films Prepared by Means of a Magnetron Co-Sputtering Process: Photocatalytic Application.* American Journal of Analytical Chemistry, 2014. **2014**.

[2] Radecka, M., et al., *Study of the TiO_2–Cr_2O_3 system for photoelectrolytic decomposition of water.* Solid State Ionics, 2003. **157**(1): p. 379-386.

[3] Dholam, R., et al., *Efficient indium tin oxide/Cr-doped-TiO_2 multilayer thin films for H_2 production by photocatalytic water-splitting.* International Journal of Hydrogen Energy, 2010. **35**(18): p. 9581-9590.

[4] Diaz-Uribe, C., W. Vallejo, and W. Ramos, *Methylene blue photocatalytic mineralization under visible irradiation on TiO_2 thin films doped with chromium.* Applied Surface Science, 2014. **319**: p. 121-127.

[5] Mardare, D., et al., *Chromium-doped titanium oxide thin films.* Materials Science and Engineering: B, 2005. **118**(1): p. 187-191.

[6] Wilke, K. and H. Breuer, *The influence of transition metal doping on the physical and photocatalytic properties of titania.* Journal of Photochemistry and Photobiology A: Chemistry, 1999. **121**(1): p. 49-53.

[7] López, R., R. Gómez, and S. Oros-Ruiz, *Photophysical and photocatalytic properties of TiO_2-Cr sol–gel prepared semiconductors.* Catalysis Today, 2011. **166**(1): p. 159-165.

[8] Jaimy, K.B., et al., *An aqueous sol–gel synthesis of chromium (III) doped mesoporous titanium dioxide for visible light photocatalysis.* Materials Research Bulletin, 2011. **46**(6): p. 914-921.

[9] Choudhury, B. and A. Choudhury, *Dopant induced changes in structural and optical properties of Cr^{3+} doped TiO_2 nanoparticles.* Materials Chemistry and Physics, 2012. **132**(2): p. 1112-1118.

[10] Michalow, K.A., et al., *Flame-made visible light active TiO_2:Cr photocatalysts: Correlation between structural, optical and photocatalytic properties.* Catalysis Today, 2013. **209**: p. 47-53.

[11] Zhang, S., et al., *Synthesis, characterization of Cr-doped TiO_2 nanotubes with high photocatalytic activity.* Journal of Nanoparticle Research, 2008. **10**(5): p. 871-875.

[12] Gong, J., et al., *A simple electrochemical oxidation method to prepare highly ordered Cr-doped titania nanotube arrays with promoted photoelectrochemical property.* Electrochimica Acta, 2012. **68**: p. 178-183.

[13] Momeni, M.M. and Y. Ghayeb, *Photoelectrochemical water splitting on chromium-doped titanium dioxide nanotube photoanodes prepared by single-step anodizing.* Journal of Alloys and Compounds, 2015. **637**: p. 393-400.

APPENDIX

First Pages of Papers Published by the Candidate during 2015-2018

Ionics (2018) 24:309–325
https://doi.org/10.1007/s11581-017-2369-2

ORIGINAL PAPER

Toward sustainable energy: photocatalysis of Cr-doped TiO_2: 1. electronic structure

Kazi Akikur Rahman[1] · Tadeusz Bak[1] · Armand Atanacio[2] · Mihail Ionescu[2] · Janusz Nowotny[1]

Received: 3 September 2017 / Revised: 8 November 2017 / Accepted: 25 November 2017 / Published online: 26 December 2017

Abstract
The present chain of five papers considers the concept of defect engineering in processing TiO_2-based photosensitive semiconductors for solar-to-chemical energy conversion. The papers report the effect of chromium on the key performance-related properties of polycrystalline TiO_2 (rutile), including (i) electronic structure, (ii) chromium-related photocatalytic properties, (iii) oxygen-related photocatalytic properties, (iv) electrochemical coupling and (v) surface versus bulk properties. The present work reports the effect of chromium on defect disorder and the related electronic structure of TiO_2, including the band gap and mid-gap energy levels. It is shown that chromium incorporation into the TiO_2 lattice results in a decrease of the band gap from 3.04 eV for pure TiO_2 to 1.4 and 1.3 eV, for Cr-doped TiO_2 (1.365 at% Cr) after annealing at 1373 K in the gas phase of controlled oxygen activity, 21 kPa and 10^{-10} Pa, respectively. The optical properties determined using the ultraviolet-vis spectroscopy (in the reflectance mode) indicate that chromium incorporation results in the formation of mid-band energy levels. In this work, we show that chromium at and above the concentrations levels of 0.04 and 0.376 at% results in the formation of acceptor-type energy levels at 0.57 and 1.16 eV (above the valence band), respectively, which are related to tri-valent chromium in titanium sites and titanium vacancies, respectively. Application of well-defined protocol leads to the determination of data that are well reproducible. The new insight involves the determination of the band gap of TiO_2 processed in the gas phase of controlled oxygen activity.

Keywords Titanium dioxide · Cr-doped TiO_2 · Defect disorder · Optical properties

Introduction

Introduction to the series

The global environment is under threat. The main factor leading to it's destruction is energy generation from fossil fuels and resulting emissions of greenhouse gases and climate changes. Therefore, there is an increasingly urgent need to reduce carbon emission through the development of new energy technologies that are environmentally clean.

Solar energy is the most widely available renewable energy. The most common approach in solar energy conversion so far is based on the generation of solar electricity. This technology, which is essentially based on silicon, is well entrenched. *The aim is to reduce the costs of photovoltaic electricity. This may be achieved by processing silicon with enhanced efficiency of solar-to-electrical energy conversion* [1].

The present series of papers considers a pioneering approach in application of defect engineering to the development of a new generation of solar materials for solar-to-chemical energy conversion, photosensitive oxide semiconductors, POSs. In has been documented that the key performance-related properties of the POSs are determined by point defects [2]. Therefore, enhanced performance of new materials may be achieved by application of defect engineering in processing the POSs with optimised defect disorder that is required for maximised performance. This series consider several aspects of defect engineering:

Highlights
1. Incorporation of chromium results in reduction of TiO_2 band gap
2. Chromium in the bulk phase is predominantly incorporated into titanium sites
3. Chromium results in the formation of both acceptor and donor-type centres

✉ Janusz Nowotny
J.Nowotny@westernsydney.edu.au

[1] Solar Energy Technologies, Western Sydney University, Penrith, NSW 2751, Australia

[2] Australian Nuclear Science and Technology Organisation, Kirrawee, NSW 2232, Australia

Ionics (2018) 24:327–341
https://doi.org/10.1007/s11581-017-2370-9

ORIGINAL PAPER

Toward sustainable energy: photocatalysis of Cr-doped TiO_2: 2. effect of defect disorder

Kazi Akikur Rahman[1] · Tadeusz Bak[1] · Armand Atanacio[2] · Mihail Ionescu[2] · Janusz Nowotny[1]

Received: 3 September 2017 / Revised: 8 November 2017 / Accepted: 25 November 2017 / Published online: 26 December 2017

Abstract

The present chain of five papers considers the concept of solar-to-chemical energy conversion using TiO_2-based semiconductors. The series reports the effect of chromium on the key performance-related properties of polycrystalline TiO_2 (rutile), including electronic structure, photocatalytic activity, intrinsic defect disorder, electrochemical coupling and surface versus bulk properties. In this work, we show that the effect of chromium on photocatalytic performance of TiO_2 depends on its elemental content and the related defect disorder that is determined by oxygen activity in the oxide lattice. At high oxygen activity, chromium leads to enhanced photocatalytic performance only for dilute solid solutions (up to 0.04–0.043 at.% Cr). Higher chromium content results in a decrease of photocatalytic activity below that for pure TiO_2, despite the observed substantial decrease of the band gap. The photocatalytic performance of Cr-doped TiO_2 annealed in reducing conditions is low within the entire studied range of compositions. The obtained results led to derivation of a theoretical model representing the mechanism of the light-induced reactivity of TiO_2 with water and the related charge transfer. The photocatalytic performance is considered in terms of a competitive effect of several key performance-related properties. The performance is predominantly influenced by the concentration of titanium vacancies acting as reactive surface sites related to anodic charge transfer.

Keywords Cr-doped TiO_2 · Defect disorder · Photocatalysis

New insight
1. Reduction of the band gap has little effect on photocatalytic performance of Cr-doped TiO_2.
2. The photocatalytic activity of Cr-doped TiO_2 formed in oxidising conditions changes with composition. The photocatalytic performance increases within dilute solid solutions, up to 0.04 at.%, and decreases at higher chromium content.
3. The effect of chromium on photocatalytic activity may be considered in terms of a competitive effect of the key performance-related properties.

Highlights 1. The incorporation of chromium into the TiO_2 lattice results in an increase of photocatalytic activity only for dilute solid solutions (up to 0.04 at% Cr) annealed in oxidising conditions.
2. Chromium results in a decrease of photocatalytic activity when annealed in reducing conditions.
3. Photocatalytic activity of Cr-TiO_2 depends on several defect-related properties that have competitive effect on performance.

✉ Janusz Nowotny
J.Nowotny@westernsydney.edu.au

[1] Solar Energy Technologies, Western Sydney University, Penrith, NSW 2751, Australia

[2] Australian Nuclear Science and Technology Organisation, Kirrawee, NSW 2232, Australia

Introduction

The most common approach in the interpretation of photocatalytic properties of oxide materials is based on the perception that the light-induced reactivity of photocatalysts, such as TiO_2, is determined by the band gap and the associated increase in light absorption. Therefore, the frequently applied research strategy in processing of TiO_2-based semiconductors aims at reduction of the band gap. The recent work shows that the performance of TiO_2-based systems is determined by a range of the key performance-related properties, KPPs, which are profoundly influenced by defect disorder, including the concentration of the reactive surface sites, Fermi level and charge transport as well as the band gap. It is shown that the latter property has a minor effect on performance [1].

The present research project, involving this work and the previous paper [2], aims at understanding the effect of chromium on the light-induced partial oxidation of water and on the associated defect disorder and defect-related properties, such as electronic structure. The previous work reported the effect of chromium on electronic structure [2]. In this work, we

Ionics (2018) 24:861–872
https://doi.org/10.1007/s11581-017-2304-6

ORIGINAL PAPER

Towards sustainable energy. Photocatalysis of Cr-doped TiO_2: 3. Effect of oxygen activity

Kazi Akikur Rahman[1] · Tadeusz Bak[1] · Armand Atanacio[2] · Mihail Ionescu[2] · Janusz Nowotny[1]

Received: 3 September 2017 / Accepted: 14 October 2017 / Published online: 4 January 2018

Abstract The present chain of five papers considers the concept of solar-to-chemical energy conversion using TiO_2-based semiconductors. The series reports the effect of chromium on the key performance-related properties of polycrystalline TiO_2 (rutile), including electronic structure, photocatalytic activity, intrinsic defect disorder, electrochemical coupling and surface vs. bulk properties. The present work reports the effect of oxygen activity in the oxide lattice on photocatalytic activity of pure and Cr-doped TiO_2 (0.04 at% Cr). Processing of specimens included annealing at 1273 K in the gas phase of controlled oxygen activity in the range 10^{-12} Pa < $p(O_2)$ < 10^5 Pa. We show that the increase of oxygen activity results initially in a decrease of photocatalytic activity, minimum around the n-p transition point, and then increase assuming maximum at $p(O_2) = 10^5$ Pa. The obtained results are considered in terms of a theoretical model that explains the effect of defect disorder on the reactivity of TiO_2 with water. The minimum of the photocatalytic activity corresponds to the n-p transition point. The maximum of performance at high $p(O_2)$ is determined by increased concentration of titanium vacancies forming surface active sites.

Keywords Defect disorder · Oxygen activity · Reactivity

✉ Janusz Nowotny
J.Nowotny@uws.edu.au

[1] Solar Energy Technologies, School of Computing, Engineering and Mathematics, Western Sydney University, Penrith, NSW 2751, Australia

[2] Institute of Environmental Research, Australian Nuclear Science and Technology Organisation, Kirrawee, NSW 2232, Australia

Introduction

The present research program aims at understanding the effect of structural imperfections, including both intrinsic and extrinsic point defects, on photocatalysis for TiO_2-based semiconductors. The former papers of the present series on photocatalysis of Cr-doped TiO_2 reported the effect of chromium on electronic structure [1] and photocatalytic activity [2]. The present work aims at the determination of oxygen activity and the associated intrinsic defect disorder on photocatalytic performance for pure and Cr-doped TiO_2. The proposed theoretical models indicate that photocatalytic performance should be considered in terms of a range of key performance-related properties, KPPs, including band gap, concentration of surface-active sites, Fermi level and charge transport.

The former work shows that the incorporation of chromium into the TiO_2 lattice results in a substantial change of the band gap that is reduced from 3 eV for pure TiO_2 to 1.4 eV for Cr-doped TiO_2 (1.37 at% Cr) [1]. It is shown that the photocatalytic activity of Cr-doped TiO_2 is enhanced only within very dilute solid solutions of chromium in TiO_2 (up to 0.04 at% Cr) [2]. It has been attested that the band gap reduction of Cr-doped TiO_2 has little effect on its photocatalytic performance. The aim of this work is to determine the effect of intrinsic defects (oxygen vacancies, titanium vacancies, titanium interstitials and electronic defects) on photocatalytic properties for pure and Cr-doped TiO_2.

Postulation of the problem

The studies on TiO_2 photocatalysis are based on common perception that the critical property affecting light-induced water oxidation is the band gap and the associated absorption of sunlight [3, 4]. Therefore, the studies on processing the TiO_2-based

Ionics (2018) 24:873–881
https://doi.org/10.1007/s11581-017-2305-5

ORIGINAL PAPER

Towards sustainable energy. Photocatalysis of Cr-doped TiO_2: 4. Electrochemical coupling

Kazi A. Rahman[1] · A. Atanacio[2] · M. Ionescu[2] · J. Davis[2] · T. Bak[1] · J. Nowotny[1]

Received: 3 September 2017 / Accepted: 14 October 2017 / Published online: 6 January 2018

Abstract The present chain of five papers considers the concept of solar-to-chemical energy conversion using TiO_2-based semiconductors. The series reports the effect of chromium on the key performance-related properties of polycrystalline TiO_2 (rutile), including electronic structure, photocatalytic activity, intrinsic defect disorder, electrochemical coupling and surface versus bulk properties. This work reports the effect of photoelectrochemical coupling of both pure and Cr-doped TiO_2 on photocatalytic partial water oxidation. The couples are annealed in oxidising and reducing conditions, at $p(O_2) = 10^5$ Pa and $p(O_2) = 10^{-10}$ Pa, respectively. The performance of the coupled system may be enhanced, or retarded, by the electrical potential barrier that is formed between the couple components as a result of the difference in Fermi levels. In this work, we show that the potential barrier results in the effect of synergy when the charge transport within the couple components is high enough. This is the case for the couples annealed in reducing conditions.

Keywords Electrochemical coupling · Fermi level · Titanium dioxide

✉ J. Nowotny
J.Nowotny@uws.edu.au

[1] Solar Energy Technologies, School of Computing, Engineering and Mathematics, Western Sydney University, Penrith, NSW 2751, Australia

[2] Institute of Environmental Research, Australian Nuclear Science and Technology Organisation, Kirrawee, NSW 2232, Australia

Introduction

The TiO_2-based systems, including solid solutions and composites, are promising candidates for solar-to-chemical energy conversion. The commonly applied research strategy in processing the systems with high performance consists in reduction of TiO_2 band gap and deposition of small islets of metals or compounds forming active sites [1–3]. An alternative approach in processing TiO_2-based systems with enhanced photocatalytic performance is based on defect engineering and modification of semiconducting properties [4].

It has been shown that deposition of metallic islets of noble metals leads to a substantial increase of photocatalytic activity [5–14]. This can be explained by enhanced charge separation and reduced recombination of photogenerated charge carriers. The enhanced photocatalytic performance may also be achieved by deposition of co-catalysts of alternative oxide phases, such as WO_3 [15, 16] and ZnO [17]. In the latter case, the reason for performance boost is probably the formation of additional active anodic sites, in addition to charge separation.

The critical issue in the formation of photocatalytically active heterogeneous system is charge transfer between the phases forming the couple. This consequently requires high charge transport in both phases involved, as well as in the interphase layer that is formed during processing. Moreover, the performance of such system depends on the height of the formed potential barrier and the direction of the potential gradient. The latter is crucial in order to achieve the charge transfer in the desired direction.

The formation of an interphase layer within the couple is easier when the system is formed of the same compound, such as TiO_2. In this case, however, imposition of the desired potential barrier requires that both couple components have different Fermi levels. The latter may be achieved by using defect engineering in order to impose desired levels.

Ionics (2018) 24:1211–1219
https://doi.org/10.1007/s11581-017-2326-0

ORIGINAL PAPER

Towards sustainable energy: photocatalysis of Cr-doped TiO_2. 5. Effect of segregation on surface versus bulk composition

Kazi Akikur Rahman[1] · **Tadeusz Bak**[1] · **Armand Atanacio**[2] · **Mihail Ionescu**[2] · **Rong Liu**[3] · **Janusz Nowotny**[1]

Received: 3 September 2017 / Revised: 22 October 2017 / Accepted: 26 October 2017 / Published online: 7 November 2017

Abstract The present chain of five papers considers the concept of solar-to-chemical energy conversion using TiO_2-based semiconductors. The series reports the effect of chromium on the key performance-related properties of polycrystalline TiO_2 (rutile), including electronic structure, photocatalytic activity, intrinsic defect disorder, electrochemical coupling and surface versus bulk properties. This work considers the effect of oxygen activity on segregation-induced surface versus bulk composition for both polycrystalline and single-crystal specimens of Cr-doped TiO_2. It has been documented that annealing of Cr-doped TiO_2 at 1273 K in oxidising conditions results in an enrichment and depletion of the surface layer with chromium. It is shown that the segregation-induced enrichment factor for single crystal is substantially larger than that for polycrystalline specimen. The effect is considered in terms of a theoretical model showing that surface segregation of solute in polycrystalline specimen is encumbered by its segregation to grain boundaries. It is also shown that the segregation-induced enrichment is profoundly influenced by oxygen activity. The new insight of this work involves (i) the determination of well-defined chromium segregation in Cr-doped TiO_2, including single-crystal and polycrystalline specimens, after annealing in the gas phase of controlled oxygen activity, and (ii) identification of the predominant driving force of segregation of chromium in Cr-doped TiO_2 that is based on electrostatic interactions between the low-dimensional surface structure (LDSS) and electrically charge segregating species.

New insight

1. The determination of well-defined chromium segregation in Cr-doped TiO_2, including single-crystal and polycrystalline specimens, after annealing in the gas phase of controlled oxygen activity.
2. The results of surface and bulk analysis are reflective of the effect of oxygen activity on bulk versus surface defect disorder of TiO_2-based solid solutions for both single-crystal and polycrystalline specimens.
3. The predominant driving force of segregation of chromium in Cr-doped TiO_2 is based on electrostatic interactions between the low-dimensional surface structure (LDSS) and electrically charged lattice elements.

✉ Janusz Nowotny
J.Nowotny@uws.edu.au

[1] Solar Energy Technologies, School of Computing, Engineering and Mathematics, Western Sydney University, Penrith, NSW 2751, Australia

[2] Australian Nuclear Science and Technology Organisation, Institute of Environmental Research, Locked Bag 2001, Kirrawee DC, NSW 2232, Australia

[3] Secondary Ion Mass Spectrometry Facility, Office of the Deputy Vice Chancellor (Research and Development), Western Sydney University, Building M8, Hawkesbury Campus, Locked Bag 1797, Penrith, NSW 2751, Australia

Keywords Titanium dioxide · Segregation · Oxygen activity · Cr-doped TiO_2

Introduction

The photocatalytic performance is determined by local properties of the surface layer. Therefore, knowledge of the local surface composition and the associated semiconducting properties is crucial in understanding and correct interpretation of the mechanism and kinetics of photocatalytic reactions.

Former papers on photocatalysis of Cr-doped TiO_2 reported a wide range of properties, including the effect of chromium on electronic structure, including the band gap [1], photocatalytic activity [2] and the effect of oxygen activity on defect

THE JOURNAL OF PHYSICAL CHEMISTRY C
Article
pubs.acs.org/JPCC

Effect of Oxygen Activity on the n−p Transition for Pure and Cr-Doped TiO_2

Janusz Nowotny,*[,†] Wojciech Macyk,[‡] Eric Wachsman,[§] and Kazi A. Rahman[†]

[†]Solar Energy Technologies, Western Sydney University, Penrith, New South Wales 2751, Australia
[‡]Faculty of Chemistry, Jagiellonian University, Ingardena 3, 30-060 Krakow, Poland
[§]Energy Research Center, University of Maryland, College Park, Maryland 20742-2115, United States

ABSTRACT: Titanium dioxide, TiO_2, is commonly considered as an n-type semiconductor. The present work shows that TiO_2 exhibits both n- and p-type semiconducting properties. It is shown that p-type properties may be imposed by either increasing of oxygen activity or incorporation of acceptor-type ions, such as chromium. This work reports the n−p transition for both pure and Cr-doped TiO_2 (0.05 at % Cr) single crystals at elevated temperatures (1023−1323 K) in the gas phase of controlled oxygen activity. The n−p transition was determined by the measurements of thermoelectric power as a function of oxygen activity in the range 10 to 10^5 Pa. It is shown that the n−p transition line for Cr-doped TiO_2 exhibits a sharp change at 1173 K that is related to the conversion in chromium oxidation state from trivalent below 1173 K to six-valent above. This effect, which is reflective of a dual mechanism of chromium incorporation into the rutile structure of TiO_2, can be used for imposition of desired semiconducting properties that are needed for specific applications, such as solar-to-chemical energy conversion.

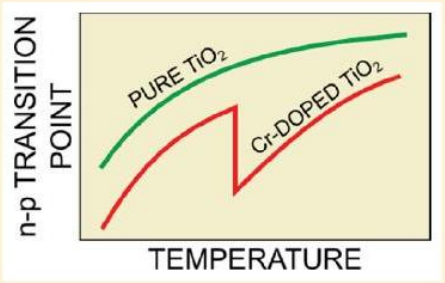

1. INTRODUCTION

Titanium dioxide, TiO_2, is the promising material for solar energy conversion.[1] Its performance is profoundly influenced by semiconducting properties.

TiO_2 is commonly considered as an n-type semiconductor.[2] In the present work we show that pure TiO_2 is an amphoteric semiconductor that exhibits both n- and p-type properties. It is shown that n-type TiO_2 may be converted into p-type semiconductor by increasing its lattice oxygen activity or incorporation of acceptor-type ions, such as chromium.

The present research strategy in processing TiO_2 with enhanced performance is commonly considered in terms of band gap reduction.[3−5] This approach is based on the perception that performance of TiO_2 is determined by the amount of absorbed light energy.

Recent studies show that the performance of TiO_2 is determined by defect disorder and defect-related properties, such as surface potential, the concentration of surface active sites, charge transport, and flat band potential.[6,7] In other words, the performance-related properties are profoundly influenced by structural imperfections, which play a key role in reactivity and photoreactivity. Recent work indicates that the population of the surface active sites is one of the key factors in solar-to-chemical energy conversion.[7] Moreover, imposition of imperfections may be used for the modification of the Fermi level position that is needed to enhance the charge transfer between TiO_2 and the adsorbed molecules.[7] In the latter case, however, the charge transfer is determined by the imperfections in the outermost surface layer, which have critical impact on performance. On the contrary, the concentration gradient within the surface layer and the related potential barrier play an important role in charge separation.[8] Therefore, the development of TiO_2 with enhanced performance requires imposition of an optimal surface versus bulk defect disorder and the related semiconducting properties. These properties may be modified by imposition of variable concentrations of both intrinsic and extrinsic defects.

The key property of amphoteric oxide semiconductors, such as TiO_2, is the n−p transition point. In this work we show that its position may be shifted back and forth by the modification of oxygen activity. The present work considers the effect of oxygen activity on the n−p transition point for pure TiO_2 and Cr-doped TiO_2.

The significance of chromium as dopant for TiO_2 can be considered in the following terms:

- It has been revealed that chromium results in a substantial reduction of bandgap.[3]
- When incorporated into titanium sites, chromium results in lowering the Fermi level and leads to imposition of the electron affinity that is favorable for anodic reactions.
- Chromium exhibits several oxidation states that may be modified by oxygen activity. The related effect may be applied for engineering of specific semiconducting properties.

Received: December 10, 2015
Revised: January 17, 2016
Published: January 19, 2016

DOI: 10.1021/acs.jpcc.5b12101
J. Phys. Chem. C 2016, 120, 3221−3228

Renewable and Sustainable Energy Reviews 81 (2018) 2541–2551

Contents lists available at ScienceDirect

Renewable and Sustainable Energy Reviews

journal homepage: www.elsevier.com/locate/rser

Towards global sustainability: Education on environmentally clean energy technologies

Janusz Nowotny[a,*], John Dodson[b], Sebastian Fiechter[c], Turgut M. Gür[d], Brendan Kennedy[e], Wojciech Macyk[f], Tadeusz Bak[a], Wolfgang Sigmund[g], Michio Yamawaki[h], Kazi A. Rahman[a]

[a] Solar Energy Technologies, Western Sydney University, Penrith, NSW 2751, Australia
[b] Institute of Earth Environment, Chinese Academy of Sciences, Yanta District, 97 Yanxiang Rd, Yanta District, Xi'an 710061, Shaanxi, China
[c] Institute for Solar Fuels, Helmholtz-Zentrum Berlin für Materialien und Energie GmbH, Hahn-Meitner-Platz 1, D-14109 Berlin, Germany
[d] Department of Materials Science and Engineering, Stanford University, Stanford, CA 94305-4034, USA
[e] School of Chemistry, The University of Sydney, Sydney, NSW 2006, Australia
[f] Faculty of Chemistry, Jagiellonian University, Ingardena 3, 30-060 Krakow, Poland
[g] Department of Materials Science and Engineering, University of Florida, Gainesville, FL 32611-6400, USA
[h] University of Tokyo, 7-3-1 Hongo, Bunkyo-ku, Tokyo 113-8654, Japan

ARTICLE INFO

Keywords:
Education-related programs
Energy-related textbooks
Sustainable Energy Network

ABSTRACT

The recent climate change agreement in Paris highlights the imperative to aggressively decarbonize the energy economy and develop new technologies, especially for the generation of electrical energy that are environmentally clean. This challenge can only be addressed by a multi-pronged approach to research and education of the next generation of scientists and engineers as well as informed public discourse. Consequently this requires the introduction of new and comprehensive education programs on sustainable energy technologies for universities and, possibly, high schools. Among others, the new programs should provide in-depth knowledge in the development of new materials for more efficient energy conversion systems and devices. The enhanced level of education is also needed for properly assessing the competing technologies in terms of their economic and social benefits. The increasing recognition of the significance of clean and efficient energy conversion indicates the need for a comprehensive education program to be developed. The purpose of the present work is to consider the structure of both an education program and the related textbook where the energy-related fundamental and applied subjects are presented in a concentrated and uniform manner. Such a textbook could be an education aid for students of energy-related courses as well as the teachers involved in the formulation of the education programs. The textbook, which should be dedicated mainly for students at the undergraduate levels at universities, and possibly high schools, should include in-depth interdisciplinary sections dedicated to energy experts and graduate students. This paper considers the present international efforts in reducing the impact of climate change and the need to develop new technologies for clean energy generation. It is argued that progress in this area requires recognition of hydrogen as the main energy carrier of the future. This work also delineates the goals of the Sustainable Energy Network, SEN, involved in the UN program of Future Earth.

1. Introduction

There is growing awareness that climate changes and the associated global environmental consequences may soon cross a critical point that could be catastrophic for humans. Therefore, there is an increasingly urgent need to take radical steps to transition to global environmental sustainability in order to secure on going global prosperity. Failure to act now will have undesired consequences for future generations who require non-contaminated water to drink, and clean air to breathe. Assuring a sustainable future requires full understanding, and appreciation, of the strong interplay and overlaps among energy, environment, food, water, and climate as schematically depicted in Fig. 1.

The recent historic Paris agreement among 195 countries on adopting a legally binding accord on climate change aims at limiting global warming to 1.5 °C to fulfil the long term goal of keeping the global average increase to less than 2 °C above its pre-industrial level. The agreement signals a global determination to reduce, and ultimately eliminate, the use of fossil fuels in energy generation and to develop alternate technologies. The enthusiastic global reaction to this agreement is reflective of community concerns of the detrimental environ-

* Corresponding author.
E-mail address: J.Nowotny@westernsydney.edu.au (J. Nowotny).

http://dx.doi.org/10.1016/j.rser.2017.06.060
Received 14 June 2016; Received in revised form 17 February 2017; Accepted 18 June 2017
Available online 29 June 2017
1364-0321/

Environmentally Clean Energy

David Black, University of New South Wales, Kensington, NSW, Australia; Sustainable Energy Initiative, Wollongong, NSW, Australia
Tadeusz Bak, Sustainable Energy Initiative, Wollongong, NSW, Australia; Western Sydney University, Penrith, NSW, Australia
John Dodson, University of Wollongong, Wollongong, NSW, Australia; Institute of Earth Environment, Shaanxi, China
Mahmudul Hasan, University of Sydney, Camperdown, NSW, Australia
Michelle Moffitt, Western Sydney University, Penrith, NSW, Australia
Kazi A Rahman, Western Sydney University, Penrith, NSW, Australia
Janusz Nowotny, Sustainable Energy Initiative, Wollongong, NSW, Australia; Western Sydney University, Penrith, NSW, Australia

Introduction

The damaging effects of climate changes on the environment are becoming increasingly apparent. Each year of inaction raises the cost of identifying and applying the measures that must be taken in order to protect Earth systems before they cross the critical thresholds which drive the planet to the point of being unable to meet the needs of ecosystems, ecosystem services and social well-being. As a result, the UN has been undertaking a range of initiatives that build international co-operation on reducing carbon-based energy systems and the emission of additional greenhouse active gases which produce global warming (Tokyo International Conference of African Development (TICAD), n.d.; United Nations Conference on Sustainable Development, n.d.; UN Climate Change Conference Paris, 2015). A key objective of the global community, realized at the Paris Summit (UN Climate Change Conference Paris, 2015) is to reduce global warming and the related climate impacts. It is believed that about 2°C warming above 1990 levels will be where many of the critical thresholds will be exceeded and that a target of no more than about 1.5°C of warming should be set (UN Climate Change Conference Paris, 2015).

A key element of this is the reduction of greenhouse gas emissions through reducing the reliance of generation of energy mainly based on fossil fuels. However, despite increasing international efforts to decarbonize the sector of energy generation, the measures undertaken by governments so far are inadequate for protection of the planet delivering sustainable services (Climate, n.d.). This can only be done through undertaking a multipronged approach to introduce solutions aimed at the transition towards sustainable development. This includes using political, economic and environmental solutions which result in a transition to affordable and environmentally clean technologies for the generation of energy.

In order to address the deterioration of the environment, the UN, through UNESCO and a consortium of global partners, was instrumental in the establishment of the program called Future Earth; which is a global platform that is expected to provide the knowledge that is required for the transformation towards global sustainability (Future Earth 2025 Vision, 2013). The consortium included:

- International Council for Science (ICSU)
- International Social Science Council (ISSC)
- The Belmont Forum of funding agencies
- United Nations Educational, Scientific and Cultural Organization (UNESCO)
- United Nations Environment Programme (UNEP)
- United Nations University (UNU)
- World Meteorological Organization (WMO)
- The Sustainable Development Solutions Network (SDSN)
- STS forum

This program, which is a necessarily very ambitious scientific project, involves three thematic areas: Dynamic Planet, Global Sustainable Development and Transformation towards Sustainability.

The first major step towards the transition to cleaner energy—already widely initiated at a global scale—is the introduction of hydrogen economy. This requires the development of new infrastructure related to hydrogen production, transportation, distribution and storage. However, the major challenge is the transition from the presently common hydrogen production technology from natural gas, which is associated with CO_2 emissions, to hydrogen generation that does not involve CO_2 emission. The application of

CHAPTER ONE

Defect Engineering of Photosensitive Oxide Materials. Example of TiO_2 Solid Solutions

Armand J. Atanacio*, Tadeusz Bak§, Kazi A. Rahman§ and Janusz Nowotny§,1

*Centre for Accelerator Science, Australian Nuclear Science and Technology Organisation, Kirrawee DC, NSW, Australia
§Solar Energy Technologies, School of Computing, Engineering and Mathematics, Western Sydney University, Penrith, NSW, Australia
1Corresponding author: E-mail: J.Nowotny@westernsydney.edu.au

Contents

Advances in Inorganic Chemistry, Volume 72
ISSN 0898-8838
https://doi.org/10.1016/bs.adioch.2018.05.006

CoO-12

Evidence of Low-Dimensional Surface Structures for Oxide Materials. Impact on Energy Conversion

Tadeusz Bak[1], Turgut M. Gür[2], Virender K. Sharma[3], John Dodson[4, 5], Kazi A. Rahman[1] and Janusz Nowotny[1*]

[1]Solar Energy Technologies, School of Computing, Engineering and Mathematics, Western Sydney University, Penrith, NSW 2751, Australia (ORCID, TB: 0000-003-1461-951X, KAR: 0000-0003-0621-7051, JN: 0000-0002-1822-750)

[2]Department of Materials Science and Engineering, Stanford University, Stanford, CA 94305-4034, USA (ORCID: 0000-0002-2218-4766)

[3]Program for the Environment and Sustainability, School of Public Health, Texas A&M University, 212 Adriance Lab Road, 1266 TAMU, College Station, TX 77845, USA (ORCID: 0000-0002-5980-8675)

[4]School of Earth, Atmosphere and Life Sciences, University of Wollongong, Wollongong, NSW 2500, Australia (ORCID: 0000-0002-0124-5910)

[5]Institute of Earth Environment, Chinese Academy of Sciences, Yanta District, 97 Yangxiang Rd, Xi'an 710061, Shaanxi, China

Abstract

Knowledge of surface properties of energy materials at elevated temperatures is essential for understanding their reactivity and performance in energy conversion. Here we show that single-phase oxide materials, such as CoO, at elevated temperatures corresponding to thermodynamic equilibrium, consists of homogeneous bulk phase and a low-dimensional surface structure, LDSS, which differs from the bulk phase in terms of crystalline structure, chemical composition, defect disorder and semiconducting properties. It has been documented that the CoO/O_2 system in gas/solid equilibrium exhibits three types of LDSSs that are formed in: (a) reducing conditions, (b) oxidizing conditions and (c) highly oxidizing conditions corresponding to the vicinity of the CoO/Co_3O_4 phase boundary. Oxidation of these LDSSs leads to: (a) decrease of the Fermi level, (b) nil change of the Fermi level, and (c) increase of the Fermi level, respectively. The effects (b) and (c), which are not observed for the bulk phase, indicate that the LDSS is quasi-isolated. This discovery has been revealed by *in situ* surface monitoring of CoO at elevated temperatures using work function, WF, measurements. The results reported in the present work are reflective of the local properties of the LDSSs that are formed on the surface of CoO single crystal, including defect disorder and the related semiconducting properties. This finding paves the way for the development of novel approaches in processing of energy conversion and refractory systems with enhanced performance through defect engineering of the surface layer.

Keywords: Surface structure, reactivity, defect disorder, defect engineering, cobalt oxide, work function

Supplementary Data

Electronic Structure

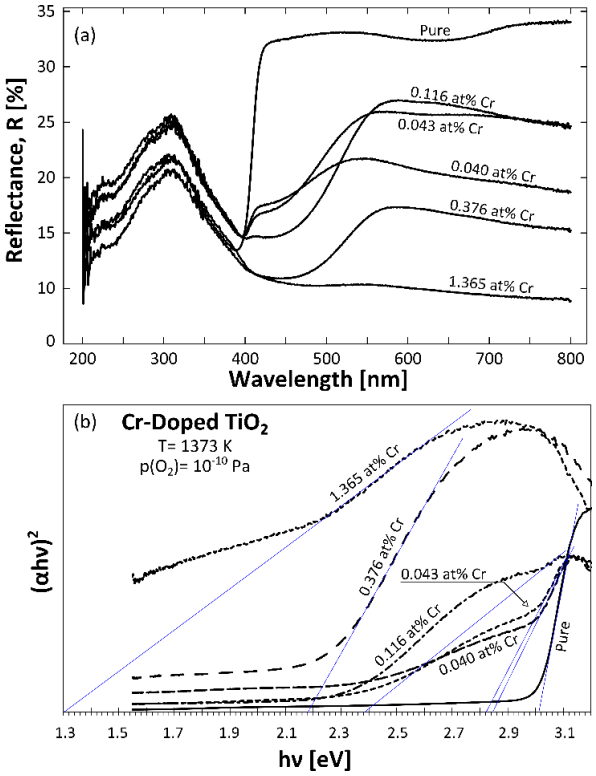

Figure A.1. *Effect of chromium concentration on the reflectance spectra (a) and the related Tauc plot (b) of TiO_2. Specimens annealed at 1373 K for 1 h in argon-hydrogen mixture ($p(O_2) = 10^{-10}$ Pa).*

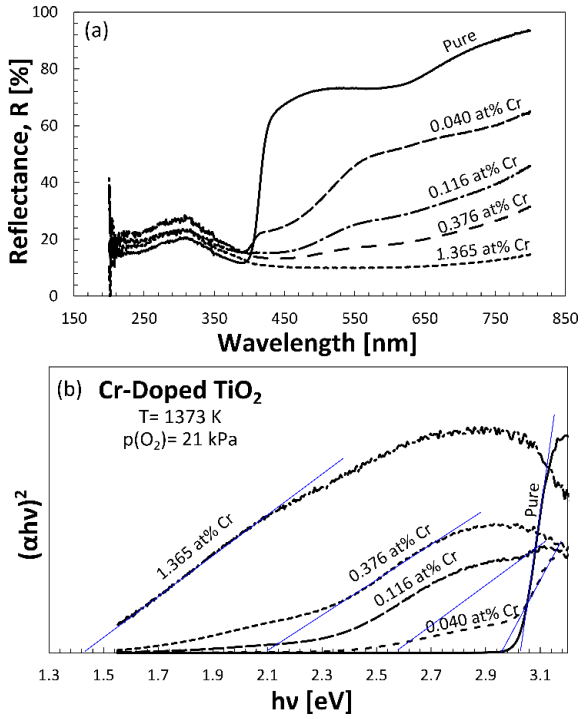

Figure A.2. *Effect of chromium concentration on the reflectance spectra (a) and the related Tauc plot (b) of TiO_2. Specimens annealed at 1373 K for 24 h in argon-hydrogen mixture ($p(O_2)$ = 21 kPa)*

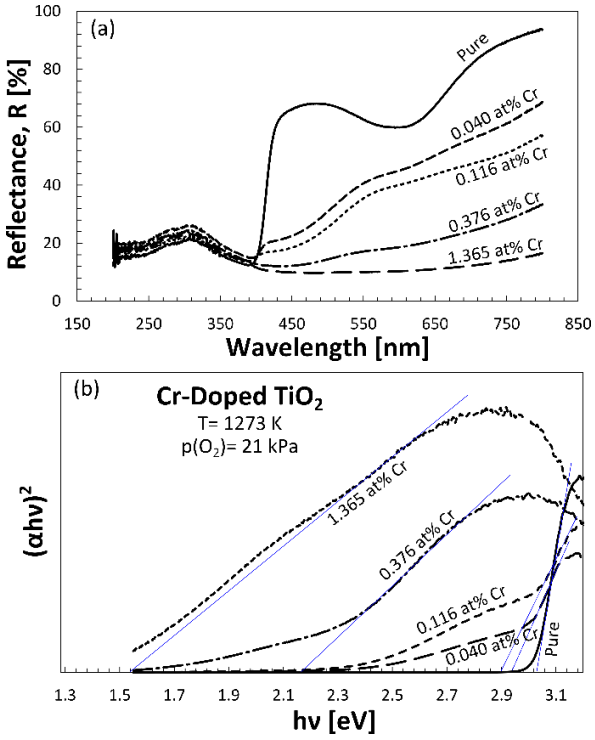

Figure A.3. *Effect of chromium concentration on the reflectance spectra (a) and the related Tauc plot (b) of TiO_2 annealed at 1273 K for 24 h in artificial air (p(O2) = 21 kPa).*